

University of Windsor
Scholarship at UWindsor

[Electronic Theses and Dissertations](#)

[Theses, Dissertations, and Major Papers](#)

1-23-2020

Thermal Modeling of Permanent Magnet Synchronous Motors for Electric Vehicle Application

Pratik Roy
University of Windsor

Follow this and additional works at: <https://scholar.uwindsor.ca/etd>

Recommended Citation

Roy, Pratik, "Thermal Modeling of Permanent Magnet Synchronous Motors for Electric Vehicle Application" (2020). *Electronic Theses and Dissertations*. 8309.
<https://scholar.uwindsor.ca/etd/8309>

This online database contains the full-text of PhD dissertations and Masters' theses of University of Windsor students from 1954 forward. These documents are made available for personal study and research purposes only, in accordance with the Canadian Copyright Act and the Creative Commons license—CC BY-NC-ND (Attribution, Non-Commercial, No Derivative Works). Under this license, works must always be attributed to the copyright holder (original author), cannot be used for any commercial purposes, and may not be altered. Any other use would require the permission of the copyright holder. Students may inquire about withdrawing their dissertation and/or thesis from this database. For additional inquiries, please contact the repository administrator via email (scholarship@uwindsor.ca) or by telephone at 519-253-3000 ext. 3208.

Thermal Modeling of Permanent Magnet Synchronous Motors for Electric Vehicle Application

By

Pratik Roy

A Thesis

Submitted to the Faculty of Graduate Studies
through the Department of Electrical and Computer Engineering
in Partial Fulfillment of the Requirements for
the Degree of Master of Applied Science
at the University of Windsor

Windsor, Ontario, Canada

2020

© 2020 Pratik Roy

Thermal Modeling of Permanent Magnet Synchronous Motors for Electric Vehicle Application

by

Pratik Roy

APPROVED BY:

G. Rankin
Department of Mechanical, Automotive & Materials Engineering

M. Azzouz
Department of Electrical and Computer Engineering

N. C. Kar, Advisor
Department of Electrical and Computer Engineering

January 23, 2020

Declaration of Co-Authorship / Publications

I hereby declare that this thesis incorporates material that is the result of joint research, as follows: this thesis includes the outcome of publications which also have graduate students or post-doctoral fellows supervised by Dr. Narayan Kar and a faculty member, Dr. Gary Rankin as co-authors. In all cases, only the primary contributions of the author towards these publications are included in the thesis. The contribution of co-authors was primarily through the provision of assistance in experimentation and analysis. I am aware of the University of Windsor Senate Policy on Authorship and I certify that I have properly acknowledged the contribution of other researchers on my thesis and have obtained written permission from each of the co-author(s) to include the above material(s) in the thesis. I certify that, with the above qualification, this thesis and the research study to which it refers, is the product of my own work. This thesis includes selected sections and extended work of research conducted in six original papers that have been published/submitted/ to be submitted in peer-reviewed International Conferences and Journals, as follows:

Thesis Chapter	Publication Title/ Full Citation	Publication Status
2	P. Roy , M. Towhidi, F. Ahmed, A. J. Bourgault, S. Mukundan, A. Balamurali, and N. C. Kar, “A Comprehensive Review of Thermal Design and Analysis of Traction Motors,” in <i>the IEEE 28th International Symposium on Industrial Electronics</i> , Vancouver, Canada, June 2019.	Published
2	P. Roy , S. Mukundan, M. Towhidi, F. Ahmed, Z. Li, and N. C. Kar, “A Comprehensive Review of Thermal Modeling of Traction Motors,” <i>the IEEE Journal of Emerging and Selected Topics in Industrial Electronics</i> , 2020.	To be submitted

3, 5, 7	<p>P. Roy, A. J. Bourgault, F. Ahmed, M. Towhidi, S. Mukundan, H. Dhulipati, E. Ghosh, and N. C. Kar “Thermal Representation of Interior and Surface Mounted PMSMs for Electric Vehicle Application,” in <i>the IEEE 45th Annual Conference of the Industrial Electronics Society</i>, Lisbon, Portugal, October 2019.</p>	Published
3, 5, 7	<p>P. Roy, S. Mukundan, H. Dhulipati, F. Ahmed, M. Towhidi, Z. Li, E. Ghosh, and N. C. Kar “Universal Thermal Representation of Interior and Surface Mounted PMSMs for Electric Vehicle Application,” <i>the IEEE Journal of Emerging and Selected Topics in Industrial Electronics</i>, 2020.</p>	To be Submitted
4, 6, 7	<p>P. Roy, M. Towhidi, F. Ahmed, S. Mukundan, H. Dhulipati, and N. C. Kar, “A Novel Hybrid Technique for Thermal Analysis of Permanent Magnet Synchronous Motor Used in Electric Vehicle Application,” in <i>SAE World Congress Experience Conference</i>, Detroit, MI, USA, April 21-23, 2020.</p>	Accepted for Presentation
8	<p>P. Roy, A. J. Bourgault, M. Towhidi, Z. Li, S. Mukundan, G. Rankin and N. C. Kar, “A Step Algorithm for Effective Cooling Design and Cooling Performance Investigation of PM Traction Motors,” in <i>IEEE International Magnetics Conference</i>, Montreal, Canada, May 2020.</p>	Submitted

I certify that I have obtained a written permission from the copyright owner(s) to include the above published material(s) in my thesis. I certify that the above material describes work completed during my registration as a graduate student at the University of Windsor.

I certify that, to the best of my knowledge, my thesis does not infringe upon anyone's copyright nor violate any proprietary rights and that any ideas, techniques, quotations, or any other material from the work of other people included in my thesis, published or otherwise, are fully acknowledged in accordance with the standard referencing practices. Furthermore, to the extent that I have included copyrighted material that surpasses the bounds of fair dealing within the meaning of the Canada Copyright Act, I certify that I have obtained a written permission from the copyright owner(s) to include such material(s) in my thesis and have included copies of such copyright clearances to my appendix.

I declare that this is a true copy of my thesis, including any final revisions, as approved by my thesis committee and the Graduate Studies office and that this thesis has not been submitted for a higher degree to any other University or Institution.

Abstract

Permanent magnet synchronous motor (PMSM) is a better choice as a traction motor since it has high power density and high torque capability within compact structure. However, accommodating such high power within compact space is a great challenge, as it is responsible for significant rise of heat in PMSM. As a result, there is considerable increase in operating temperature which in turn negatively affects the electromagnetic performance of the motor. Further, if the temperature rise exceeds the permissible limit, it can cause demagnetization of magnets, damage of insulation, bearing faults, etc. which in turn affect the overall lifecycle of the motor. Therefore, thermal issues need to be dealt with carefully during the design phase of PMSM. Hence, the main focus of this thesis is to develop efficient ways for thermal modeling to address thermal issues properly.

Firstly, a universal lumped parameter thermal network (LPTN) is proposed which can be used for all types of PMSMs regardless of any winding configuration and any position of magnets in the rotor. Further, a computationally efficient finite element analysis (FEA) thermal model is proposed with a novel hybrid technique utilizing LPTN strategy for addressing the air gap convection in an efficient way. Both proposed LPTN and FEA thermal models are simplified ways to predict motor temperature with a comparatively less calculation process. Finally, the proposed thermal models have been experimentally validated for the newly designed interior and surface mounted PMSM prototypes.

Again, a procedure for effective cooling design process of PMSM has been suggested by developing an algorithm for cooling design optimization of the motor. Further, a computational fluid dynamics (CFD) model with a proposed two-way electro-thermal co-analysis strategy has been developed to predict both thermal and electromagnetic performance of PMSM more accurately considering the active cooling system. The developed step algorithm and CFD modeling approach will pave the way for future work on cooling design optimization of the newly designed interior and surface mounted PMSM prototypes.

Dedication

Dedicated to my parents, sister, and brother-in-law.

Acknowledgements

Firstly, I would like to express my sincere thanks and heartfelt gratitude to my supervisor, Dr. Narayan Kar who guided me into and supported me throughout my master's program. He recognized my potential and gave me all the necessary tools to become an exceptional researcher. His vision and passion inspired a large part of my thesis work. In addition, he provided me with an abundant amount of opportunities to attend several international conferences and technical workshops to gain research experience as well as confidence. Further, he gave me the opportunity to pursue a research internship in a recognized industry and work on several industrial projects during my master's program which help me grow as a professional researcher in the field of electric vehicle application. Furthermore, such an opportunity to pursue the research internship program and work on several industrial projects helped me to pay my tuition fees for the master's program. For that, I am really grateful to Dr. Kar.

Secondly, I would like to sincerely thank Dr. Gary Rankin who took the time to sit with me in spite of his busy schedule and have technical discussions with me regarding my research work. He provided me with many attractive insights in the field of numerical thermal optimization process using ANSYS software tool. I would also like to thank Dr. Maher Azzouz who provided me with valuable feedback to improve the thesis writing.

Thirdly, I would like to sincerely thank the entire CHARGE labs team especially Dr. Shruthi Mukundan and Dr. Himavarsha Dhulipati for providing all information related to their designed motor prototypes which were their five years' dedicated Ph.D. work. I am grateful for their trust in me. Their unwavering support made completion of my master's program possible within the time. Again, I want to thank Dr. Firoz Ahmed for his valuable directions. I was lucky to have him working on the same field for his Ph.D. program at the same time. He involved me in his work without any hesitation which helped me to understand the overall research field in depth. Finally, I want to thank the whole CHARGE labs team

specially Dr. Wenlong Li, Dr. Emine Bostanci, Dr. Eshaan Ghosh, Dr. Sukanta Halder, Mr. Ze Li, Mr. Muhammad Towhidi, Mr. Alexandre J. Bourgault, Mr. Rao Fu, Mr. Animesh Kundu, Mr. Pronay Kumar Chakrobarty, Mr. Philip Korta, Mr. Brad Sato, Mr. Donovan O'Donnell, Mr. Soumava Bhattacharjee, Mr. Steven Turco and Mrs. Eunha Chu who selflessly helped me whenever I needed assistance.

At last but not least, I would like to express my sincere thanks and heartfelt gratitude to my parents who have always inspired me to pursue higher education at North American University. Their mental and financial support made completion of my master's program possible. Further, I want to thank my sister and brother-in-law for their valuable directions during my master's program. I am really grateful for their selfless support both mentally and financially during my master's program. Finally, I want to thank Dr. Nihar Biswas and my uncle and aunt, Mr. and Mrs. Paul for their valuable suggestions during my master's program.

Table of Contents

Declaration of Co-Authorship / Publications	iii
Abstract.....	vi
Dedication.....	vii
Acknowledgements	viii
List of Tables	xiv
List of Figures.....	xv
List of Abbreviations	xix
Nomenclature	xx
Chapter 1 Introduction.....	1
<i>1.1 Electric Vehicle: A Clean and Safe Transportation Mode.....</i>	1
<i>1.2 Electric Machine for Electrically Dominant Vehicle Propulsion System</i>	3
<i>1.3 Permanent Magnet Synchronous Motors for Traction Application</i>	5
<i>1.4 Thermal Aspects of Traction Permanent Magnet Synchronous Motor.....</i>	6
<i>1.5 Research Motivation</i>	6
<i>1.6 Research Objectives</i>	7
<i>1.7 Research Contributions.....</i>	8
<i>1.8 Organization of Thesis</i>	10
Chapter 2 A Comprehensive Review of Thermal Modeling of Traction Motors	13
<i>2.1 Thermal Design and Analysis of Traction Motor.....</i>	13
<i>2.1.1 Significance of Thermal Design and Analysis for Traction Motor</i>	14
<i>2.1.2 Different Ways for Thermal Analysis of Traction Motor</i>	16
<i>2.1.3 Challenges in Traction Motor Thermal Analysis Process</i>	18
<i>2.1.4 Published Works on LPTN Modeling of Traction Motor</i>	27
<i>2.1.5 Published Works on FEA Thermal Modeling of Traction Motor.....</i>	30
<i>2.2 Thermal Management of Traction Motor.....</i>	32

2.2.1 Significance of Thermal Management in Traction Motor	33
2.2.2 Different Ways of Motor Thermal Management.....	34
2.2.3 CFD Analysis for Motor Cooling Performance Investigation	34
2.3 Thermal Testing of Traction Motor.....	36
2.3.1 Significance of Motor Thermal Testing	36
2.3.2 Different Ways of Thermal Testing of Traction Motor.....	37
Chapter 3 Traction PMSM Prototypes for Thermal Performance Analysis	38
3.1 Designed PMSM Prototypes	38
3.1.1 Specifications of Designed IPMSM Prototype	39
3.1.2 Specifications of Designed SPMSM Prototype.....	40
3.2 Design Parameters of Analyzed Motors.....	41
3.3 Materials Properties of Analyzed Motors	42
Chapter 4 Loss Estimation of PMSMs for The Proposed Two-way Electro-thermal Co-analysis	43
4.1 Electromagnetic Finite Element Model for PMSMs	43
4.2 Electromagnetic Losses in PMSMs	44
4.2.1 Core Loss.....	44
4.2.2 Copper Loss.....	45
4.2.3 Magnet Loss.....	45
4.3 Mechanical Losses in PMSMs	45
4.3.1 Bearing Loss	45
4.3.2 Air Friction Loss.....	45
4.3.3 Other Mechanical Losses	46
4.4 Loss Data of IPMSM and SPMSM Prototypes.....	46
4.5 Temperature Dependency of Motor Losses.....	47
Chapter 5 A Universal Lumped Parameter Thermal Network Model of PMSMs for Traction Application.....	50
5.1 Proposed LPTN Model.....	50
5.2 Simplification Strategy for LPTN Modeling.....	53
5.3 Thermal Resistance Calculation in Proposed LPTN Model	54
5.3.1 Heat Transfer between Active Cooling System and Stator Frame	55

<i>5.3.2 Heat Transfer in Stator Yoke</i>	56
<i>5.3.3 Heat Transfer in Stator Teeth</i>	56
<i>5.3.4 Heat Transfer in Windings</i>	57
<i>5.3.5 Heat Transfer through Air Gap</i>	60
<i>5.3.6 Heat Transfer in Magnet</i>	60
<i>5.3.7 Heat Transfer in Rotor</i>	62
<i>5.3.8 Heat Transfer in Shaft</i>	62
<i>5.3.9 Heat Transfer in Bearing</i>	62
<i>5.3.10 Heat Transfer in End Region.....</i>	64
<i>5.4 Thermal Capacitance Calculation in Proposed LPTN Model</i>	65
<i>5.5 Temperature Calculation in Proposed LPTN Model</i>	65
<i>5.5.1 Steady State Thermal Analysis</i>	65
<i>5.5.2 Transient Thermal Analysis.....</i>	65
<i>5.6 Predicted Temperature of PMSM Prototypes from Proposed LPTN Model</i>	65
Chapter 6 A Novel Hybrid Technique for Computationally Efficient FEA Thermal Modeling Approach of PMSMs	69
<i>6.1 FEA Process for Thermal Analysis of Motor</i>	69
<i>6.2 Proposed FEA Thermal Model</i>	69
<i>6.2.1 Meshing for FEA Thermal Model.....</i>	70
<i>6.2.2 Strategy and Boundary Conditions in Proposed FEA Thermal Model</i>	71
<i>6.2.3 Simplification Strategy for FEA Thermal Modeling.....</i>	71
<i>6.2.4 Air Gap Creation Strategy in Proposed FEA Thermal Model</i>	72
<i>6.3 Predicted Temperature of PMSM Prototypes from Proposed FEA Model.....</i>	74
Chapter 7 Validation of The Proposed LPTN and FEA Thermal Models.....	77
<i>7.1 Comparison of LPTN and FEA Thermal Models.....</i>	77
<i>7.2 Experimental Validation of Thermal Models</i>	78
<i>7.3 Comparison of One-way and Two-way Electro-thermal Analysis Results</i>	81
<i>7.4 Validation of Thermal Analysis Strategy of Windings in LPTN</i>	83
<i>7.5 Validation of Equivalent Space Strategy of Magnets in LPTN</i>	84
<i>7.6 Explanation of Air Gap Creation Strategy in FEA</i>	85

Chapter 8 Cooling Design Process and Cooling Performance Investigation of PMSMs.....	86
<i>8.1 Cooling Design Process</i>	86
<i>8.2 Cooling Performance Investigation</i>	88
Chapter 9 Conclusions.....	93
<i>9.1 Overall Research Summary.....</i>	93
<i>9.2 Future Scopes</i>	95
<i>9.2.1 Future Work in the area of Thermal Design and Analysis</i>	95
<i>9.2.2 Future Work in the area of Thermal Management.....</i>	97
References	99
Appendices.....	111
<i>Appendix A: List of Publications.....</i>	111
<i>Journals</i>	111
<i>Conference Publications.....</i>	111
<i>Technical Report.....</i>	112
<i>Appendix B: Research Activities, Memberships, Scholarships and Courses</i>	113
<i>Industrial Project Contributions</i>	113
<i>Other Activities</i>	114
<i>Memberships.....</i>	114
<i>Scholarships.....</i>	114
<i>Courses Taken</i>	114
<i>Appendix C: Permission for Using Publications</i>	115
Vita Auctoris.....	117

List of Tables

Table 2.1 Comparison of thermal analysis processes of traction motors	17
Table 2.2 Nusselt number equations for various active cooling techniques	19
Table 2.3 Consideration of heat flow directions in LPTN model of electric motor	28
Table 2.4 Drawbacks of heat flow direction strategies in LPTN model of electric motor	29
Table 2.5 Drawbacks of 3D and 2D FEA thermal model.....	32
Table 3.1 Main specifications of IPMSM	40
Table 3.2 Main specifications of SPMSM.....	41
Table 3.3 Main design parameters of both PMSMs	42
Table 3.4 Material properties of both PMSMs	42
Table 4.1 Initial motor loss data at two different operating conditions for PMSMs	46
Table 4.2 Final loss data at 70 Nm and base speed for PMSMs using two-way electro-thermal co-analysis	48
Table 5.1 Thermal resistance parameters of proposed LPTN model.....	52
Table 5.2 Thermal capacitance and loss parameters of proposed LPTN model.....	52
Table 5.3 Steady state temperature of major motor components from LPTN model using initial loss	66
Table 5.4 Steady state temperature of major motor components from LPTN model using final loss results at 70 Nm and base speeds	66
Table 7.1 Comparison of LPTN and FEA temperature results at the rated condition in IPMSM.....	77
Table 7.2 Comparison of LPTN and FEA temperature results at the rated condition in SPMSM.....	77
Table 7.3 Comparison of LPTN and measured temperature results in SPMSM....	79
Table 7.4 Comparison of FEA and measured temperature results in SPMSM	80
Table 7.5 Comparison of windings thermal resistance	84
Table 7.6 Comparison of predicted rotor temperature from FEA Models	85
Table 8.1 Predicted torque considering the operating temperature of IPMSM.....	92

List of Figures

Figure 1.1 Basic diagram of electrically dominant vehicle propulsion system	3
Figure 1.2 Torque-speed and power-speed characteristics of a traction motor.....	4
Figure 2.1 Power flow diagram for PMSM.	13
Figure 2.2 Conversion of loss into heat energy source causing motor temperature rise.....	13
Figure 2.3 Impact of high operating temperature on overall motor performance [6].	15
Figure 2.4 Different ways for thermal analysis of traction motors.....	16
Figure 2.5 Convection heat transfer coefficient versus inner air velocity in the end space region based on several proposed empirical equations [21] – [28].....	21
Figure 2.6 Rotor structure of a scale down surface mounted PMSM prototype for future electric vehicle application from CHARGE labs.	24
Figure 2.7 3D LPTN model strategy. (a) An arc–segment element in radial, axial and circumferential directions [75]. (b) A cuboidal element in x , y and z directions [76].....	25
Figure 2.8 Hollow cylindrical structure having outer radius, r_1 and inner radius r_2	27
Figure 2.9 Heat flow direction through a hollow cylinder. (where, q_r , q_a and q_c = radial, axial and circumferential heat flow).	28
Figure 2.10 Convection boundaries in conventional FEA thermal model of motor.	31
Figure 2.11 Importance of cooling in traction motors [97].	33
Figure 2.12 Different ways of motor thermal management.....	34
Figure 2.13 Motor Thermal testing at CHARGE Labs.....	36
Figure 3.1 Radial sections of designed scale down IPMSM and SPMSM prototypes.....	38
Figure 3.2 Designed scale down IPMSM prototype.....	39
Figure 3.3 Several components of designed scale down IPMSM prototype.	39
Figure 3.4 Designed scale down SPMSM prototype.....	40
Figure 3.5 Several components of designed scale down SPMSM prototype.	41
Figure 4.1 Electromagnetic finite element models for analyzed motors. (a) IPMSM and (b) SPMSM.	43

Figure 4.2 Initial total loss density maps from electromagnetic finite element models for analyzed IPMSM and SPMSM at 70 Nm and base speeds after one full cycle.....	44
Figure 4.3 Two-way electro-thermal co-analysis.....	47
Figure 4.4 Final total loss density maps from electromagnetic finite element models for analyzed IPMSM and SPMSM at 70 Nm and base speeds after one full cycle.....	49
Figure 5.1 A general longitudinal sectional view of PMSM	50
Figure 5.2 Proposed LPTN model of PMSM. (where, T_{inlet} = constant inlet temperature of coolant as initial input).....	51
Figure 5.3 Considered heat transfer phenomena in different motor sections for LPTN calculation.....	53
Figure 5.4 Stator teeth designs of IPMSM and SPMSM prototype respectively ...	57
Figure 5.5 Winding configurations of IPMSM and SPMSM prototype. (a) FSDW. (b) FSCW.....	58
Figure 5.6 Universal representation strategy of rotor and magnet in proposed LPTN model for SPMSM and IPMSM prototype respectively.....	61
Figure 5.7 Bearing thermal model.....	63
Figure 5.8 Inner air passive cooling model.....	64
Figure 5.9 Predicted temperature in IPMSM at 70 Nm and 3,000 rpm from LPTN model.....	67
Figure 5.10 Predicted temperature in IPMSM at 35 Nm and 3,000 rpm from LPTN model.....	67
Figure 5.11 Predicted temperature in SPMSM at 70 Nm and 405 rpm from LPTN model.....	67
Figure 5.12 Predicted temperature in SPMSM at 35 Nm and 405 rpm from LPTN model.....	68
Figure 6.1 The overall process in ANSYS for thermal analysis of motor.....	69
Figure 6.2 Basic steps for numerical FEA thermal model.....	69
Figure 6.3 Two different mesh structures for numerical FEA thermal model.....	70
Figure 6.4 Strategies and boundary conditions for numerical FEA thermal model.....	70
Figure 6.5 Simplification strategy for numerical FEA thermal model in both IPMSM and SPMSM	72

Figure 6.6 Heat flow in air gap. (a) Low operating temperature. (b) High operating temperature.....	73
Figure 6.7 Created geometric region with assigned air properties for air gap in the motor geometry.....	73
Figure 6.8 Temperature distribution maps in IPMSM at 405 rpm from FEA thermal model. (a) 70 Nm. (b) 35 Nm.....	75
Figure 6.9 Temperature distribution maps in SPMSM at 3,000 rpm from FEA thermal model. (a) 70 Nm. (b) 35 Nm.....	74
Figure 6.10 Temperature distribution maps in IPMSM at 70 Nm and 3,000 rpm from FEA thermal model. (a) One-way analysis and (b) Two-way analysis.....	75
Figure 6.11 Temperature distribution maps in SPMSM at 70 Nm and 405 rpm from FEA thermal model. (a) One-way analysis. (b) Two-way analysis.....	76
Figure 6.12 Temperature distribution maps at 70 Nm and base speeds from numerical 3D FEA thermal models. (a) IPMSM. (b) SPMSM.....	76
Figure 7.1 Comparison of LPTN and FEA temperature results for IPMSM at 70 Nm and 3,000 rpm	78
Figure 7.2 Comparison of LPTN and FEA temperature results for SPMSM at 70 Nm and 405 rpm.	78
Figure 7.3 Loading test of SPMSM at 35 Nm and 100 rpm.	79
Figure 7.4 Captured temperature profile during loading test of SPMSM at 35 Nm and 100 rpm. (a) Winding temperature. (b) Magnet Temperature.	80
Figure 7.5 Comparison of LPTN and measured temperature results in SPMSM at 35 Nm and 100 rpm.	81
Figure 7.6 Comparison of FEA and measured temperature results in SPMSM at 35 Nm and 100 rpm.	81
Figure 7.7 Comparison of one-way and two-way electro-thermal co-analysis results for both FEA and LPTN in IPMSM at rated condition.	82
Figure 7.8 Comparison of one-way and two-way electro-thermal co-analysis results for both FEA and LPTN in SPMSM at rated condition.	82
Figure 7.9 DC Test of SPMSM and IPMSM prototypes respectively.....	83
Figure 7.10 Comparison of magnet temperatures in IPMSM prototype from FEA thermal model. (a) V-shape magnets. (b) Horizontally positioned magnets.	84
Figure 7.11 Motor temperature results from conventional FEA process using convection boundary at air temperature, 22°C in airgap.	85
Figure 8.1 Basic step algorithm for cooling design optimization of motor.....	87

Figure 8.2 Two-way electro-thermal co-analysis process during CFD analysis.	89
Figure 8.3 3D motor geometry with cooling channel for CFD analysis.....	91
Figure 8.4 Predicted temperature distribution of IPMSM from CFD analysis.....	92
Figure 9.1 Layer by layer temperature prediction topology in LPTN model for n^{th} layer winding configurations. (a) FSDW. (b) FSCW.	96
Figure 9.2 Cooling design optimization process for targeted electromagnetic performance using CFD analysis in ANSYS Workbench.	97

List of Abbreviations

HEV	Hybrid Electric Vehicle
EV	Electric Vehicle
PM	Permanent Magnet
PMSM	Permanent Magnet Synchronous Motor
IM	Induction Motor
SPMSM	Surface Mounted Permanent Magnet Synchronous Motor
IPMSM	Interior Permanent Magnet Synchronous Motor
UDDS	Urban Dynamometer Driving Schedule
HWFET	Highway Fuel Economy Driving Schedule
WLTP	Worldwide Harmonised Light Vehicle Test Procedure
WLTC	Worldwide Harmonised Light Vehicle Test Cycle
LPTN	Lumped Parameter Thermal Network
FEA	Finite Element Analysis
CEFEA	Computationally Efficient Finite Element Analysis
CFD	Computational Fluid Dynamics
FEM	Finite Element Model
FSDW	Fractional Slot Distributed Winding
FSCW	Fractional Slot Concentrated Winding
EPA	Environmental Protection Agency
SST	Steady State Thermal
TTA	Transient Thermal Analysis
DC	Direct Current
AC	Alternative Current
HC	Hydrocarbon
RTD	Resistance Temperature Detector

Nomenclature

L	Length of heat path (m).
A	Cross-sectional area of heat path (m^2).
h	Convection heat transfer coefficient ($\text{W}/\text{m}^2\text{K}$).
ε	Emissivity of the surface.
σ	Stefan-Boltzmann constant ($\text{kgs}^{-3}\text{K}^{-4}$).
T_1, T_0	Nodal temperatures (K).
F	View factor in between two surfaces.
k	Thermal conductivity of corresponding substance (W/mK).
Re	Reynolds number.
Re_r	Rotational Reynolds number.
Pr	Prandtl number.
Gr	Grashof number.
Nu	Nusselt number.
D	Hydraulic diameter of cooling channel (m).
d	Inner diameter of cooling channel (m)
H	Height of cooling channel / fin (m).
W	Width of cooling channel (m).
f	Friction factor of coolant flow.
ρ	Density of corresponding fluid (kg/m^3).
v	Velocity of corresponding fluid (m/s^2).
μ	Dynamic viscosity of corresponding fluid (kg/ms).
C_p	Specific heat capacity of corresponding substance (J/kg).
q_l	Latent heat (J/kg).

ΔT	Temperature rise / difference (K).
ω	Angular velocity of rotor (rad/s).
r_{ro}	Outer radius of rotor (m).
R_{ec}	End–cap axial thermal resistance (K/W).
g	Gravitational constant for earth (m/s ²).
β	Coefficient of cubical expansion (K ⁻¹).
N	Number of fins.
S	Fin pitch (m).
α_T	Temperature coefficient (K ⁻¹)
l_r	The axial length of the rotor
k_1, k_2, k_3	Proportionality coefficients that are dependent on air turbulence intensity
η	Geometrical factor based on surface geometry and roughness
Q	Amount of heat flow (W)
q	Amount of heat flow per unit area (W/m ²)
T_{body}	Body temperature (K)
T_{fluid}	Temperature of fluid (K)
$T_{amb.}$	Ambient temperature (K)
p_e	Eddy current loss (W)
p_h	Hysteresis loss (W)
p_a	Additional loss component on core loss (W)
P_c	Core loss (W)
k_e	Variable eddy current loss coefficient
k_h	Variable hysteresis loss coefficient
k_a	Variable additional loss coefficient
B_m	Maximum magnetic induction (T)

f_e	Electrical frequency (Hz)
n	Number of phase
I	Current (A)
R_e	Electrical resistance (Ω)
P_b	Bearing loss at certain angular velocity (W)
P_{bmax}	Bearing loss at maximum angular velocity
ω_{max}	Maximum angular velocity (rad/s)
P_{ag}	Air friction loss (W)
ρ_{air}	Density of air (kg/m^3)
μ_{air}	Dynamic viscosity of air (kg/ms)
δ	Air gap thickness (m)
t_{fr}	Average thickness of the stator frame (m)
l_s	Stack length (m)
r_{so}	Outer radius of stator yoke (m)
k_{Al}	Thermal conductivity of aluminum (W/mK)
r_{si}	Inner radius of stator yoke (m)
h_{st}	Tooth height (m)
l_u	Useful length of stator core (m)
k_{sf}	Stacking factor
k_l	Thermal conductivity of lamination (W/mK)
N_s	Number of stator slots
$x_d(r)$	Tooth width where y is the radial coordinate
l_{av}	Average length of half a turn of coil (m)
A_{Cu}	Total copper area in one slot (m^2)
k_{Cu}	Thermal conductivity of copper (W/mK)

r_{av}	Average of rotor and stator radii (m)
p	Pole pairs
θ_m	Angle occupied by magnets in one pole pitch (radians)
t_r	Thickness of the rotor yoke in SPMSM(m)
t_m	Thickness of the magnet (m)
r_{ri}	Inner radius of rotor (m)
w	Width of magnet (m)
t_{ru}	Thickness of rotor upper part in IPMSM (m)
t_{rl}	Thickness of rotor lower part in IPMSM (m)
l_{bb}	Effective axial length of shaft (bearing to bearing) (m)
r_{sh}	Radius of shaft (m)
k_{steel}	Thermal conductivity of steel (W/mK)
d_b	Average diameter of the bearing (m)
A_1	Surface area of end cap and partially frame (m^2)
A_2	Surface area of end winding (m^2)
A_3	Surface area of rotor end (m^2)
l_{airgap}	Length of air gap (m)
R_{Cu}	Resistance of windings after temperature rise (Ω)
R_{Cu0}	Resistance of windings at initial temperature (Ω)
v_x, v_y, v_z	Velocity components of fluid element in x, y, z direction (m/s)
p	Pressure (Pa)
F_x, F_y, F_z	Volume force in x, y, z direction of fluid element (N)
S_T	Viscous dissipation
k_e, ε_e	Turbulent kinetic energy and dissipation rate

Chapter 1

Introduction

1.1 Electric Vehicle: A Clean and Safe Transportation Mode

Nowadays climate change is one of the most burning issues all over the world, as the temperature of the earth is rising at the fastest rate because of global warming. To combat climate change, different measures are being taken all over the world. The recent Paris agreement is the promising action plan in which the central aim is to strengthen the global response to the threat of climate change by keeping global temperature rise this century well below 2 degrees Celsius and this target can be achieved by reducing CO₂ emission significantly [1]. However, in a recent study, global light duty vehicles such as cars, minivans, SUVs, etc. are predicted to be triple in number and CO₂ emissions are predicted to be double in amount by 2050 [2], [3]. As a result, in order to reduce the rise in CO₂ emissions, the number of light duty vehicles dependent on fossil-fuels such as oil, gas, etc. needs to be replaced by electrically driven vehicles due to its eco-friendly zero CO₂ emission characteristics. That is why electrically dominant vehicle propulsion system is one of the emerging research areas nowadays.

Further, due to the drastic change in climate and the concern about other environmental issues, electric vehicles are gaining significant thrust from governments, automobile manufacturers and consumers globally. Moreover, the significant rise in fossil-fuel cost and also, recently imposed tax on fossil-fuel in most developed countries, for example, the recently imposed carbon tax in Canada in order to reduce fossil-fuel dependency are significantly shifting the research trends towards the electrically dominant vehicle propulsion system. Although the initial price of electric vehicles is higher, it can be compensated later by comparatively lower operating costs which are mainly fuel and maintenance costs in the long run. Therefore, more research focus has been given to increase both speed range and distance range of electric vehicles to make it a more preferable choice for consumers rather than fossil-fuel dependent vehicles. Therefore, there are lots of research activities currently going on the development of more efficient

electric vehicles so that it can become the most popular transportation mode all over the world in the not too distant future.

Furthermore, although the innovation of internal combustion (IC) engine vehicles is one of the greatest revolutions for modern technology, it is also one of the main reasons for environmental pollution in recent days. It is undeniable that IC engine vehicles have significant contributions to the development of modern human society. These vehicles are considerably satisfying most of the mobility needs in our daily to daily life. As a result, the number of IC engine vehicles in use around the world has been continuously increasing. Such huge numbers of IC engine vehicles in use all over the world have already caused and are still continuously causing serious damage to the environment which is actually one of the most rising concerns in recent days. All these IC engine vehicles around the world consume mainly hydrocarbon (HC) fuels for combustion to derive the necessary energy for engine propulsion. Since the combustion of hydrocarbon (HC) fuels are not ideal combustion in nature, there are other harmful by-products also other than carbon dioxide (CO_2). Such a nonideal combustion process also produces a good amount of nitrogen oxides (NO_x) and carbon monoxides (CO). Further, there are always some unburned HCs remaining after completion of the combustion process. All these by-products are harmful to the environment as well as to both human and animal health since these are toxic chemicals. Nitrogen oxides cause smog, acid rain, etc. which have a significant negative impact on the environment such as the destruction of forests. Again, carbon monoxide also causes damage to the environment. Further, it is poisonous gas for animals and human beings. Inhaling carbon monoxide can cause several serious damages to both human and animal health. Further, inhaling too much carbon monoxide can eventually cause death. Besides these by-products, remaining unburned HCs can also cause harm to the environment and human and animal health depending on the type such as highly toxic benzene. Further, there are some impurities in the HCs fuel which also results in the emission of more pollutants into the environment. The major impurity in HCs is basically sulfur which produces sulfur oxides (SO_x) after direct chemical reaction with oxygen from air during the IC engine combustion process. Sulfur oxides are also harmful chemicals for the environment, human and animal health. Sulfur oxides are one of the main reasons for acid rain like nitrogen oxides which is harmful to trees [4]. For all

these reasons, the research activities have been shifted towards the development of high efficiency, clean and safe transportation mode which has significantly increased the research activities on eco-friendly vehicles. Therefore, it is high time to pursue research in the area of electric vehicle application.

1.2 Electric Machine for Electrically Dominant Vehicle Propulsion System

The heart of electrically dominant vehicle propulsion system is traction motor which is the connection between the electrical and mechanical control system shown in Figure 1.1. Further, traction motor is the main powerhouse of electric vehicles (EVs). It provides power partially to hybrid electric vehicles (HEVs) and solely to fully electric vehicles.

As traction motor provides the power, the main focus of research in the area of electrically dominant vehicle propulsion system is basically traction motor. The further increase in speed range capability of electric vehicles is mainly dependent on the progress of traction motor in terms of torque and speed capability which is mainly total power capability. Traction motors should be capable of adopting some definite operational requirements such as high torque at low speed, high constant power at high speed and high efficiency along with high power density shown in Figure 1.2.

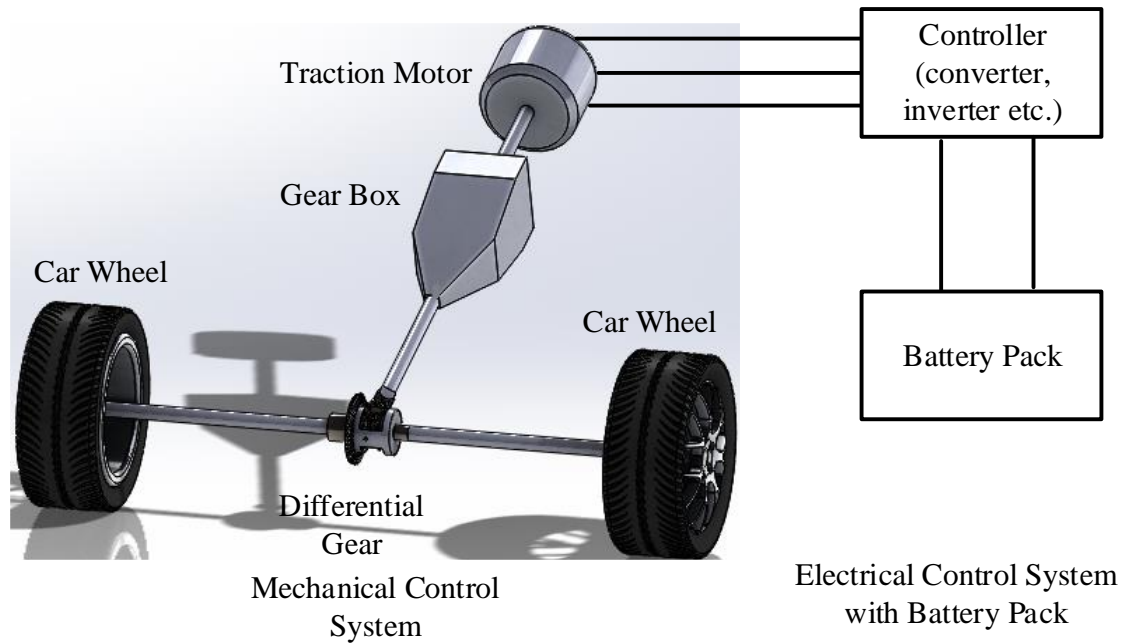


Figure 1.1 Basic diagram of electrically dominant vehicle propulsion system.

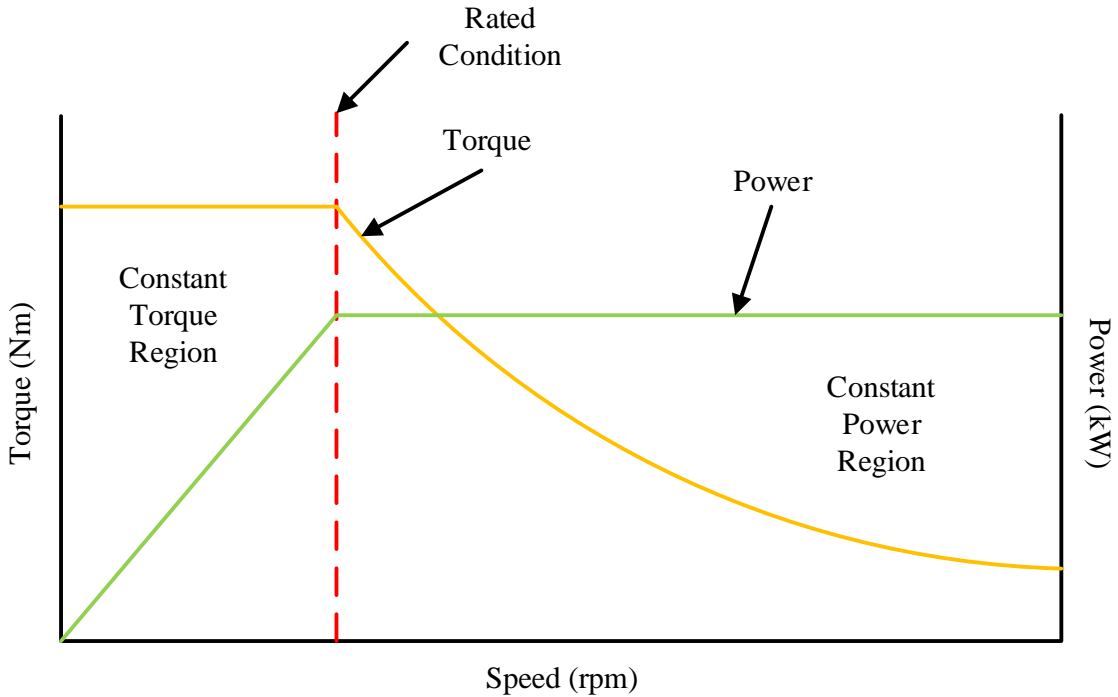


Figure 1.2 Torque-speed and power-speed characteristics of a traction motor.

Further, as vehicles require frequent starts and stops, traction motor should have higher rates of acceleration and deceleration. Besides that, there are always concerns about the size and weight of traction motor. Traction motor should be smaller in size and lighter in weight which means traction motor should have a compact structure. Adopting these definite operational requirements in one specific motor with smaller size and lighter weight at the same time is more challenging. Because such high torque and high power density within compact structure can make any motor unstable if it is not designed properly to handle that high power and torque rating. Therefore, careful motor design needs to be carried out for traction motor so that it has enough mechanical strength to withstand such high torque and high power and also it has the ability to provide better performance both electromagnetically and thermally during the operating condition. Further, it must ensure proper dynamic balance in terms of electromagnetic, thermal, structure, and acoustic during operation. As a result, the design optimization process of traction motor needs extra care. Hence, the main focus of motor designers is the design of traction motors to overcome all these challenges for better dynamic performance of traction motor. Such a better dynamic performance of traction motor can further open the door for more consumer friendly electric vehicles. For this reason, traction motor has

been selected as the main focus of this research in the area of electrically dominant vehicle propulsion system.

1.3 Permanent Magnet Synchronous Motors for Traction Application

At present, induction motor (IM) and permanent magnet synchronous motor (PMSM) are mainly used as traction motors. However, PMSM is more efficient compared to IM. PMSM has much higher efficiency than IM over a wide speed and torque range. For example, it was found from an investigation that the efficiency of PMSM was 92.5%, much higher than the efficiency of copper rotor IM, 88.2% under the same speed and torque ratings, 900 rpm and 118 Nm respectively [5]. Even PMSM is more advantageous than IM in terms of torque-speed and power-speed characteristics. As high energy permanent magnets are used for field excitation, PMSMs can be designed with high power and high torque capability. Therefore, it can provide higher torque during low-speed application especially during starting condition and hill-climbing and can provide higher constant power during high-speed application for electric vehicles. Further, PMSM has a compact structure compared to IM. Therefore, it is also comparatively smaller in size and lighter in weight than IM with the same power rating. Furthermore, PMSM is easy to control because of easily accessible control variables that are constant throughout the operation of PMSM [4]. Again, PMSM has great longevity and thus it possesses good reliability also. Another great advantage of PMSM is the ease of cooling. Unlike IM, it has permanent magnets in the rotor instead of copper bars that do not consume any current. As a result, the rotor of PMSM is cooler compared to IM, although PMSM is more thermally challenging than IM. For this reason, the rotor of PMSM does not need any separate cooling like most of the IMs in electric vehicle application. Therefore, the cooling system of PMSM has a simple structure that is basically built around the stator frame only. Due to such a simple cooling structure, the cooling system of PMSM is really easy to operate. Further, it gives the operation of PMSM more flexibility [4]. For these reasons, PMSM is the most viable candidate as a traction motor at present in electric vehicle application. Hence, PMSM is being widely used as a traction motor in electric vehicle application compared to other traction motor types. That is why extensive research on PMSM is getting more and more attention from automotive industries all over the world for electric vehicle application. For this reason, PMSM has

been selected as the focus of this research study among all other traction motor types used in electric vehicle application.

1.4 Thermal Aspects of Traction Permanent Magnet Synchronous Motor

A significant portion of motor losses converts into heat which results in a considerable rise in operating temperature, while the motor is in operation. Since traction motors are mainly high power motors, the amount of loss in traction motor during operation is also large. As a result, the rise in operating temperature of traction motor is significant which makes the motor thermally challenging. Permanent magnet synchronous motor (PMSM) mainly used in traction application is thermally more challenging than any other traction motor type. Due to high torque and power density within the compact structure, temperature rise within PMSM is comparatively quicker than other traction motor types. Moreover, it has thermally sensitive permanent magnets which are susceptible to heat. If the motor temperature rises more than the permissible limit, it can cause permanent demagnetization of the magnets which in turn can cause permanent damage to PMSM. Therefore, extra care is needed on the thermal side during the design phase of PMSMs.

1.5 Research Motivation

An integrated electromagnetic and thermal analysis should be done carefully for designing high torque and high power PMSM to ensure both electromagnetic and thermal stability within the compact motor structure. However, most of the traction motor designers were from the Electrical Engineering background in past, as traction motor is one kind of electric machine. Therefore, significant progress has been made in the area of electromagnetic design optimization of traction motors. On the other hand, the area of thermal design optimization of traction motors has got less attention, as thermal experts are mainly from Mechanical Engineering background. As a traction motor, permanent magnet synchronous motor (PMSM) is not out of that. However, such condition is changing day by day since there are a lot of research opportunities available in the area of thermal design optimization of PMSM. Therefore, pushing the thermal operation limit of PMSM into a further advanced level is the main focus nowadays to achieve a better thermal performance of PMSM. For this reason, the research study emphasis is on thermal aspects of PMSM mainly to provide a better thermal modeling approach for

PMSM. Thermal design and analysis, thermal management and thermal testing are three main research branches in the research area of motor thermal study. Thermal design and analysis are mainly used to analyze motor thermal behavior and predict the motor temperature and further to provide better suggestions regarding thermal design optimization process of the motor. Thermal management is mainly used to provide several solutions for better motor thermal performance such as cooling. Finally, thermal testing is mainly used for experimental testing of the motor to get a better practical direction regarding motor thermal behavior. All three branches of motor thermal study are discussed in the research study to a certain extent for PMSMs used in electric vehicle application.

1.6 Research Objectives

The major purpose of this research is to analyze thermal stability and thermal performance of newly designed scale down surface mounted and interior PMSM prototypes in CHARGE labs at the University of Windsor by developing efficient thermal modeling processes. To fulfill this purpose, three specific research areas on the thermal side of traction motors have been selected as stated in the previous section. These three research areas are thermal design and analysis, thermal management and thermal testing. In these three research areas, three main work goals have been set up which are mentioned below:

- Work goal in the area of thermal design and analysis:

Developing simplified thermal models for newly designed scale down surface mounted and interior PMSM prototypes to predict the rise in motor temperature while the motor prototypes are operating. This process is helpful for ensuring thermal stability of the motor prototypes by ensuring that the rise in the operating temperature of both motor prototypes is within the acceptable limit. Further, this process is also helpful for identifying motor design faults if there are any, from the predicted temperature distribution of the motors.

- Work goal in the area of thermal testing:

Experimental validation of the developed thermal models to prove the reliability of the models. Such experimental validation will then provide more reliable ways to predict and monitor temperatures of several motor components of PMSM while the motor is operating. Further, such practical testing is helpful to detect any manufacturing defects on the motor prototypes if any from the sudden rise in measured temperature in any motor components during testing.

- Work goal in the area of thermal management:

Developing a basic step algorithm for cooling design process and a CFD modeling for cooling performance investigation of newly designed scale down IPMSM prototype. Such step algorithm process can form basic guidelines for the cooling design process of PMSM. Such investigation process is helpful to find out the proper flow rate of coolant to get better thermal performance for the motor prototype at a certain operating condition. Further, the implementation of a two-way electro-thermal co-analysis strategy in the developed CFD model enables the process to determine the proper flow rate of coolant to achieve the targeted electromagnetic performance of the motor also at the same operating condition.

1.7 Research Contributions

Author's own research contributions are described below:

- Developed a **simplified analytical LPTN model** for PMSMs to reduce both over-complexity and calculation time for thermal analysis.

Such simplification strategy for the analytical LPTN model has been developed by considering only major heat transfer phenomena for thermal resistance calculation. This simplification strategy is helpful to simplify the process by reducing the over-complexity of thermal resistance calculations. As a result, it will save the calculation time for the overall thermal analysis process. Further, considering all major heat transfer phenomena for thermal resistance calculation will keep the accuracy level of the developed LPTN model within the acceptable range.

- Developed a **universal thermal representation strategy** to use the same analytical LPTN model for all types of PMSMs.

Such a universal thermal representation strategy has been achieved by developing common thermal analysis strategies for both wide range of winding configurations and any position of magnets in the rotor. As mainly winding configurations and magnet positions vary with different PMSM structures, incorporation of such common thermal analysis strategies for both wide range of winding configurations and any position of magnets in the developed LPTN model will provide an efficient way to use the developed LPTN model as a universal thermal representation model of all types of PMSMs.

- Developed a **simplified FEA thermal model** for PMSMs with better accuracy.

Such simplification has been achieved by assigning an additional conduction boundary to characterize the heat flow from shaft to housing through bearing and end cap. Such strategy minimizes the need for complex bearing and end cap geometry for FEA thermal model. Therefore, only the radial 2D geometry section can be considered for the FEA thermal model instead of complex 3D geometry, if the end region temperature is not needed. Even in the 3D FEA thermal model, this additional conduction boundary strategy between shaft and stator frame can be implemented without considering complex bearing and end cap geometry for simplification. On the other hand, heat flow from shaft to stator frame through the end cap and bearing addressed by assigning conduction boundary will keep the accuracy level of results within the desired limit.

- Developed a **unique strategy to address the heat transfer through the air gap** in the proposed FEA thermal model for PMSMs in an efficient way.

By creating a separate geometric region with assigned air properties for air gap in the motor geometry, the heat transfer through the air gap has been characterized in an efficient way for better accuracy of the developed FEA thermal model. Such a geometric region for air gap also makes a way to address the air friction loss as one of the heat generation sources in the FEA thermal model. Further, this strategy allows the rise of air temperature in the air gap with the rise in the operating temperature of the motor.

Therefore, it provides a better solution to address the air gap convection in the most practical way.

- Developed **an algorithm strategy for the cooling design optimization process** for PMSMs.

From an in-depth background study of cooling design optimization processes for PMSMs, an algorithm strategy has been developed. This algorithm for the cooling design optimization process describes the basic steps in a proper sequence to achieve an optimal cooling design for PMSMs in a simpler and quicker way. However, cooling design optimization is not the concern of this research study, since the analyzed motors have already inbuilt active cooling systems. The main purpose of the developed algorithm is to provide the basic guidelines regarding the cooling design process of PMSM which will pave the way for the cooling design optimization process in the future.

- Proposed **a strategy addressing temperature dependency of electromagnetic properties** during the thermal and cooling performance investigation process of PMSMs.

By developing a two-way electro-thermal co-analysis strategy, such temperature dependency of electromagnetic properties has been addressed during the thermal and cooling performance investigation process of the designed motor prototypes. Such a two-way electro-thermal co-analysis is helpful to get the final motor temperature rise after dynamic equilibrium reaches between electromagnetic and thermal analysis which is the actual practical case for the motor while in operation. Further, such a two-way electro-thermal co-analysis is helpful to address the electromagnetic performance of the motor under consideration of the active cooling system during CFD analysis.

1.8 Organization of Thesis

This thesis including the introduction chapter has nine chapters that present the research conducted and the novel contributions made to the area of work to achieve the overall research objectives stated above. The chapters are organized as follows:

Chapter 2 focuses on background study of the discussed research areas in the thesis. The background study considers the fundamental basics, classifications, challenges and their

solutions, and previously published works, etc. to get a proper understanding regarding the research areas.

Chapter 3 presents the information about the newly designed scale down IPMSM and SPMSM prototypes. The information about the designed motors basically contains the main specifications, design parameters, properties of construction materials of the designed motors.

Chapter 4 introduces the loss analysis of the designed motor prototypes which will be used later for thermal study. In detail, the chapter discusses the calculation of electromagnetic and mechanical losses considered in the thermal design model as the heat generation sources. This chapter also discusses the electromagnetic FEM to a certain extent from which losses are analyzed. Further, this chapter also discusses the two-way electro-thermal co-analysis process briefly which has been used to consider temperature dependent electromagnetic losses of the motor.

Chapter 5 utilizes thermal resistance and capacitance equations to develop the proposed analytical LPTN model for thermal design and analysis of the designed motor prototypes. This chapter also presents the new insights such as simplification and universal representation strategy of the developed LPTN model in detail. Further, this chapter also discusses the motor temperature results obtained from the LPTN model.

Chapter 6 presents the methodology of the developed FEA thermal model briefly. This chapter presents the new insights such as simplification and air gap creation strategy of the developed FEA thermal model in detail. The presented strategies have been discussed for both 2D and 3D FEA thermal model. Further, this chapter also discusses the motor temperature distribution obtained from the FEA thermal model.

Chapter 7 extends the research work of thermal design and analysis to experimental validation. Analyzed results from the developed LPTN and FEA thermal models are compared with the experimental results from the loading test for practical validation of the models and then the comparison is presented in this chapter. Further, the calculated thermal resistances from the developed thermal analysis strategy for windings used in the proposed LPTN are compared with the measured thermal resistances from the DC test.

The procedures of loading test and DC test of the designed motor prototypes have been presented briefly in this chapter. Further, this chapter also discusses the different aspects of analyzed results for a better understanding of the thermal behavior of the designed motor prototypes.

Chapter 8 outlines the active cooling system and cooling performance investigation process of the cooling system for the designed IMPSM prototype. This chapter presents the developed algorithm for the cooling design optimization process of PMSM. In the future, using that process optimal cooling design of any cooling technologies for traction motors can be obtained, if equations related to the specific cooling technology is known. Moreover, CFD modeling is presented in this chapter for the cooling performance investigation process to find out the proper flow rate of coolant for better thermal performance of IPMSM. Further, this chapter presents the implementation of a two-way electro-thermal co-analysis strategy into the developed CFD model to find out electromagnetic performance under the consideration of the active cooling system of IPMSM.

Chapter 9 summarizes the significance of the overall research work and provides potential future work in this area of research.

Chapter 2

A Comprehensive Review of Thermal Modeling of Traction Motors

2.1 Thermal Design and Analysis of Traction Motor

Generally, during the working condition, all the energy losses in permanent magnet synchronous motors subsequently convert into heat energy which has a negative impact on the motor's performance. Only a very small portion of the energy loss may be converted into sound energy, leading to high acoustic noise emitted from the motor.

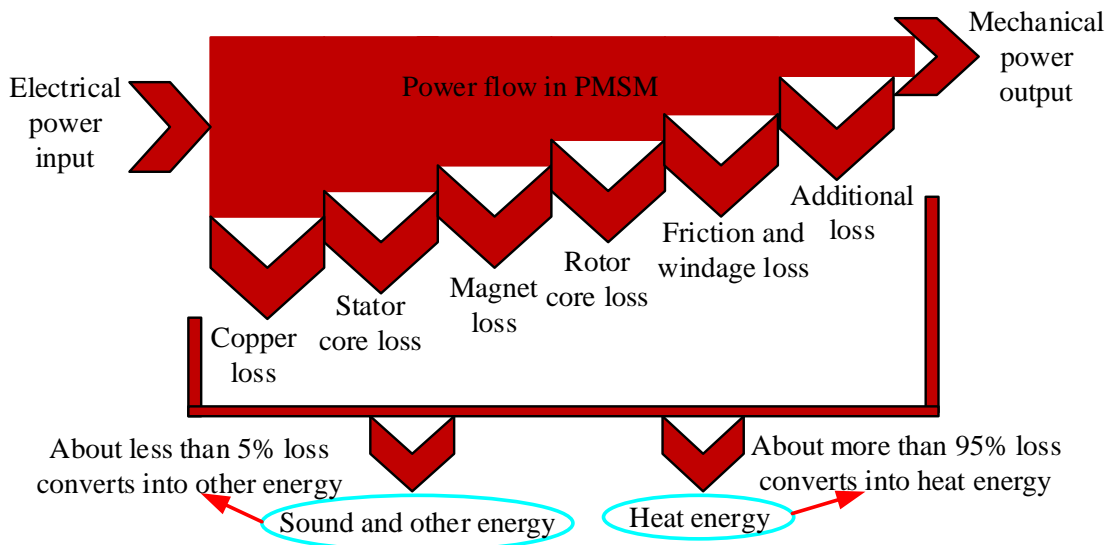


Figure 2.1 Power flow diagram for PMSM.

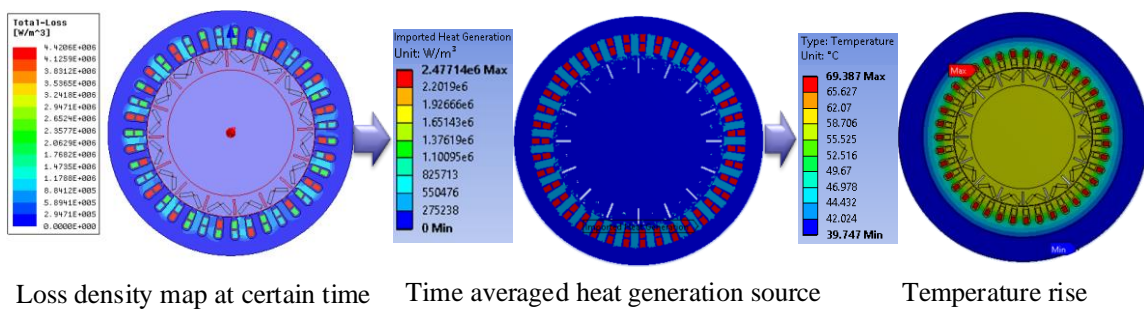


Figure 2.2 Conversion of loss into heat energy source causing motor temperature rise.

As the vast part of the energy losses is related to the production of heat energy causing significant temperature rise, the motor's performance is also absolutely governed by its thermal design like its electromagnetic design. Therefore, thermal design and analysis are

mandatory steps for the design phase of permanent magnet synchronous motors to ensure its thermal stability during operation.

In order to analyze the thermal aspects of motors, most of the researchers follow different basic methods that already exist which can generally be divided into analytical and numerical methods. The analytical method includes Lumped Parameter Thermal Network (LPTN) modeling where the thermal system is represented as a network of thermal resistances. Unlike LPTN modeling, the numerical method considers the geometry of the overall system and calculates the heat transfer parameters. Depending on the implementation of Thermodynamics or Fluid dynamics equations, the numerical method can further be divided into Finite Element Analysis (FEA) and Computational Fluid Dynamics (CFD) respectively. Only the simplified geometry and material properties are not sufficient to give an accurate prediction of the thermal performance of motors. Some critical parameters such as interference gaps between components, the uncertainty of material property, critical winding geometry, coating, and insulation properties, etc. must be implemented into the basic thermal design and analysis to reflect the accurate thermal behavior of the motor.

2.1.1 Significance of Thermal Design and Analysis for Traction Motor

The major part of power losses in the motors converted into heat must be eventually dissipated from the motor to its surrounding environment. Otherwise, generated heat in the motor can substantially increase the temperature in the windings and other parts of the motor.

Such temperature rise can deteriorate the performance characteristics of the motor. Figure 2.3 shows clearly how high operating temperature negatively impacts the torque and power capability of traction motors [6]. Such a decrease in torque and power capability at high operating temperatures in traction motor surely affects the performance of electric vehicles. Hence, high operating temperature is not a desired condition for the traction motor. Therefore, the thermal stability of the traction motor is a very important issue to be considered so that the motor temperature does not exceed the permissible temperature limit during operation.

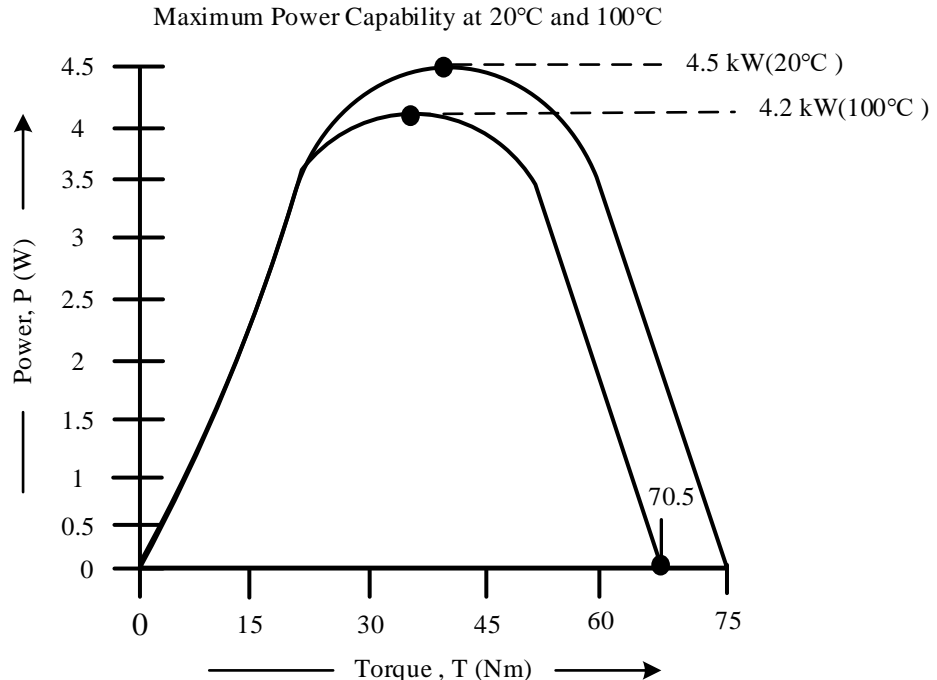


Figure 2.3 Impact of high operating temperature on overall motor performance [6].

Again, the motor failures happen because of the conversion of power losses into heat energy causing the excessive internal temperature of the motor. A good percentage of motor failures such as damage of insulations, bearing faults, and demagnetization of magnets, etc. occurs due to overheating during operation [6]. Moreover, the efficiency of the machine is defined as the ratio of power output (which is equal to the total power input minus power losses) to the total power input. As a result, the higher the power losses, the lower the machine efficiency. The same is true for the PMSM as it is also one kind of electric machine. Therefore, besides electromagnetic modeling and analysis, thermal modeling and analysis should be an integral part of the motor design to ensure its thermal stability.

The past research related to this specific area indicates that thermal design and analysis of electric machines had less attention than electromagnetic design and analysis. At present, the condition has already changed. Recently, thermal design and analysis of electric machines have started to receive more attention as well as electromagnetic design and analysis of electric machines. It is due to extensive research on common causes of failures of electric machines. The fact is that most of the failures are caused by overheating. Therefore, researchers are now also focusing on thermal design and analysis

of electric machines. Therefore, the research study includes thermal design and analysis of both newly designed IPMSM and SPMSM prototypes to ensure the selection of correct insulation and bearing types to prevent motor faults. Further, it will ensure the stable operating temperatures for the motors to prevent demagnetization, breakdown of insulation and bearing faults.

2.1.2 Different Ways for Thermal Analysis of Traction Motor

There are mainly two types of methods for thermal analysis of traction motor – analytical and numerical methods. The analytical method involves necessary calculations based on theoretical equations related to the problem that needs to be solved. In the thermal study, the analytical method is basically called a lumped parameter thermal network (LPTN) modeling in which a thermal network is built using thermal resistances and capacitances. On the other hand, the numerical method is an iterative process to solve any critical mathematical problem until the solution converges. Such numerical methods can be utilized for the thermal study also.

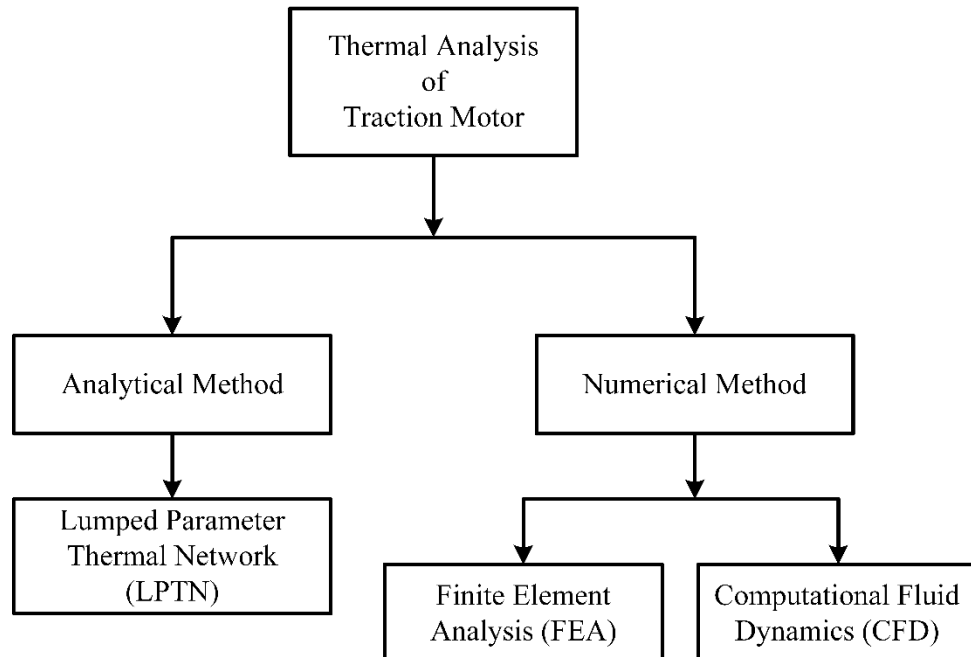


Figure 2.4 Different ways for thermal analysis of traction motors.

In the thermal study, there are mainly two types of numerical methods. One method is finite element analysis (FEA) in which the overall problem domain is divided into lots of small elements called sub-domains. A set of necessary equations related to the

problem are utilized to represent each element. Finally, all sets of equations for all elements are merged into a global system equation for calculation. In the thermal study, energy equations for heat transfer are basically utilized for FEA. Another numerical process is computational fluid dynamics (CFD) that utilizes the finite control volume strategy in most cases. The sharp difference compared to the FEA method is that CFD is capable of analyzing dynamic fluid flow, as it includes the fluid dynamics equations in addition to energy equations for heat transfer during the thermal analysis process.

Among these three methods, analytical LPTN modeling is easy to understand and can predict motor temperature faster. However, it considers motor parts as nodes. Therefore, it can predict only a uniform temperature rise for any specific node which represents mainly a specific motor part. Therefore, LPTN is mainly used as a faster temperature monitoring method for traction motor while in operation. On the other hand, numerical methods are used to get the temperature distribution map of traction motors. Such a temperature distribution map of traction is helpful to detect motor design faults. If any sudden temperature rise occurs in any single magnet or winding, the motor design has some faults in that specific part. Unlike numerical methods, the uniform temperature rises for all magnets and winding considered as a magnet node and a winding node respectively in LPTN can not detect such design faults. Among FEA and CFD, FEA is less complex and takes less time for the thermal analysis process. Therefore, FEA is the easiest and fastest approach to get the temperature distribution map.

Table 2.1 Comparison of thermal analysis processes of traction motors

Method	Process	Description	Accuracy	Process Time
Analytical	LPTN	Simple and easy to understand. Based on electric circuit concepts.	Less	Less
Numerical	FEA	Slightly complex. Simply utilize the concepts of heat transfer.		
	CFD	More complex. Utilize the concepts of fluid dynamics and heat transfer.	More	More

In this research study, an analytical LPTN model has been proposed to develop a quicker but also more reliable way for the motor temperature monitoring method for PMSMs. Further, numerical FEA has been proposed to get the temperature distribution

map for PMSMs in a more simplified and accurate way within less analysis time for motor fault diagnosis purposes.

2.1.3 Challenges in Traction Motor Thermal Analysis Process

In this section, recent challenges in the area of thermal design and analysis of traction motors are described and the best approaches to address these challenges are stated from the in-depth background study.

Thermal analysis of the active cooling system: As most of the traction motors produce lots of heat energy, there is always an active cooling system in the traction motor in the form of forced cooling. It may be air forced cooling, water or water-glycol cooling, oil cooling, etc. The main purpose of the active cooling system is to remove the extra heat produced in the traction motor for better thermal stability and better thermal performance. Therefore, the thermal analysis of the active cooling system needs to be carried out to get accurate motor temperature prediction. In the LPTN method, there are some analytical calculation approaches available to address the active cooling effect which involves Nusselt number equations. As convection heat transfer is the major phenomenon in the cooling system, coefficient due to convection heat transfer is being calculated for determining the thermal resistance due to convection heat transfer. The most common active cooling system of traction motors is circumferential cooling jackets around the whole stator frame. As the coolant flow rate is high to get sufficient cooling effect, usually fully developed turbulent flow i.e. $3000 < \text{Re} < 10^6$ occurs in the active cooling system. The most common Nusselt number equation for calculating the convection heat transfer coefficient of the circumferential cooling jacket is [8], [9],

$$\text{Nu} = \frac{hD_h}{k_f} = \frac{\left(\frac{f}{8}\right)(\text{Re}-1000)\text{Pr}}{1+12.7\left(\frac{f}{8}\right)^{\frac{1}{2}}(\text{Pr}^{\frac{2}{3}}-1)} \quad (2.1)$$

where, dimensionless numbers – Reynolds number and Prandtl number can be determined as,

$$\text{Re} = \frac{\rho v D}{\mu} \quad (2.2)$$

$$\text{Pr} = \frac{\mu C_p}{k_f} \quad (2.3)$$

Also, the frictional coefficient can be determined as,

$$f = [0.79 \times \ln(\text{Re}) - 1.64]^2 \quad (2.4)$$

According to different flow patterns such as laminar or turbulence and also further variation in turbulence intensity of turbulence flow, the Nusselt number equation can vary [10] – [12].

Table 2.2 Nusselt number equations for various active cooling techniques

Cooling system	Nusselt Number Equation	Reference
Round channel	$\text{Nu} = 3.66 + \frac{0.065 \times (\frac{D}{L}) \times \text{Re} \times \text{Pr}}{1 + 0.04[(D/L) \times \text{Re} \times \text{Pr}]^{\frac{2}{3}}}$ <p style="text-align: center;">For laminar flow</p>	[13]
Rectangular channel	$\text{Nu} = 7.49 - 17.02 \left(\frac{H}{W}\right) + 22.43 \left(\frac{H}{W}\right)^2 - 9.94 \left(\frac{H}{W}\right)^3 + \frac{0.065 \times (\frac{D}{L}) \times \text{Re} \times \text{Pr}}{1 + 0.04[(D/L) \times \text{Re} \times \text{Pr}]^{\frac{2}{3}}}$ <p style="text-align: center;">For laminar flow</p>	[13]
Concentric cylinder	$\text{Nu} = 7.54 + \frac{0.03 \times (\frac{D}{L}) \times \text{Re} \times \text{Pr}}{1 + 0.016[(D/L) \times \text{Re} \times \text{Pr}]^{\frac{2}{3}}}$ <p style="text-align: center;">For laminar flow</p>	[13]
Rotational hollow shaft	$\text{Nu} = \begin{cases} 0.019 \text{Re}^{0.93} + 8.51 \times 10^{-6} \text{Re}_r^{1.45}; 1.6 \times 10^3 < \text{Re}_r < 2.77 \times 10^5 \\ 2.85 \times 10^{-4} \text{Re}_r^{1.19}; \text{Re}_r > 2.77 \times 10^5 \end{cases}$	[14]
Spray cooling	$\text{Nu} = \text{Pr}^{0.4} \left[0.785 \text{Re}^{0.5} \times \left(\frac{L}{D} \right) \times A_r + 0.0258 \text{Re}^{0.83} \times \left(\frac{L}{L^*} \right) \times (1-A_r) \right]$ <p style="text-align: center;">where, $A_r = \pi(1.9d)^2/L^2$ and $L^* = \{0.5(1+\sqrt{2})L - 2.8d\}/2$</p>	[15]
Heat Pipe	$\text{Nu} = 4.728 \times 10^{-7} \text{Re}^{1.986} C_p \Delta T / q_i$	[16]

Furthermore, according to different cooling techniques such as round channel cooling jacket, rectangular channel cooling jacket, spray cooling, heat pipe, etc., some of the papers have also suggested several alternative Nusselt number equations to determine the convection heat transfer coefficient for forced convection occurred in the active cooling system. Some of these Nusselt number equations are shown in Table 2.2. But during

forced air cooling which is mainly used in induction motors by means of fans or blowers, a validated equation is used for convection heat transfer coefficient [17] – [19] as,

$$h = k_1 \times [1 + (k_2 v)^{k_3}] \quad (2.5)$$

In case of numerical methods, CFD is the best way for thermal analysis of the active cooling system of traction motors, as the fluid flow is involved. In CFD, turbulence modeling of coolant is done using different approaches such as standard $k-\epsilon$, realizable $k-\epsilon$, standard $k-\omega$, shear stress transport (SST) $k-\omega$, and Reynolds stress transport (RST), etc. based on applications to determine the convection heat transfer coefficient [12], [20]. Although the CFD process gives more accurate results, the accuracy of the results completely depends on how meshing, boundary conditions, and flow modeling are addressed in the CFD process. For that, the user should have good background knowledge in the area of fluid dynamics.

Thermal analysis of the passive cooling system: There is always a certain amount of natural air flow within the end space between the motor active parts and the end cap which is responsible for natural passive cooling. Because of the compact construction of traction motors, it is challenging to address the natural passive cooling effect. Although equation (5) can also be used to determine the convection coefficient of natural air convection, it is difficult to estimate the velocity of inner air within the end space because of complex surface geometry of end space especially end winding. The surface roughness factor plays an important role in inner air velocity estimation. The change in inner air velocity mostly depends on the rotational speed of the rotor. Therefore, to avoid complexity, inner air velocity estimation has been done mainly based on the rotational speed of the rotor as equation (6) [18]. Further to estimate inner air velocity accurately, sometimes a geometrical factor, η is used additionally in equation (2.6). The main reason behind this is to address inner air flow near complex end winding geometry. Such geometrical factor is dependent on the surface geometry and surface roughness of end windings.

$$v = \omega r_{ro} \eta \quad (2.6)$$

Several empirical equations have been already developed to determine convection heat transfer coefficients for natural air convection within the end space by using equations

(2.5) and (2.6) based on different geometrical factors and proportionality constants through practical experiment [21] – [28]. As inner air has a cooling effect on the rotor, end winding and end cap within the end space region, convection heat transfer coefficients need to be determined separately for these areas to address overall passive cooling effect in the thermal model.

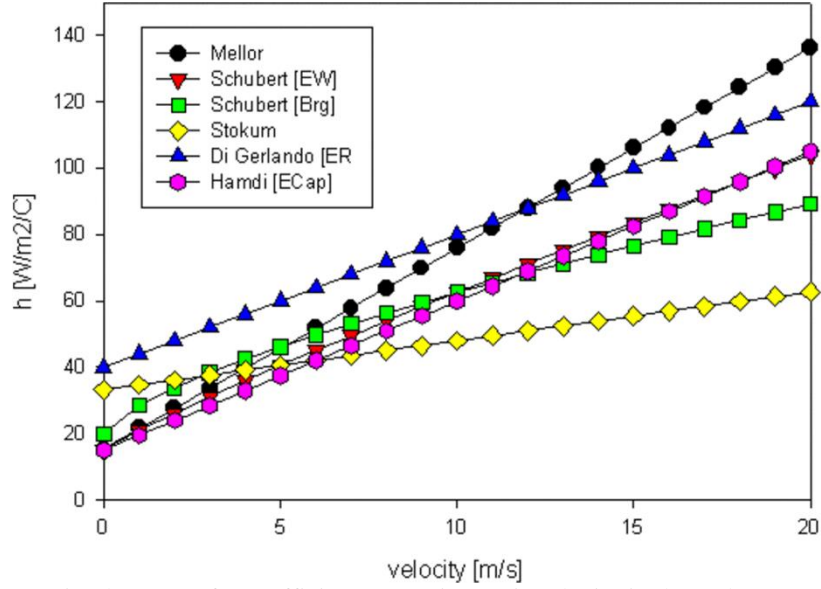


Figure 2.5 Convection heat transfer coefficient versus inner air velocity in the end space region based on several proposed empirical equations [21] – [28].

Moreover, other analytical approaches have been suggested also regarding the thermal model of inner air in several works of literature. For example, equations (2.7) and (2.8) have been considered to determine the convection heat transfer coefficients, h_t and h_l of natural air flow within the end space near the rotor and the end cap respectively [29].

$$h_t = \begin{cases} 0.35k\left(\frac{\omega}{v}\right)^{0.5} ; \text{Re} < 30000 \\ 0.0195 \frac{k}{r_{ro}} \left(\frac{\omega r_{ro}}{v}\right)^{0.8} ; \text{Re} \geq 30000 \end{cases} \quad (2.7)$$

$$h_l = \frac{0.59(\text{Gr Pr})^{0.25}}{R_{ec}} \quad (2.8)$$

where, dimensionless Grashof number, Gr can be determined as,

$$\text{Gr} = \frac{\beta g \Delta T \rho^2 L^3}{\mu^2} \quad (2.9)$$

Although these analytical approaches are common methods, CFD analysis is the better way for calculation of heat transfer coefficient for natural convection within the end space region similar to the active cooling system.

In some cases, fins are used to improve the natural air cooling effect. To incorporate the cooling effects of fins, in LPTN modeling, thermal resistances due to all three types of heat transfer processes are determined in the fin section [17], [18]. To address the convection heat transfer process between air and fins, below mentioned Nusselt number equation (2.10) can be used to determine the convection heat transfer coefficient [12], [30]. On the other hand, in numerical methods, geometry and material properties of fins are considered to address heat transfer through fins.

$$\text{Nu} = \begin{cases} 5.22 \times 10^{-3} \left(\frac{\text{GrPrNS}}{L} \right)^{0.57} \left(\frac{S}{L} \right)^{0.412} \left(\frac{H}{L} \right)^{0.656}; \\ 10^6 < \frac{\text{GrPrNS}}{L} < 2.5 \times 10^7 \\ 2.78 \times 10^{-3} \left(\frac{\text{GrPrNS}}{L} \right)^{0.57} \left(\frac{S}{L} \right)^{0.412} \left(\frac{H}{L} \right)^{0.656}; \\ 2.5 \times 10^7 < \frac{\text{GrPrNS}}{L} < 1.5 \times 10^8 \end{cases} \quad (2.10)$$

Structural design characteristics: Traction motors have structural differences according to the types of motor used for the application. At present, two types of traction motors are mainly used in the electric vehicle application – synchronous and induction motors. Among synchronous motors, permanent magnet synchronous motor (PMSM) is mostly used in the automotive sector due to its high efficiency and reduced size. PMSM has a unique construction where permanent magnets are placed in the rotor to create a constant magnetic field. Therefore, an additional node for permanent magnet associated with magnet loss is considered in the LPTN modeling of PMSM [31] – [39]. Similarly, in numerical methods, magnet loss is also considered during the thermal analysis of PMSM [40] – [47]. PMSM is further divided into two categories according to their rotor construction. One is rotor with surface mounted permanent magnets called surface mounted PMSM and another one is rotor with embedded permanent magnets called interior PMSM. According to their construction geometry differences i.e. position of the magnet, thermal designs of both surface mounted [9] and interior [10] PMSMs are carried

out differently. Although other synchronous motors are rarely used in electric vehicles, there are still some papers on thermal analysis of switch reluctance motor [48] and electrically excited synchronous motor [49] where thermal design has been done by following the structural design of each motor type using both analytical and numerical methods.

Besides synchronous motors, induction motors are also used as traction motors because of low maintenance, low cost and ability to operate even in hostile conditions. Unlike PMSM, induction motors do not have any permanent magnet but have rotor bars that must be taken into consideration during thermal design and analysis. There are several papers on both analytical LPTN method [50] – [58] and numerical methods [57] – [69] which show how the structural design characteristics are addressed for thermal design of induction motors.

Besides these general structural differences, some other unique differences in the design can also be seen in traction motors. As there is a significant push towards the reduction of both the size and weight of the traction motors, manufacturers are coming with new structural design ideas for traction motors. This trend is making the process of thermal design of traction motors more challenging in terms of addressing structural design characteristics into the thermal design. For example, sometimes materials are discarded from different active parts of the traction motors to reduce the weight. This process can also be helpful in reducing core losses if material is discarded from stator or rotor. At the same time, it leaves additional gaps for natural air flow which directly contributes to passive cooling. To address this additional cooling, the convection heat transfer coefficient is determined from the Nusselt number. The appropriate Nusselt number equation for the natural air flow of such additional gaps can be formed by considering the flow domain, the direction of flow driving force and surface geometry of the gaps [70] – [74]. However, identifying air flow characteristics in the motor is challenging. Air flow must be treated differently based on the position of additional air gaps in stationary parts and rotating parts of the motor.

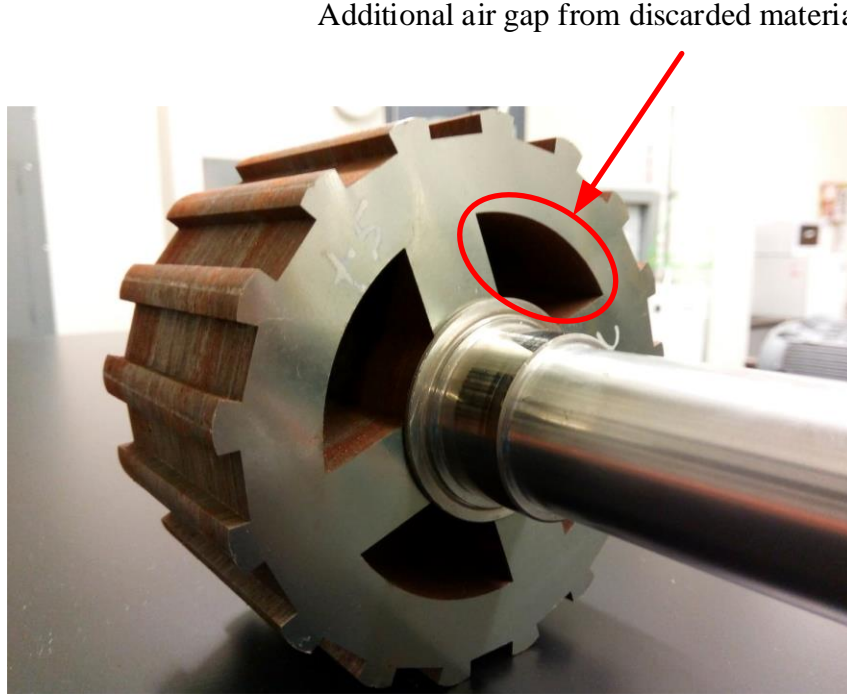


Figure 2.6 Rotor structure of a scale down surface mounted PMSM prototype for future electric vehicle application from CHARGE labs.

Geometrical Anisotropy: Anisotropy mainly refers to the directional dependence of the physical properties of materials. That means thermal conductivities of anisotropic materials are different in each direction which leads to a different amount of heat flow in different directions through the materials. Although construction materials of motor do not have such anisotropic behavior, still the amount of heat flow of the motor is still different in all three directions because of the geometrical structure of the motor. For example, due to inter-lamination gaps, there is negligible heat flow in both axial and circumferential directions for both stator and rotor of the motor compared to heat flow in the radial direction. For accuracy, such geometrical anisotropic behavior needs to be addressed in the thermal design of motors. There are some unique approaches such as general arc-segment element [75] and cuboidal element [76] strategies shown in Figure 2.7 for three-dimensional LPTN thermal modeling to address that anisotropic behavior in all three directions. For numerical methods, 3D geometry needs to be considered to implement directional thermal conductivities and address geometrical anisotropic behavior.

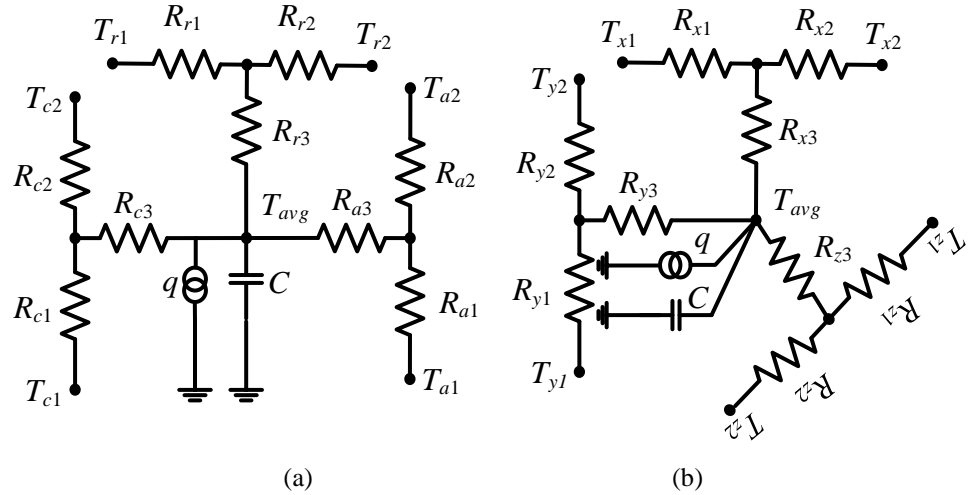


Figure 2.7 3D LPTN model strategy. (a) An arc–segment element in radial, axial and circumferential directions [75]. (b) A cuboidal element in x , y and z directions [76].

Manufacturing Mismatches: There are always some defects in every manufacturing process. Therefore, some mismatches exist between designed and manufactured motor geometry. For example, irregular surface edges create air film in the contact region and change the surface roughness. These factors also impact the temperature distribution within the manufactured motor due to the change in temperature gradients. Therefore, an identical 3D CAD geometry of the manufactured motor is necessary to address these factors in numerical thermal designs. Recent 3D scanning technology is helpful to create identical 3D CAD geometry of manufactured motor [77].

Mechanical Interference Gap: Imperfect contact between surfaces creates interference gaps in the motors where the temperature gradient exists. This creates thermal contact resistances in the interference gaps such as in between stator lamination and housing, slot liner and lamination, two layers of laminations, etc. Therefore, the accuracy of the thermal design depends on the numbers of thermal contact resistances considered [19]. The common way to address this thermal contact resistance is to consider the gap as interference air gap where thermal resistance can be determined as [28], [78],

$$R_{contact} = \frac{l_g}{kA} \quad (2.11)$$

where, l_g is the interference air gap thickness which is dependent on material hardness, interface pressure, surface roughness, and air pressure. Several works of literature related

to heat transfer analysis have already come up with lots of typical thickness values for interference air gaps which can be used for determining thermal contact resistances in motors [79] – [81].

Uncertainty of Material Properties: The thermal behavior of laminations and wires inside the slots is complex. It depends on which conditions i.e. pressure, temperature, etc. stacking process of laminations and impregnation process inside the slots are carried out respectively. Therefore, effective or equivalent thermal conductivity needs to be determined instead of using the usual thermal conductivity of the material to address the change in thermal behavior.

If the thickness t of one lamination, thermal contact resistance R_C and thermal resistance of one lamination R_L is known, the effective thermal conductivity of lamination can be determined as [82],

$$k_{\text{effective}} = \frac{t}{R_L + R_C} \quad (2.12)$$

On the other hand, equivalent thermal conductivity is determined instead of effective thermal conductivity inside the slot area, as insulation and residual air film besides the copper wire also play an important part in complex thermal behavior inside the slot. If the slot space or filling factor K_f , the slot area A_{slot} and the axial core length L_{core} are known, then equivalent thermal conductivity will be [83], [84],

$$k_{eq} = 0.2749[(1-K_f)A_{\text{slot}}L_{\text{core}}]^{-0.4471} \quad (2.13)$$

Another alternative approach is to subdivide whole space inside the slot consisting of wire, insulation and air film into a number of thermal resistances [19].

Dynamic Workload: Temperature distribution prediction under continuous load can ensure the thermal stability of traction motors. However, for predicting thermal performance, it is mandatory to consider the drive cycle as a dynamic workload. This process is challenging, as losses are changing rapidly with respect to time. There are several works of literature [85] – [87] on integrated electromagnetic and thermal analysis of traction motors under the drive cycle load to analyze the motor performance while using in operation.

2.1.4 Published Works on LPTN Modeling of Traction Motor

Analytical LPTN model is mainly a thermal circuit consisting of several thermal resistances and capacitances which accurately model the nature and path of the heat transfer. It is done by calculating thermal resistances based on conduction, convection and radiation heat transfer using (2.14), (2.15) and (2.16) respectively [88], [89].

$$R_k = \frac{L}{kA} \quad (2.14)$$

$$R_h = \frac{1}{hA} \quad (2.15)$$

$$R_\sigma = \frac{(T_1 - T_2)}{(\sigma \epsilon F (T_1^4 - T_0^4) A)} \quad (2.16)$$

Due to the ease and simplicity of modeling, LPTN has been implemented for thermal design and analysis of electric motors in numerous papers. As it is analogous to the electric circuit network, it is a well-adopted method in electric motors. LPTN model generally consists of several temperature nodes that represent different motor components as lumped heat capacity elements where the temperature is considered to be uniform. Therefore, the LPTN model of a motor always predicts a uniform temperature rise for each individual motor component. LPTN model must be detailed enough to cover all major motor components such as stator yoke, stator teeth, rotor, winding, etc. which have bulk thermal storages and heat generation sources due to internal energy and losses [90].

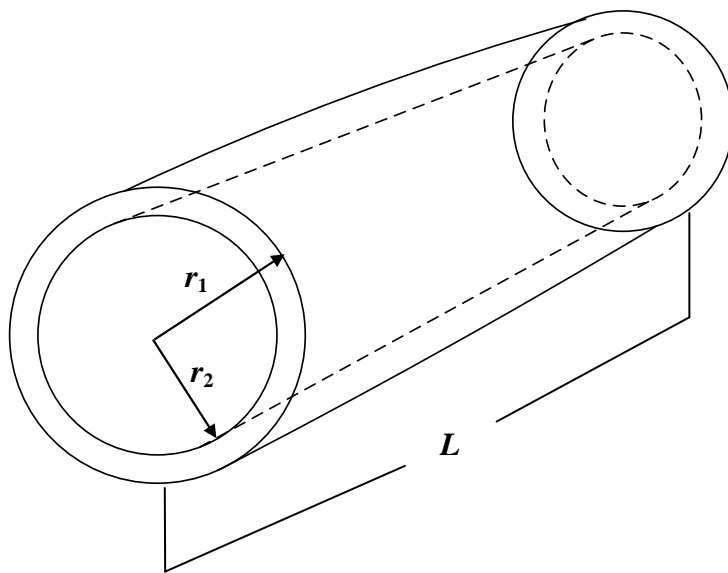


Figure 2.8 Hollow cylindrical structure having outer radius, r_1 and inner radius, r_2 .

Finally, thermal resistances and capacitances in between those motor components are calculated and incorporated into transient or steady state thermal model equations to determine the nodal temperature rise.

There are abundant published works on LPTN modeling of electric motors as it is a simple and faster process and also easy to understand. The basic strategy for thermal resistance calculation in most of the LPTN models of electric motors is to consider the motor components as cylindrical structures. Only except shaft, all other motor components are considered as hollow cylindrical structures that have both inner and outer radius as shown in Figure 2.8. Internal heat generation source within any hollow cylindrical structure creates three directional heat flow such as radial, axial, and circumferential heat flow as shown in Figure 2.9. It is an actually similar phenomenon to three directional stress such as radial, longitudinal or axial, and hoop or circumferential stress acting upon a hollow cylinder due to the acting force on the cylinder surface. Based on these three directional heat flow within the hollow cylinder, there are basically three strategies to calculate thermal resistances of motor components for LPTN modeling so far available in the published works of literature. To develop 3D LPTN models for motor, one strategy for thermal resistance calculation has been developed by considering the heat flow of all three directions such as radial, axial and circumferential heat flow. Further, the other two strategies for thermal resistance calculation used in LPTN model for the motor are developed by considering only radial and axial heat flow or only radial heat flow.

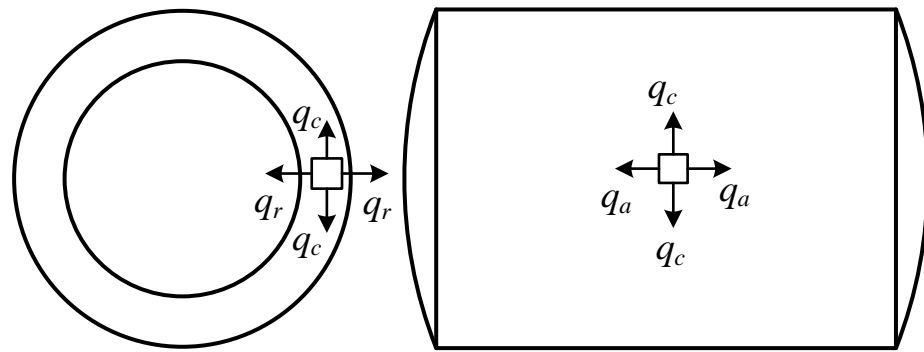


Figure 2.9 Heat flow direction through a hollow cylinder. (where, q_r , q_a and q_c = radial, axial and circumferential heat flow).

Table 2.3 Consideration of heat flow directions in LPTN model of electric motor

Heat flow direction	Error in results	References
Radial, axial, and circumferential	About 1-3°C	[91]
Radial, axial, and circumferential	About 1-4°C	[89]
Radial and axial	About 1-4°C	[29]
Radial and axial	About 1-3°C	[92]
Radial and axial	About 1-4°C	[93]
Radial	About 1-5°C	[28]

It is clear from the above table that there is no significant change in the predicted temperature of the motor while considering axial or circumferential heat flow direction in the LPTN model. It is due to negligible heat flow in both axial and circumferential directions because of inter-lamination gaps, coating and insulation layers. On the contrary, it makes the thermal resistance calculation more complex and time consuming process. On the other hand, consideration of only radial conduction heat flow cannot address the heat flow in the shaft and winding correctly. In the shaft, the major conduction heat flow is in the axial direction towards bearing and end cap. In case of winding, the conduction heat flow in the main winding is in both radial and circumferential direction and the conduction heat flow in end winding is in axial direction mainly. Therefore, this strategy of thermal resistance calculation is less accurate.

Finally, major drawbacks of published works of literature on LPTN modeling of electric motors have been summarized in Table 2.4 which will be addressed in the developed LPTN model in this thesis.

Table 2.4 Drawbacks of heat flow direction strategies in LPTN model of electric motor

Consideration of heat flow direction	Major drawbacks
Radial, axial and circumferential	<ul style="list-style-type: none"> • No significant improvement in terms of accuracy • Very complex and time consuming process
Radial and axial	<ul style="list-style-type: none"> • No significant improvement in terms of accuracy • Complex and time consuming process
Radial	<ul style="list-style-type: none"> • Less accuracy as heat flow in shaft and winding is not correctly addressed

2.1.5 Published Works on FEA Thermal Modeling of Traction Motor

Since the LPTN model can only predict the uniform temperature rise of each motor component, FEA or CFD numerical process is needed for thermal analysis of electric motor to get overall temperature distribution of motor. These numerical processes are helpful to identify motor design faults from the temperature distribution map of the motor. Compared to FEA, CFD process is more complex and time consuming. Therefore, the FEA process has been chosen in this thesis for thermal analysis of motor to get overall temperature distribution of motor. In the FEA thermal model of electric motor, motor losses are converted into heat generation sources and finally, temperature rise within the motor is predicted based on basic heat transfer phenomena such as conduction, convection, and radiation due to heat generation sources [94].

Conduction heat transfer happens due to molecular interaction basically. According to Fourier's law, overall heat flux is directly proportional to the temperature gradient of any system. The mathematical expression of this law is basically utilized to predict the amount of conduction heat flow within the system in the FEA thermal model which further indicates the temperature rise of the system due to conduction heat flow. Three directions x, y, and z are considered according to the 3D or 2D motor geometry is considered during the FEA thermal model.

$$\frac{\vec{Q}}{A} = \vec{q} = -k\nabla T = -k \left(\frac{\partial T}{\partial x} \hat{x} + \frac{\partial T}{\partial y} \hat{y} + \frac{\partial T}{\partial z} \hat{z} \right) \quad (2.17)$$

Convection heat transfer happens due to fluid motion basically. In motor, convection heat transfer occurs due to air and coolant flow. Although there are mainly three types of convection heat transfer such as natural, forced and boiling convection, there are only natural and forced convection heat transfer phenomena to exist in case of the motor. The general mathematical expression of Newton's law of cooling is utilized to predict the amount of convection heat flow within the system in FEA thermal model.

$$q = h(T_{body} - T_{fluid}) = h\Delta T \quad (2.18)$$

Radiation heat transfer happens due to the emission of heat energy from any system via electromagnetic waves. At high temperatures, radiation heat transfer has a significant contribution to the thermal behavior of the motor. The general mathematical

expression of the Stefan-Boltzmann law for heat emission of the real body by radiation is utilized to predict the amount of radiation heat flow within the system in FEA thermal model.

$$Q = \epsilon A \sigma (T_{body}^4 - T_{amb}^4) \quad (2.19)$$

Based on these three basic equations for three types of heat transfer phenomena, FEA thermal model predicts the amount of heat flow within the system and determines temperature rise.

There are less published works of literature on the FEA thermal model of electric motors compared to the LPTN model due to complexity and time consuming numerical process. Basically, in conventional FEA thermal models, convection boundary at constant air temperature is used in the motor air gap similarly like convection boundary at constant inlet coolant temperature for cooling. However, in practical cases, air temperature in the motor air gap increases with motor temperature rise. Further, air friction loss generated in the air gap contributes to heat generation and thus further increases air temperature within the motor air gap.

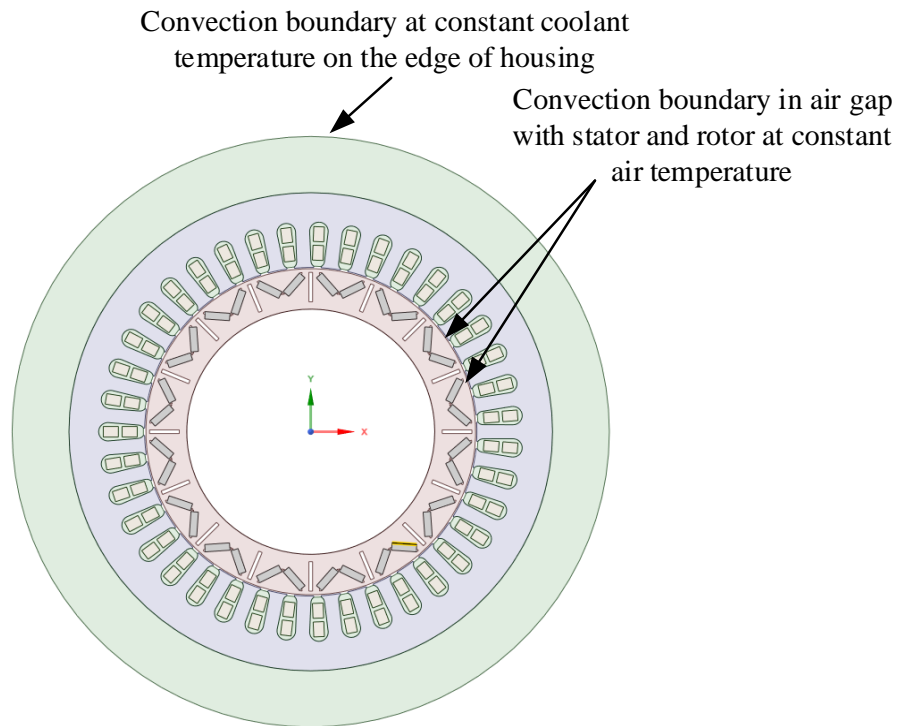


Figure 2.10 Convection boundaries in conventional FEA thermal model of motor.

Therefore, the major drawback of conventional FEA thermal model is the implementation of the convection boundary at a constant air temperature in the motor air gap which cannot address the actual practical situation.

Furthermore, 3D or 2D FEA thermal analysis can be carried out based on 3D and 2D motor geometry respectively. Like the LPTN model, 3D FEA is a complex and time consuming process. Yet, there is no significant improvement in terms of accuracy due to negligible axial and circumferential heat flow within the motor. On the other hand, the 2D FEA process is less accurate due to the inability to address heat flow between shaft and housing through bearing and end cap.

Finally, major drawbacks of published works of literature on 3D and 2D FEA thermal models of electric motors have been summarized in Table 2.5 which will be addressed in the developed FEA thermal model in this thesis.

Table 2.5 Drawbacks of 3D and 2D FEA thermal models

Type	Error	Drawbacks	References
3D FEA	About 1-3°C	<ul style="list-style-type: none"> No significant improvement in terms of accuracy Complex and time consuming process 	[95]
2D FEA	About 2-5°C	<ul style="list-style-type: none"> Less accuracy due to inability to address heat flow between shaft and housing 	[96]

2.2 Thermal Management of Traction Motor

When heat is the by-product of any process, proper thermal management is mandatory for the system to provide better ways for heat dissipation. Otherwise, the system will be heated more than the permissible limit. As a result, there will be a significant rise in the operating temperature of the system that will have a negative impact on the system's overall performance. Since a significant portion of motor losses convert into heat, heat energy is also a by-product during the conversion of electrical energy into mechanical energy while the motor is operating. Therefore, thermal management is necessary to get better thermal performance in traction motor. That is why motor thermal management is one of the important branches in the thermal study of the motor.

2.2.1 Significance of Thermal Management in Traction Motor

Traction motors have always higher speed and torque compared to regular electric motors to fulfill the dynamic drive cycle loading conditions. Therefore, traction motors must perform beyond its continuous operating limit. However, beyond the continuous operating limit, due to higher speed and torque that means higher power ratings, there is always higher heat generation in that region. This higher heat generation ultimately constrains the motor performance capability, if the level of heat generation goes beyond the tolerance limit. Therefore, such a region is called the thermally limited area of operating for traction motors as shown in Figure 2.11 [97].

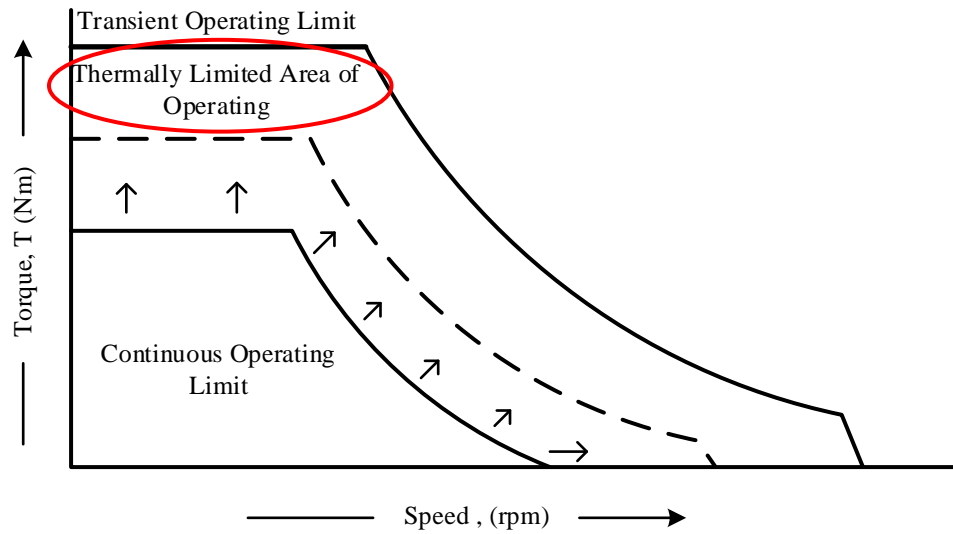


Figure 2.11 Importance of cooling in traction motors [97].

To operate in this region smoothly, the motor needs a better way for continued extra heat dissipation from the system. Therefore, every traction motor structure has an inbuilt active cooling system to dissipate the extra generated heat and cool down the motor quickly so that the motor can operate beyond the continuous operating limit at higher speed and torque. Further, such a cooling system is capable of providing better thermal performance while the motor is in operation so that ultimately motor can fulfill the goal of targeted electromagnetic performance at the thermally limited area of operating. That is why an active cooling system is the major way of motor thermal management. However, there are other means used also directly or indirectly for motor thermal management. For example, lubrication in the motor bearings is used to prevent the damage of bearing, thermal protection system is sometimes used to prevent

demagnetization or insulation breakdown due to overheating of the motor and so on. Due to these reasons, proper motor thermal management is absolutely necessary for smooth operation and better performance of traction motors.

2.2.2 Different Ways of Motor Thermal Management

There are several ways for proper thermal management of motor. The major way of motor thermal management is cooling. Two types of cooling systems exist in traction motor. One is the active cooling system due to forced liquid or air cooling and another one is the passive cooling system due to natural air flow. The other ways for motor thermal management are bearing lubrication, motor thermal protection system, extended fins to enhance natural passive cooling further, etc. However, the main research focus in this thesis is only the active cooling system of the traction motor. Both analyzed motors have water-glycol circumferential cooling jackets as active cooling systems. Cooling performance investigation of the cooling system has been carried out in this thesis by using numerical CFD analysis.

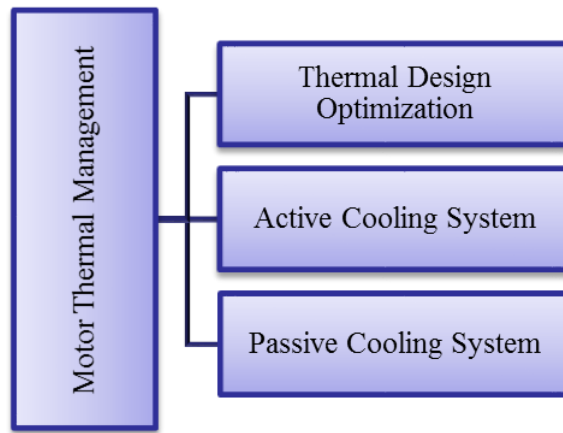


Figure 2.12 Different ways of motor thermal management.

2.2.3 CFD Analysis for Motor Cooling Performance Investigation

As fluid flow is involved in motor cooling, computation fluid dynamics (CFD) analysis is a better approach for motor cooling performance investigation. Although both CFD and FEA are the numerical processes, the CFD process considers fluid dynamics equations in addition to thermodynamics equations, unlike FEA. Any fluid flow can be briefly expressed by mathematical expressions of three basic laws of physics. They are

the Continuity equation where the mass of fluid is considered to be conserved, the Momentum equation which is widely known as Navier-Stokes equation derived from Newton's second law, and the Energy equation where the total energy of the fluid is considered to be conserved [98]. The basic theory of mass conservation is that the rate of increase of mass in a fluid element is equal to the net rate of flow of mass into the same fluid element. Further, the basic theory of the momentum equation is that the rate of increase of momentum of a fluid particle is equal to the sum of forces on the fluid particles. Furthermore, the basic theory of energy equation is that the rate of increase of energy of a fluid particle is equal to the net rate of heat added to the fluid particle and net rate of work done on the fluid particle [98].

The CFD analysis is also established based on these three basics principles for fluid flow analysis. Therefore, CFD analysis is capable of effective 3D or 2D fluid flow analysis. In traction motor, a high amount of heat dissipation is needed by the active cooling system due to higher heat generation. Therefore, the active cooling system of traction motor must have a higher cooling effect which is actually achieved by a considerably high flow rate of coolant. As a result, turbulence fluid flow is a common phenomenon in traction motor cooling. The CFD analysis is the best way to characterize such critical turbulent fluid flow in traction motor cooling for better results regarding cooling performance investigation.

There are few published works of literature about traction motor cooling design optimization and cooling performance investigation [12], [20], [99] - [102]. In most cases, complex and time consuming CFD analysis is utilized only for cooling design optimization of the traction motor. Therefore, in this thesis, a basic step algorithm process has been developed to get an optimal cooling design for traction motors which can avoid repetitive CFD analysis for cooling design optimization of traction motor and thus can simplify the overall cooling design optimization process. Further, conventional CFD analysis for motor cooling performance investigation in most of the published works of literature is capable of showing the only thermal performance improvement due to motor cooling. Therefore, the major drawback of conventional CFD analysis for motor cooling performance investigation is the inability to address the improvement in the

electromagnetic performance of the traction motor under consideration of motor cooling. Two-way coupling electro-thermal co-analysis is carried out in this thesis to address this drawback of conventional CFD analysis.

2.3 Thermal Testing of Traction Motor

Thermal testing of traction motor basically means any practical test carried out while the motor is in operation for determining thermal parameters such as thermal resistances, operating temperatures of different motor components, etc. Thermal testing is one of the core parts of the thermal study. In the case of traction motor, there are both stationary and rotating parts. Therefore, thermal testing is a very complex process for traction motor. There is abundant literature on thermal testing methods of traction motor [103] - [105].

2.3.1 Significance of Motor Thermal Testing

In any actual practical case, no system operates at ideal condition. Lots of factors are always in play in actual practical cases while the motor is running which cannot be considered in the simulation process sometimes. Thus, there is always a difference between predicted and measured results which is the error of the developed model. Further, there are always some variations between designed and manufactured motor, as the manufacturing process is not ideal also which will further result in more error in predicted temperature.

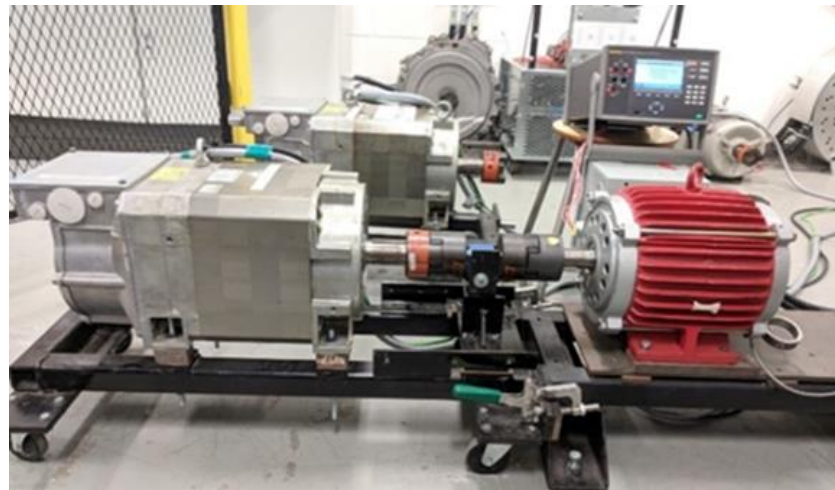


Figure 2.13 Thermal testing at CHARGE Labs.

Therefore, thermal testing plays a vital role to identify the error of the developed thermal model which can suggest a way or solution to improve the thermal model further.

For this reason, experimental validation is always necessary for any developed thermal model so that it can actually reflect the results close to the practical situation. Further, thermal testing can identify the manufacturing defects of the motor also, if there is any.

2.3.2 Different Ways of Thermal Testing of Traction Motor

There are mainly two types of testing carried out for analyzing the thermal behavior of the traction motor. They are the measurement of thermal parameters such as thermal resistance or conductivity and the measurement of the operating temperature of the traction motor. For example, the DC test is basically conducted to measure thermal resistance or conductivity of windings. During the DC test, only DC current is supplied to the motor and the rotor stays still. Therefore, there is only winding loss as a heat generation source from which winding thermal resistance is determined [26], [104]. Further, the loading test is basically conducted for measuring temperatures of several motor components. The load condition can be the continuous loading or dynamic drive cycle loading condition based on the testing purpose.

There are many ways to measure the temperature of the motor. There are several temperature sensors based on the principle of thermocouple, RTD (Resistance Temperature Detector), etc. to detect the temperature of several motor parts. Further, there is also a thermal imager technology that can be used to get the temperature distribution map of the motor. In this thesis, the DC test and the load test at a continuous loading condition are carried out to validate the developed thermal models.

Chapter 3

Traction PMSM Prototypes for Thermal Performance Analysis

3.1 Designed PMSM Prototypes

Recently, two PMSMs have been designed for future electric vehicle application in CHARGE labs at the University of Windsor. One is interior permanent magnet synchronous motor (IPMSM) and another one is surface mounted permanent magnet synchronous motor (SPMSM).

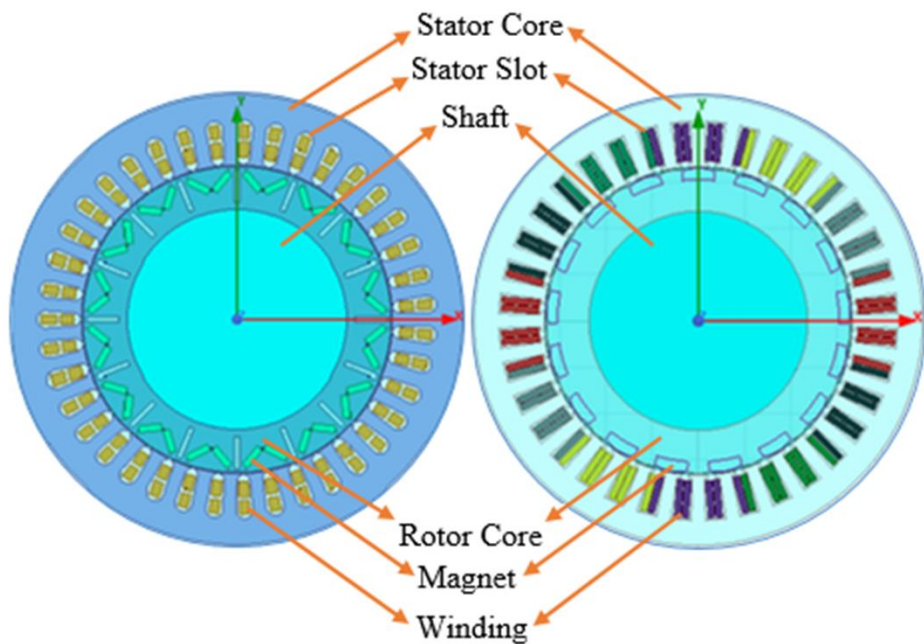


Figure 3.1 Radial sections of designed scale down IPMSM and SPMSM prototypes.

Both newly designed motors have fulfilled more than the targeted performance ratings. Both motors have less torque ripple percentage than the target value, less weight than the target value, more torque density, and efficiency than the target values. Such critical motor design with more torque density within the compact structure makes the motors thermally challenging. Therefore, a detail thermal investigation has been carried out in this thesis for both motors.

3.1.1 Specifications of Designed IPMSM Prototype

IPMSM prototype has been designed for future high-speed electric vehicle application. The peak efficiency of the newly designed scale down IPMSM prototype is 96.3% which is more than the target value of 95%.



Figure 3.2 Designed scale down IPMSM prototype.



Figure 3.3 Several components of designed scale down IPMSM prototype.

The IPMSM motor prototype has double layers fractional-slot distributed windings (FSDW) with a coil pitch of only 2 for reduced end winding length. Minimum torque ripple has been achieved in the motor by star-delta windings connection for odd slot numbers. Further, the torque density of the motor has been maximized with v-shaped magnets embedded in the rotor structure and spoke type barriers. Furthermore, it is lighter in weight which is beneficial for electric vehicle application. The use of less material for weight reduction has further reduced the manufacturing cost. Finally, one special feature of this designed IPMSM prototype is that it can be used for the integrated charging application [106].

Main specifications of the motor prototype are given below:

Table 3.1 Main specifications of IPMSM

Parameters	Values
Current	78 A
Voltage	120 V
Continuous Power	22 kW
Peak Power	45 kW
Continuous Torque	70 Nm
Peak Torque	150 Nm
Frequency	400 Hz
Base Speed	3000 rpm
Maximum Speed	10000 rpm
Poles	16

3.1.2 Specifications of Designed SPMSM Prototype

SPMSM prototype has been designed for direct-drive low-speed electric vehicle application. The efficiency of the newly designed scale down SPMSM prototype is 95.3% which is more than the target value of 95%.



Figure 3.4 Designed scale down SPMSM prototype.

The SPMSM prototype has been designed with an optimized slot-pole combination for minimum torque ripple. Again, shaped magnets were used for further reduction of torque ripple. Moreover, there is an optimal consequent pole rotor for increasing torque per volume of permanent magnet (PM). That strategy is helpful for

saving PM volume and the cost of magnets. In SPMSM, double layers concentrated dual-three phase winding configurations are used for reduced end-winding length. Finally, reduction in material consumption such as copper and PM results in reduced weight and high torque density. Therefore, the motor is lighter in weight and less costly.



Figure 3.5 Several components of designed scale down SPMSM prototype.

Main specifications of the motor prototype are given below:

Table 3.2 Main specifications of SPMSM

Parameters	Values
Current	15 A
Voltage	115 V
Continuous Power	3 kW
Peak Power	6 kW
Continuous Torque	70 Nm
Peak Torque	140 Nm
Frequency	114.75 Hz
Base Speed	405 rpm
Maximum Speed	1400 rpm
Poles	34

3.2 Design Parameters of Analyzed Motors

For both motor prototypes, the major design dimensions such as stator diameter, rotor diameter, etc. are similar. Further, both motors have water-glycol circumferential cooling jackets as an active cooling system and design dimensions of cooling jackets are also similar. Furthermore, housing and end cap structure and design dimensions are also similar. However, magnet design dimensions are different for both motors and they have completely different winding configurations. IPMSM has FSDW and SPMSM has FSCW

configurations and thus design dimensions are different for windings also. Major design dimensions for both motors are given below:

Table 3.3 Main design parameters of both PMSMs

Design Parameters	Values
Outer diameter of housing	241 mm
Outer diameter of stator core	195 mm
Inner diameter of stator core	134 mm
Airgap thickness	0.5 mm
Outer diameter of rotor	133 mm
Shaft diameter	100 mm
Stack length	75 mm

3.3 Materials Properties of Analyzed Motors

Materials are similar for both motor prototypes. Lamination core is made of electrical steel, DW310–35 and magnet is made of permanent magnet material, NdFeB45. Other motor parts are made of conventional materials.

Table 3.4 Material properties of both PMSMs

Motor Sections	Material	Properties		
		Density (kg/m ³)	Specific Heat (J/kg-k)	Thermal Conductivity (W/m-k)
Shaft	Steel	7650	475	50
Stator and Rotor	Electrical Steel, DW310-35	7650	500	25
Winding	Copper	8900	385	379
Air gap and End region	Inner Air	1.009	1009	0.02624
Insulation	Epoxy	1200	1500	0.22
Housing	Aluminium	2700	921	205
Magnet	Permanent Magnet, NdFeB45	7400	460	8.95

Chapter 4

Loss Estimation of PMSMs for The Proposed Two-way Electro-thermal Co-analysis

4.1 Electromagnetic Finite Element Model for PMSMs

As most of the amount of motor loss converts into heat, the accuracy of thermal design and analysis of motors mostly depends on the accuracy of the loss model. There are mainly two types of losses that occurred in motors during operation – electromagnetic and mechanical losses. To address electromagnetic losses, thermal analysis is always coupled with electromagnetic loss analysis which is carried out through an analytical approach [107] or electromagnetic finite element model (FEM) approach [108]. The analytical approach results in a considerable error in loss calculation because of the use of several empirical equations which in turn directly affects the accuracy of temperature prediction by thermal design. On the contrary, electromagnetic FEM is a numerical process that ensures the use of variable loss coefficients through an iterative method for the accuracy in loss calculation. Therefore, electromagnetic FEM is always recommended for the loss model during thermal design to predict accurate temperature rise. Therefore, both PMSMs have been designed in ANSYS RMxprt and further electromagnetic finite element models have been developed using the designed motors in ANSYS RMxprt for motor loss analysis in ANSYS Maxwell. Both ANSYS RMxprt and ANSYS Maxwell are widely used features of ANSYS Electronics for motor design.

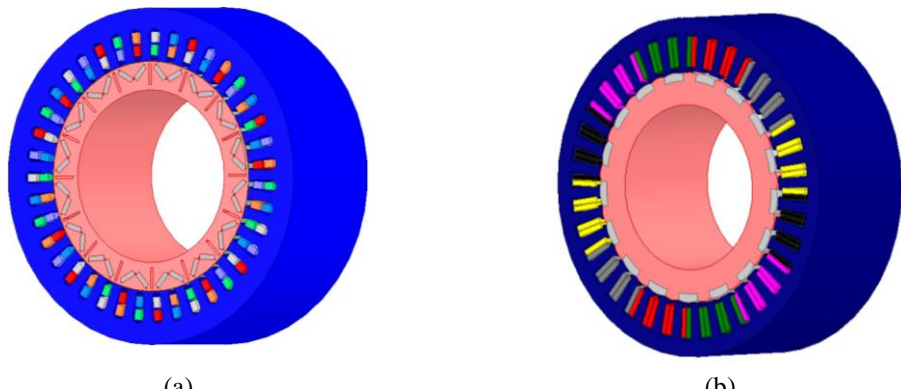


Figure 4.1 Electromagnetic finite element models. (a) IPMSM. (b) SPMSM.

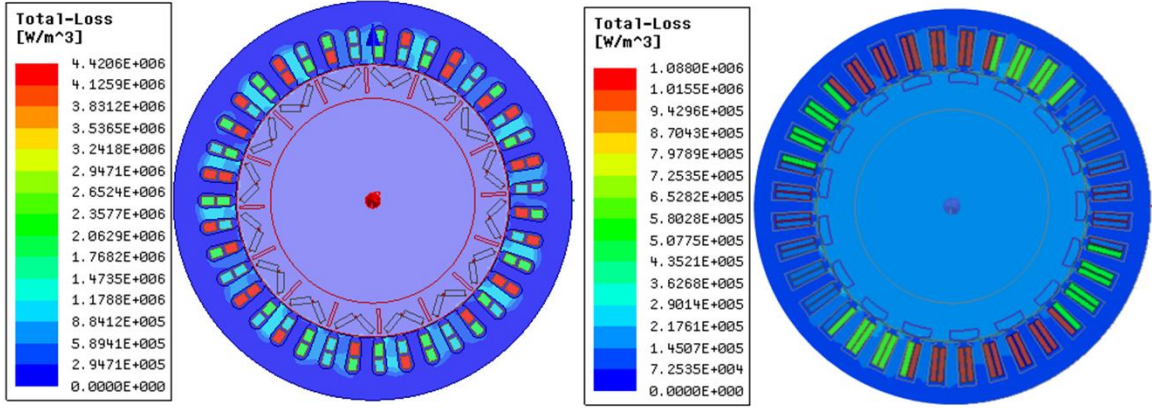


Figure 4.2 Initial total loss density maps from electromagnetic finite element models for analyzed IPMSM and SPMSM at 70 Nm and base speeds after one full cycle.

4.2 Electromagnetic Losses in PMSMs

Since traction motor is one kind of electric machines, electromagnetic losses are the major portion of total losses. Core loss in stator and rotor, copper loss in windings, solid loss in magnets are the main electromagnetic losses in PMSMs while the motor is in operation.

4.2.1 Core Loss

As consideration of constant loss coefficients results in a significant error, the core loss model needs to be developed by considering variable loss coefficients with the variation of frequency and flux density [8], [29], [109]. Hence, variable loss coefficients have been used for core loss calculation in the developed electromagnetic FEMs.

Core or iron loss mainly consists of eddy current, hysteresis and some additional losses [110].

Eddy current losses,

$$p_e = k_e (f_e B_m)^2 \quad (4.1)$$

Hysteresis losses,

$$p_h = k_h f_e B_m^2 \quad (4.2)$$

Additional losses,

$$p_a = k_a (f_e B_m)^{1.5} \quad (4.3)$$

Total core losses,

$$P_c = p_e + p_h + p_a \quad (4.4)$$

4.2.2 Copper Loss

Copper loss is mainly resistive loss in winding and is determined as follows:

$$P_{cu} = nI^2R_e \quad (4.5)$$

4.2.3 Magnet Loss

Magnet losses can be calculated considering solid losses in the developed electromagnetic finite element models. Solid loss is basically determined from the distribution of eddy current density of the motor while in operation.

4.3 Mechanical Losses in PMSMs

Friction losses at different motor sections are mainly considered as mechanical losses in PMSM.

4.3.1 Bearing Loss

As bearings are used to bear the load of the whole rotating section of the motor, most of the portion of friction losses in motors occurs in the bearings and the bearing sealing. From the manufacturer's manual, maximum friction loss of bearing can be found at maximum allowable angular speed. Therefore, bearing losses, P_b at any rotational speed of the motor can be determined by using linear approximation as [78],

$$P_b = P_{bmax} \frac{\omega}{\omega_{max}} \quad (4.6)$$

4.3.2 Air Friction Loss

In most cases, air friction loss within the air gap is neglected, as it is small and hardly contributes to heat generation in the motors. But, in traction motors, due to high rotational speed, a considerable amount of air friction loss occurs within the air gap which has a direct impact on heat generation. Therefore, air friction loss must be considered during the thermal design of traction motors. As air friction loss varies with the rotational speed, it can be calculated as [29],

$$P_{ag} = C_f \pi \rho_{air} \omega^3 r_{ro}^4 l_r \quad (4.7)$$

where, frictional coefficient of air,

$$C_f = \frac{0.0152}{Re^{0.24}} \quad (4.8)$$

Reynold's number of air,

$$Re = \frac{\rho_{air} \omega r_{ro} \delta}{\mu_{air}} \quad (4.9)$$

4.3.3 Other Mechanical Losses

There may be some other losses such as windage loss due to fans or blowers which is completely utilized to accelerate cooling air in traction motors. Therefore, windage loss does not lead to heating of the motors and thus it is not considered during thermal design [28].

4.4 Loss Data of IPMSM and SPMSM Prototypes

Motor loss analysis is carried out for different operating conditions to get temperature distribution at different operating conditions. However, in this thesis, only loss data at two operating conditions are presented. For IPMSM, motor losses are presented at 70 Nm and 35 Nm at base speed, 3,000 rpm and for SPMSM, motor losses are presented at also 70 Nm and 35 Nm at base speed, 405 rpm.

Table 4.1 Initial motor loss data at two different operating conditions for PMSMs

Name of motor sections	Losses at different loading torques at base speeds for PMSMs			
	70 Nm		35 Nm	
	IPMSM	SPMSM	IPMSM	SPMSM
Stator yoke	137.55 W	26.44 W	98.816 W	22.9 W
Rotor core	16.642 W	1.28 W	8.2787 W	0.8147 W
Windings	375.48 W	152.15 W	93.869 W	36.4 W
Magnet	8.28 W	1.8 W	4.9558 W	0.968 W
Air gap	0.403 W	0.0016 W	0.403 W	0.0016 W
Bearing	1.05 W	0.4725 W	1.05 W	0.4725 W
Total loss	539.405 W	182.1441 W	207.3725 W	61.5568 W

4.5 Temperature Dependency of Motor Losses

Most of the published works of literature used the one-way process for thermal analysis where initial loss from electromagnetic analysis of PMSM is taken into consideration as a heat generation source to predict final motor temperature. However, in practical cases, motor losses vary due to the change in materials properties with the rise in motor temperature. One-way process for thermal analysis cannot address the variation in motor losses which further affects the accuracy of motor temperature prediction. Therefore, the two-way coupling between ANSYS Maxwell and Steady State Thermal has been utilized for electro-thermal co-analysis. Such electro-thermal co-analysis is helpful to establish a dependency relationship between electromagnetic and thermal analysis of PMSM as shown in Figure 4.3. This process predicts the final motor temperature while both electromagnetic and thermal analyses reach the dynamic equilibrium condition. Therefore, the predicted temperature results are more accurate and close to practical situations.

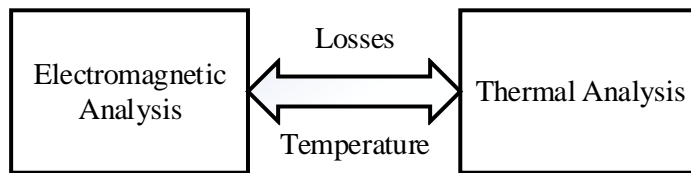


Figure 4.3 Two-way electro-thermal co-analysis.

In this process, a parameter, p has been introduced to address the change in materials properties due to temperature rise as follows,

$$p = 1 \pm \alpha_T \Delta T \quad (4.10)$$

Properties of steel are almost stable even at the high range of operating temperatures of traction motors. Therefore, there is no significant variation in the permeability of steel during the operation of the motor in which the core loss is mainly dependent. However, the resistivity of copper increases at a considerable rate with the rise in motor temperature which further increases copper loss. Again, magnets are thermally sensitive materials. Therefore, temperature dependency relationships for both resistivity and coercivity of magnets that affect solid loss have been considered in this process in addition to the resistivity of copper.

Now, the parameter to consider the change in resistivity of copper,

$$p_{cu} = 1 + 0.0039 \times \Delta T \quad (4.11)$$

The parameter to consider the change in resistivity of magnet,

$$p_{mag_R} = 1 + 0.0002 \times \Delta T \quad (4.12)$$

The parameter to consider the change in coercivity of magnet,

$$p_{mag_H} = 1 - 0.005 \times \Delta T \quad (4.13)$$

The change in motor losses after two-way electro-thermal co-analysis has been presented in below table at 70 Nm and base speed for both motors:

Table 4.2 Final loss data at 70 Nm and base speed for PMSMs using two-way electro-thermal co-analysis

Name of the motor sections	Motor losses at 70 Nm and base speed			
	IPMSM	Percentage of change from one-way	SPMSM	Percentage of change from one-way
Stator yoke	132.6 W	3.6%	25.46 W	3.7%
Rotor core	16.02 W	3.8%	1.23 W	3.9%
Main Winding	438.56 W	16.8%	163.43 W	6.9%
Magnet	8.13 W	1.8%	1.78 W	1.1%
Air gap	0.403 W	Not applicable	0.0016 W	Not applicable
Bearing	1.05 W	Not applicable	0.4725 W	Not applicable
Total loss	596.79 W	10.6%	192.3741 W	5.6%

From the above table 4.2, it is clear that due to a more increase in resistivity of copper resulting from high temperature rise in windings, there is a considerable increase in copper loss. On the contrary, since both temperature rise in magnet and coefficient for resistivity of the magnet is comparatively much less than windings, the change in resistivity of the magnet is not considerable. However, the magnet has a comparatively higher reversible temperature coefficient for coercivity which is actually the resistance to demagnetization. Such a higher reversible temperature coefficient indicates the considerable reduction in coercivity of magnet with motor temperature rise. Further, due to the reduction in magnetic coercivity, the *B-H* characteristics curve of magnets changes and overall magnetic flux density decreases for which solid loss slightly decreases.

Moreover, there is a slight reduction in core loss also, since, core loss depends on magnetic flux density. Such changes in motor losses have a significant effect on motor operating temperature. Therefore, a two-way electro-thermal co-analysis is necessary to predict a more accurate final operating temperature of the motor. In this two-way coupling electro-thermal co-analysis has been carried out at 70Nm and base speeds for both motor prototypes to show the effect in motor temperature.

In conclusion, it can be said that there is always a dependency relationship exist between electromagnetic and thermal analyses. Until both of the processes reach a dynamic equilibrium state, changes in both processes are visible. So, it is necessary to take the temperature-dependent electromagnetic loss model in account during thermal design to get temperature prediction close to the practical results. Previously, thermal designs of motors were one-way process i.e. from loss to temperature estimation only. But at present, there are several strong industrial standard software tools available that allow two-way coupling of both electromagnetic and thermal analysis processes. This strategy is helpful to predict results close to the practical motor temperature.

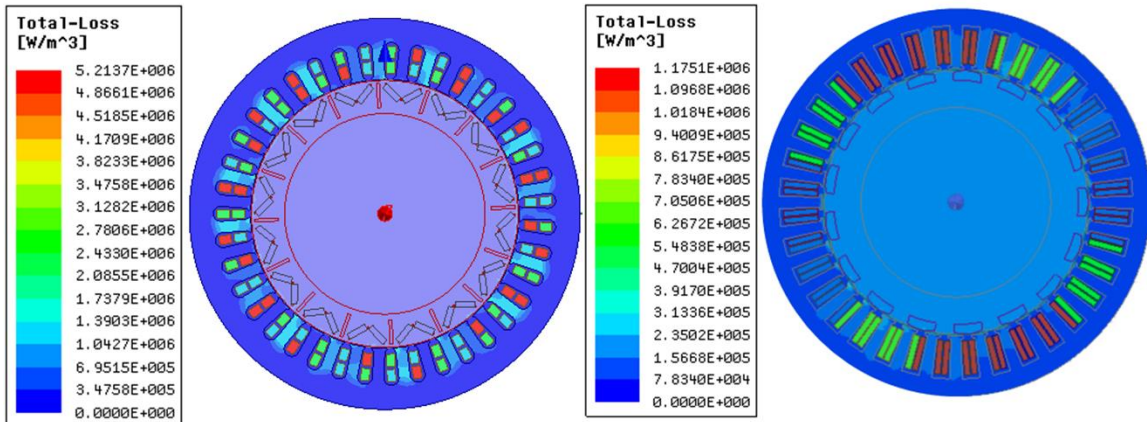


Figure 4.4 Final total loss density maps from electromagnetic finite element models for analyzed IPMSM and SPMSP at 70 Nm and base speeds after one full cycle.

Chapter 5

A Universal Lumped Parameter Thermal Network Model of PMSMs for Traction Application

5.1 Proposed LPTN Model

A general longitudinal sectional view of PMSM is helpful for understanding major motor components having bulk thermal storages and heat generation sources due to internal energy and motor losses respectively. All the major motor components are considered as temperature nodes in our proposed LPTN model shown in Figure 5.1. Thermal resistances are addressed between the nodes following heat transfer types and paths such as conduction, convection, and radiation. Instead of designing large and complex LPTN model of whole motor geometry, geometrical symmetry of the motor is considered so that the LPTN model can be small and easy to understand.

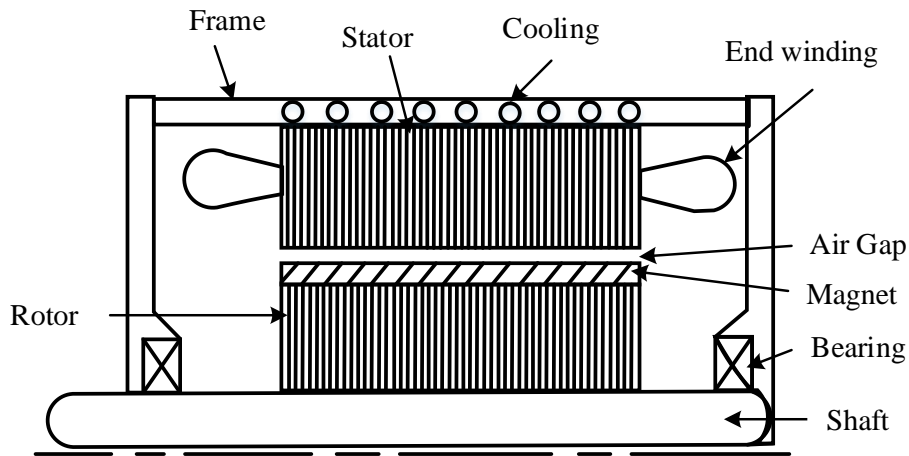


Figure 5.1 A general longitudinal sectional view of PMSM.

Further, thermal capacitances are determined to address the internal heat energy capacity of each node and placed in each node individually and defined as $C_1, C_2, C_3, C_4, C_5, C_6, C_7, C_8, C_9, C_{10}$, and C_{11} respectively. Determined losses in chapter 4 are used as heat generation sources and placed in each node individually and defined as $q_{sy}, q_{st}, q_{ag}, q_m, q_r, q_b, q_w$, and q_{ew} respectively.

The proposed LPTN model in this thesis is the modified higher-order model based on [18] and [78] for thermal analysis of all types of PMSM regardless of any position of

magnets in the rotor. Moreover, a unique thermal optimization strategy has been adopted in the proposed LPTN model to cover the thermal analysis of a wide range of recent multi-layer winding configurations. Such thermal analysis strategies for both magnets and windings enable the LPTN model to be used as a universal thermal representation model for all types of PMSM. Therefore, the same LPTN model can be used for both SPMSM and IPMSM prototypes. Further, the thermal resistance calculation strategy has been developed considering only major heat flow directions in different motor parts for simplification. Thus, the proposed LPTN model is one of the simplified ways to predict motor temperature which will reduce over-complexity as well as calculation time of the overall process.

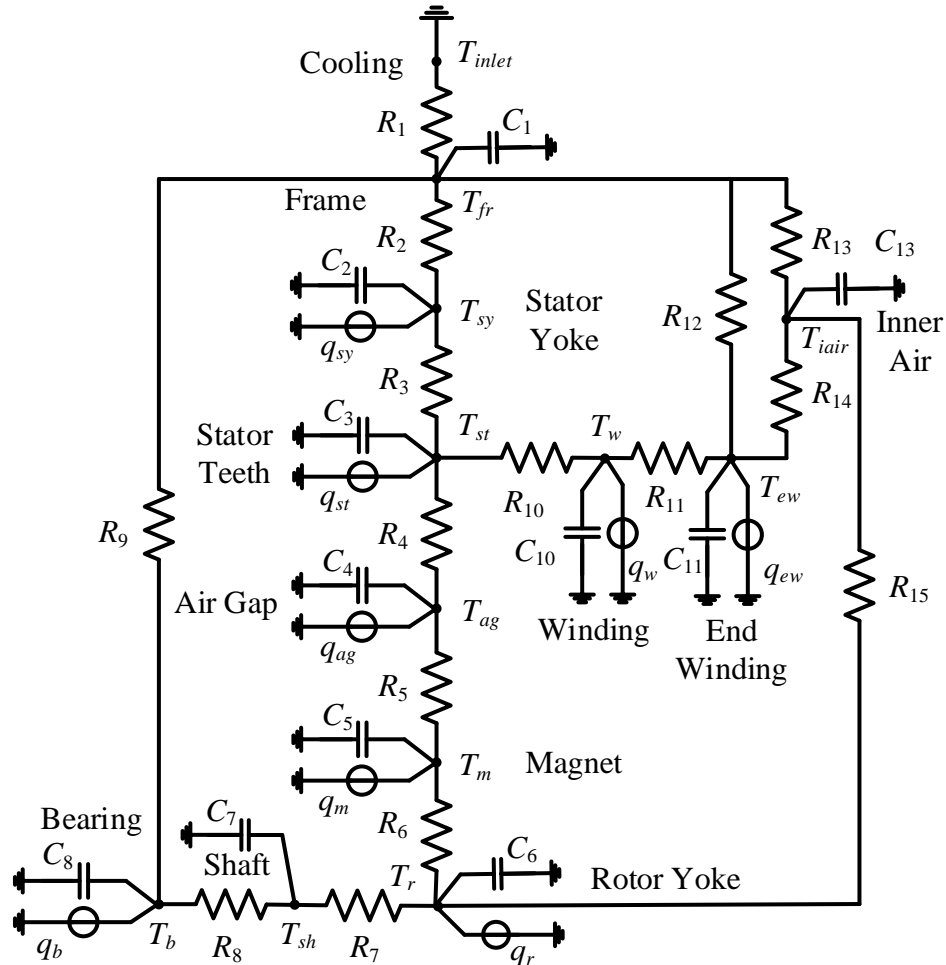


Figure 5.2 Proposed LPTN model of PMSM. (where, T_{inlet} = constant inlet temperature of coolant as initial input).

Table 5.1 Thermal resistance parameters of proposed LPTN model

Parameters	Description of Parameters
R_1	Thermal resistance between frame and cooling system
R_2	Thermal resistance between stator yoke and frame
R_3	Thermal resistance between stator teeth and stator yoke
R_4	Thermal resistance for air gap
R_5	Thermal resistance between magnet and air gap
R_6	Thermal resistance between rotor and magnet
R_7	Thermal resistance between shaft and rotor
R_8	Thermal resistance between bearing and shaft
R_9	Thermal resistance between bearing and frame
R_{10}	Thermal resistance between main winding and stator
R_{11}	Thermal resistance between end winding and main winding
R_{12}	Thermal resistance between end winding and frame
R_{13}	Thermal resistance between inner air and frame
R_{14}	Thermal resistance between inner air and end winding
R_{15}	Thermal resistance between inner air and rotor

Table 5.2 Thermal capacitance and loss parameters of proposed LPTN model

Parameters	Description of Parameters
C_1	Thermal capacitance of stator frame
C_2	Thermal capacitance of stator yoke
C_3	Thermal capacitance of stator teeth
C_4	Thermal capacitance of air in air gap
C_5	Thermal capacitance of magnet
C_6	Thermal capacitance of rotor
C_7	Thermal capacitance of shaft
C_8	Thermal capacitance of bearing
C_{10}	Thermal capacitance of main winding
C_{11}	Thermal capacitance of end winding
C_{13}	Thermal capacitance of inner air in end region
q_{sy}, q_{st}	Losses in stator yoke and stator teeth
q_r, q_m	Losses in rotor core and magnet
q_{ag}, q_b	Friction losses in air gap and bearing
q_w, q_{ew}	Copper losses in windings and end windings

5.2 Simplification Strategy for LPTN Modeling

All the major heat transfer phenomena that have a great impact on the accuracy of the final results have been identified for developing the calculation strategy. Such a simplification strategy will keep balance within the calculation time and accuracy of the LPTN model.

The considered heat transfer phenomena in several motor sections are given below:

Stator and rotor: Due to interlamination gaps there is negligible heat flow in both axial and circumferential directions. Therefore, only radial conduction heat transfer has been considered for stator and rotor sections.

Magnets: LPTN nodes are considered as lumped heat capacity that means the temperature is uniform. Unless in the radial direction, due to the same magnet material, uniform heat transfer is taken into consideration. Therefore, only radial conduction heat transfer has been considered for magnets to characterize the heat flow from the magnet to the rotor.

Winding: In windings, all three directions are taken into account for calculation, as the significant amount of heat energy transfers both radially and circumferentially from the coil sides into the stator core through slot insulation and axially from end windings to the coil sides.

Shaft: In the shaft, axial direction is taken into account, as most of the heat transfers axially through the shaft towards the bearing and endcap.

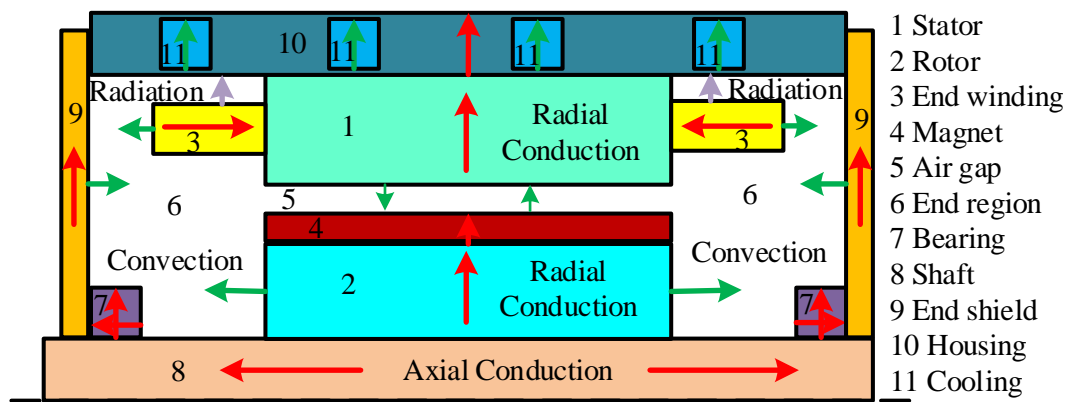


Figure 5.3 Considered heat transfer phenomena in different motor sections for LPTN calculation.

Convection: Natural convection heat transfer has been taken into consideration in the end region and air gap due to air flow. Further, forced convection heat transfer has been taken into consideration for the active cooling system around the housing.

Radiation: End windings are the most heated part of the motor and housing is the less heated part of the motor. Therefore, a significant temperature gradient exists between end windings and housing and thus a small amount of radiation occurs which has been considered also for better accuracy in temperature prediction of the most heated part of the motor, end windings.

Others: Other considered heat transfers are also conduction heat transfers in bearing, end cap and housing as shown in Figure 5.3.

5.3 Thermal Resistance Calculation in Proposed LPTN Model

Basic LPTN calculation strategies for thermal resistances considering different heat transfer phenomena are given step by step below:

Conduction heat transfer: Thermal resistance of a hollow cylindrical motor component for radial heat conduction is,

$$R_r = \frac{\ln(r_o) - \ln(r_i)}{kl\theta} \quad (5.1)$$

where, r_o is the outer radius, r_i is the inner radius, l is the axial length, θ is angular span and k is the thermal conductivity.

Further, the thermal resistance of a cylindrical motor component of radius r and axial length l for axial heat conduction is,

$$R_a = \frac{1}{\pi r^2 k} \quad (5.2)$$

Furthermore, thermal resistance due to conduction heat transfer for motor components considered as rectangular structure such as windings is determined using basic equation (2.14) stated in the background study of chapter 2. In this case, the axial length will be dependent on the direction that has been considered for conduction heat transfer in a specific motor part.

Convection heat transfer: For convection heat transfer, thermal resistance is determined using basic equation (2.15) stated in the background study of chapter 2.

Radiation heat transfer: For radiation heat transfer, thermal resistance is determined using basic equation (2.16) stated in the background study of chapter 2.

Based on these above basic principles, thermal resistances in different motor sections are determined and described below in individual subsections.

5.3.1 Heat Transfer between Active Cooling System and Stator Frame

To determine thermal resistance, $R_{cooling}$ due to convection in the active cooling system, convection heat transfer coefficient of coolant, h_f needs to be determined. Since, for both motors, the active cooling system is a circumferential water-glycol cooling jacket, the Nusselt number equation (2.1) stated in the background study of chapter 2 has been used to determine the convection heat transfer coefficient.

The stator frame is assumed as a cylinder having a diameter much larger than thickness for resistance calculation due to radial conduction through the stator frame.

Now, thermal resistance due to radial conduction in a hollow cylinder [78],

$$R_r = \frac{r_o - r_i}{r_o - r_i} \times \frac{\ln(r_o) - \ln(r_i)}{2\pi k l} = \frac{r_o - r_i}{\left(\frac{k[2\pi r_o - 2\pi r_i]}{\ln(2\pi r_o / 2\pi r_i)} \right)} = \frac{r_o - r_i}{k A_{lm}} \quad (5.3)$$

where, $A_{lm} = (A_o - A_i) / \ln(A_o / A_i)$ is a log mean area that is almost equal to the average of two areas, $(A_o + A_i) / 2$.

Now, in case of a cylinder having a diameter much larger than thickness, t , $r_o - r_i = t$ and $(A_o + A_i) / 2 = \pi l(r_o + r_i) = \pi l(d_i + t)$. Therefore, the thermal resistance of the stator frame due to radial conduction will be [78],

$$R_{fr} = \frac{t_{fr}}{\pi l_s k_{Al} (d_{so} + t_{fr})} \quad (5.4)$$

Now, the thermal resistance between the stator frame and cooling system,

$$R_1 = R_{cooling} + \frac{1}{2} R_{fr} \quad (5.5)$$

5.3.2 Heat Transfer in Stator Yoke

Stator yoke is considered as a hollow cylinder and thermal resistance of the stator yoke due to radial conduction will be,

$$R_{sy} = \frac{\ln(r_{so}) - \ln(r_{si} + h_{st})}{2\pi l_u k_l} \quad (5.6)$$

where, the useful length, $l_u = k_s d_s$.

Further, the temperature gradient exists in mechanical interference gaps due to imperfect contacts between the surface of the stator frame and yoke. Thermal contact resistance, $R_{contact}$ has been addressed by considering the gap as an interference air gap and can be calculated using equation (11) stated in the background study of chapter 2.

Now, thermal resistance, R_2 can be determined as,

$$R_2 = \frac{1}{2}(R_{fr} + R_{sy}) + R_{contact} \quad (5.7)$$

5.3.3 Heat Transfer in Stator Teeth

As the stator core part involves a large portion of the motor, another node has been taken into consideration in the LPTN model which is for heat transfer between stator teeth and stator yoke. Due to the coating of lamination and the interlamination gap, axial and circumferential conduction is neglected. For thermal resistance for stator teeth due to radial conduction heat transfer can be determined using the integration method [78].

Therefore, thermal resistance for stator teeth due to radial conduction [78],

$$R_{st} = \int_{y=0}^{h_{st}} \frac{1}{k_l N_s l_u x_d(r)} \quad (5.8)$$

Therefore, for IPMSM stator teeth design,

$$R_{st} = \frac{1}{k_l N_s l_u} \left[\frac{y_{d1}}{x_{d1}} + \frac{y_{d3}}{x_{d3}} + \frac{y_{d2}}{x_{d1}-x_{d2}} \left(\ln \left| \frac{x_{d1} y_{d2}}{x_{d1}-x_{d2}} \right| - \ln \left| y_{d2} - \frac{x_{d1} y_{d2}}{x_{d1}-x_{d2}} \right| \right) - \frac{\pi}{4} + \frac{a}{\sqrt{a^2-1}} \arctan \left(\frac{a+1}{\sqrt{a^2-1}} \right) \right] \quad (5.9)$$

where, parameter, $a = (x_{d3}+2y_{d4})/ 2y_{d4}$.

and for SPMSM, stator teeth design,

$$R_{st} = \frac{1}{k_l N_s l_u} \left[\frac{y_{d1}}{x_{d1}} + \frac{y_{d3}}{x_{d3}} + \frac{y_{d2}}{x_{d1}-x_{d2}} \left(\ln \left| \frac{x_{d1}y_{d2}}{x_{d1}-x_{d2}} \right| - \ln \left| y_{d2} \cdot \frac{x_{d1}y_{d2}}{x_{d1}-x_{d2}} \right| \right) \right] \quad (5.10)$$

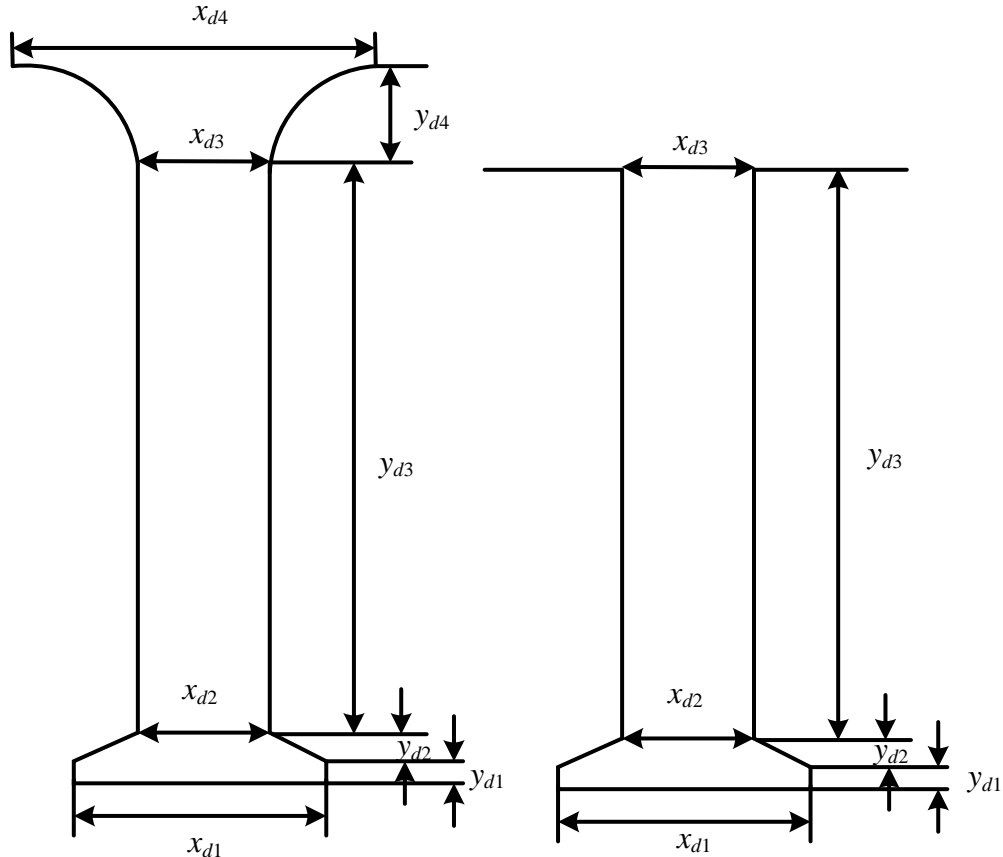


Figure 5.4 Stator teeth design of IPMSM and SPMSM prototype respectively.

Now, thermal resistance, R_3 can be determined as,

$$R_3 = \frac{1}{2} (R_{sy} + R_{st}) \quad (5.11)$$

5.3.4 Heat Transfer in Windings

Windings are a very important and complex part of thermal modeling involving wire, insulation and air film. In most LPTN models of the motor, the winding region is specifically susceptible to inaccuracies of theoretical predictions of temperature. Thus,

the maximum error in predicted temperature from LPTN models occurs in the winding region.

There is a simplified strategy of converting stator slot geometry into an equivalent rectangular shape for calculating thermal resistance between single-layer winding and stator teeth [28], [78]. However, our newly designed IPMSM and SPMSM have double layers fractional slot distributed and concentrated windings respectively. Therefore, the strategy has been modified according to the recent winding configurations. This strategy considers all the major heat flow directions in the windings and also the contribution of both insulation and air film in winding thermal phenomena for better accuracy. As the temperature gradient is near about zero between two winding layers, heat transfer between two winding layers across the slot insulation is neglected for simplification. Such a rectangular shape strategy shown in Figure 5.5 can be used for any multi-layers winding configuration.

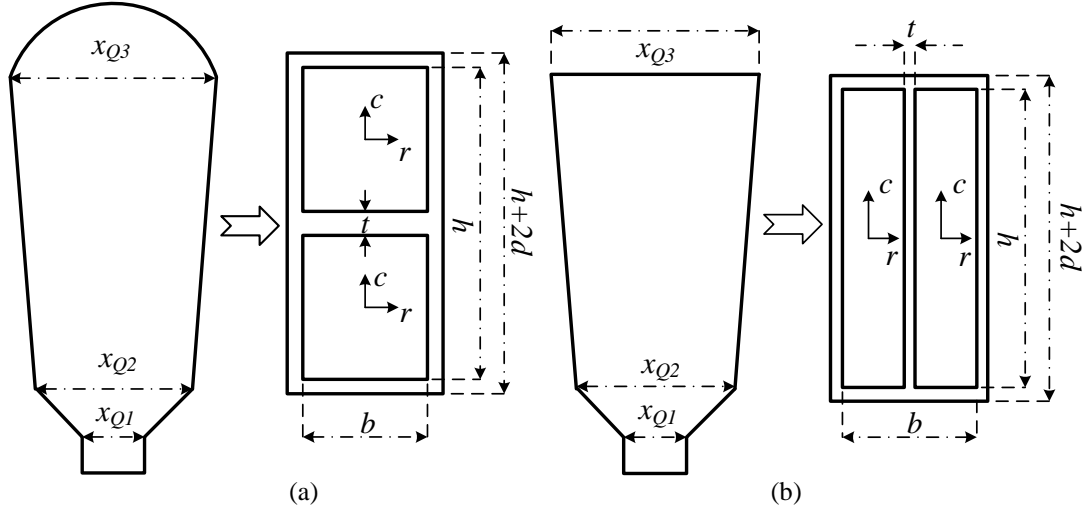


Figure 5.5 Winding configurations of IPMSM and SPMSM prototype. (a) FSDW. (b) FSCW.

In Figure 5.5, t is the distance between two layers, d is the equivalent thickness consisting of insulation thickness, d_i and equivalent air film thickness, d_a . Other two parameters, b and h can be calculated from stator slot geometry as [28] and [78],

$$b = \frac{x_{Q3} + x_{Q2}}{2} - 2d \quad (5.12)$$

$$h = \frac{2A_{slot}}{x_{Q3} + x_{Q2}} - 2d \quad (5.13)$$

Now, the contribution of slot material in thermal resistance,

$$\begin{aligned} R_{r0} &= \frac{b}{(h-t)k_{eq}}; \text{ FSDW} \\ &= \frac{(b-t)}{hk_{eq}}; \text{ FSCW} \end{aligned} \quad (5.14)$$

$$\begin{aligned} R_{c0} &= \frac{(h-t)}{bk_{eq}}; \text{ FSDW} \\ &= \frac{h}{(b-t)k_{eq}}; \text{ FSCW} \end{aligned} \quad (5.15)$$

and contribution of insulation and air film in thermal resistance,

$$R_{ir} = \frac{d_i}{hk_i} + \frac{d_a}{hk_{air}} \quad (5.16)$$

$$R_{ic} = \frac{d_i}{bk_i} + \frac{d_a}{bk_{air}} \quad (5.17)$$

where, k_i and k_{air} are the thermal conductivities of insulation material and air film respectively. Also, if the slot filling factor is K_f , then equivalent thermal conductivity, k_{eq} due to the impregnation process can be determined using (2.13) stated in chapter 2.

Now, the per unit-length thermal resistances due to radial and circumferential conduction will be [28], [78],

$$R_r = \frac{1}{2} \left(R_{ir} + \frac{R_{r0}}{6} \right) \quad (5.18)$$

$$R_c = \frac{1}{2} \left(R_{ic} + \frac{R_{c0}}{6} \right) \quad (5.19)$$

Now, thermal resistance, R_{10} between the coil side and teeth can be derived as [28], [78],

$$R_{10} = \frac{R_r R_c}{N_s l_u (R_r + R_c)} \left(1 - \frac{R_{r0} R_{c0}}{720 R_r R_c} \right) \quad (5.20)$$

For axial conduction heat transfer between end winding and coil sides, thermal resistance will be,

$$R_{11} = \frac{l_{av}}{N_s A_{cu} k_{cu}} \quad (5.21)$$

As radiation heat transfer is very small, it is mostly neglected in the proposed LPTN model. Only radiation between the end winding and end shield, A_{ew} and A_{es} with respect to absolute temperatures T_{ew} and T_{fr} is considered as,

$$R_{12} = \frac{\frac{1-\varepsilon_1}{\varepsilon_1 A_{ew}} + \frac{1}{A_{ew} F} + \frac{1-\varepsilon_2}{\varepsilon_2 A_{es}}}{\sigma(T_{ew} + T_{fr})(T_{ew}^2 + T_{fr}^2)} \quad (5.22)$$

where, ε_1 and ε_2 are surface emissivity, and F is the form factor of the relative orientation of two surfaces. Only at higher operating conditions, this radiation needs to be considered, since end winding has highest temperature and large temperature gradient between frame surface and end winding surface exists at higher operating conditions.

5.3.5 Heat Transfer through Air Gap

For determining thermal resistance due to air gap convection, $R_4 = 1/A_{ag} h_{ag}$, the convection coefficient, h_{ag} is calculated as [18],

$$h_{ag} = \frac{Nu k_{air}}{l_{airgap}} \quad (5.23)$$

According to Becker and Kaye [111],

$$Nu=2 \quad \text{for } Ta_m < 1,700$$

$$Nu=0.409Ta_m^{0.241}-137Ta_m^{-0.75} \quad \text{for } 1,700 < Ta_m < 10^4$$

By assuming smooth surfaces, the modified Taylor number, Ta_m can be considered the same as Taylor number and can be determined as [18],

$$Ta_m = \frac{\rho_{air}^2 \omega^2 r_{av} \delta^3}{\mu_{air}^2} \quad (5.24)$$

5.3.6 Heat Transfer in Magnet

As the magnet is mounted on the rotor surface in SPMSM, the magnet node can be defined directly after the air gap in the LPTN model. Therefore, thermal resistance between the air gap and magnet nodes can be calculated by using (5.1) for magnet only.

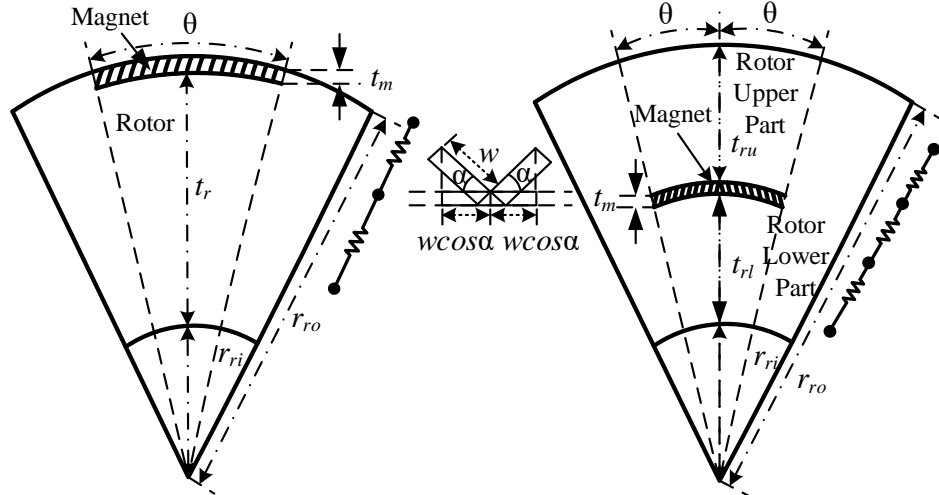


Figure 5.6 Universal representation strategy of rotor and magnet in proposed LPTN model for SPMSM and IPMSM prototype respectively.

On the other hand, the magnet is embedded in the rotor in IPMSM. Therefore, the whole rotor structure is divided into two parts for defining the same magnet node in the proposed LPTN model. One is the upper part of the rotor above the magnet and another is the lower part of the rotor below the magnet. Hence, thermal resistance between the air gap and magnet nodes consists of thermal resistances of both the rotor upper part and magnet in this case. Further, an equivalent space has been defined horizontally from the inclined angle of V-shape magnets in the designed IPMSM to use the same simplified equation (5.1) for calculating thermal resistance of magnet. This equivalent space strategy will be helpful to calculate magnet thermal resistance in a specific and simplified way for any position of magnets in PMSM, if the horizontally inclined angle, α is known.

Now, for SPMSM, thermal resistance for magnet due to radial conduction,

$$R_m = \frac{\ln\left(\frac{r_{ri}+t_r+t_m}{r_{ri}+t_r}\right)}{2p\theta_m l_s k_m} \quad (5.25)$$

Therefore, for SPMSM, the thermal resistance, R_5 can be determined as,

$$R_5 = \frac{1}{2} R_m \quad (5.26)$$

Now, for IPMSM, thermal resistance for rotor upper part due to radial conduction,

$$R_{upper} = \frac{\ln\left(\frac{r_{ro}}{r_{ri}+t_{rl}+t_m}\right)}{2\pi l_u k_l} \quad (5.27)$$

Again, for IPMSM, thermal resistance for magnet due to radial conduction,

$$R_m = \frac{\ln(\frac{r_{ri}+t_{rl}+t_m}{r_{ri}+t_{rl}})}{2p\theta_m l_s k_m} \quad (5.28)$$

Therefore, for IPMSM, the thermal resistance, R_5 can be determined as,

$$R_5 = R_{upper} + \frac{1}{2} R_m \quad (5.29)$$

5.3.7 Heat Transfer in Rotor

For the thermal resistance through rotor core due to radial conduction heat transfer,

$$R_r = \frac{\ln(\frac{r_{ro}}{r_{ri}})}{2\pi l_u k_l} \quad (5.30)$$

Therefore, the thermal resistance, R_6 can be calculated as,

$$R_6 = \frac{1}{2} R_r \quad (5.31)$$

5.3.8 Heat Transfer in Shaft

As the shaft is not hollow in the middle, it is considered as a thick cylindrical rod of radius r . Therefore, thermal resistance due to axial conduction through the shaft is,

$$R_{shaft} = \frac{l_{bb}}{\pi r_{sh}^2 k_{steel}} \quad (5.32)$$

Now, the thermal resistance, R_7 can be calculated as,

$$R_7 = R_{shaft} + \frac{1}{2} R_r \quad (5.33)$$

5.3.9 Heat Transfer in Bearing

The thermal behavior of ball bearings mounted on the motor shaft is complicated. For simplification, the conductivity of sealing and lubrication is neglected. Only physical dimensions of the bearing are used for the determination of thermal resistance of bearing. Now, the below general expression for the thermal resistance of bearing can be used [28], [78],

$$R_b = k_1(0.12 - k_2 d_b)(33 - k_3 \omega d_b) \quad (5.34)$$

where, values of empirical constants are taken from [78],

$$k_1=0.45 \text{ K/W}$$

$$k_2=1 \text{ m}^{-1}$$

$$k_3=1 \text{ s/m}$$

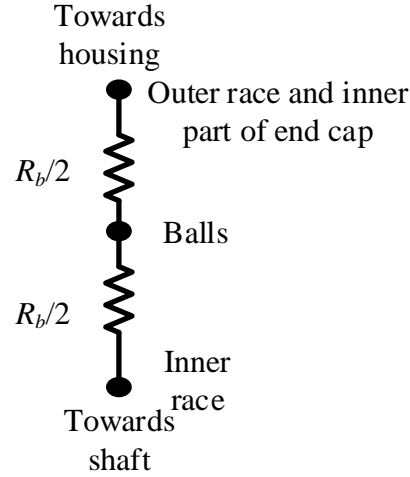


Figure 5.7 Bearing thermal model.

In equation (65), the speed dependence is neglected for further simplification. Even in the worst case, the neglected speed dependence does not have a significant impact [78].

Since symmetry of the motor is considered in the LPTN model, the same amount of heat flows through two bearings in a parallel position. Now, according to bearing thermal model shown in Figure 5.7 and consideration of the same amount of heat flows through two bearings in a parallel position,

The thermal resistance between bearing and shaft, R_8 will be,

$$R_8 = \frac{1}{4} R_b \quad (5.35)$$

and the thermal resistance between bearing and frame, R_9 will be,

$$R_9 = \frac{1}{4} R_b \quad (5.36)$$

5.3.10 Heat Transfer in End Region

The proposed LPTN model has a Y-connected thermal circuit approach for end region air cooling effect in the frame, end windings and rotor end shown in Figure 5.8.

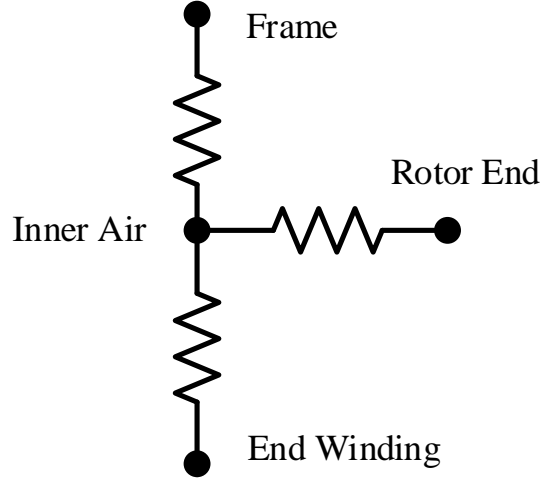


Figure 5.8 Inner air passive cooling model.

Since the change in inner air velocity is fully dependent on motor rotation, the peripheral speed of the rotor, v_r can be considered to estimate the inner air velocity, $v_{air} = v_r \eta$, where, η is the factor for surface geometry. Several empirical equations are available to determine the convection coefficients of inner air based on equation (2.5) stated in the background study of chapter 2 [21] – [28] and [78]. In the proposed model, the empirical equations from [78] are used for convection heat transfer coefficients for passive cooling.

The convection heat transfer coefficient between inner air and frame,

$$h_1 = 15 + 6.75^{0.65} v_r^{0.65} \quad (5.37)$$

The convection heat transfer coefficient between inner air and end windings,

$$h_2 = 6.5 + 5.25^{0.65} v_r^{0.6} \quad (5.38)$$

The convection heat transfer coefficient between inner air and rotor end,

$$h_3 = 16.25^{0.65} v_r^{0.65} \quad (5.39)$$

Now, thermal resistances due to the end region convection will be,

$$R_{13} = \frac{1}{A_1 h_1} \quad (5.40)$$

$$R_{14} = \frac{1}{A_2 h_2} \quad (5.41)$$

$$R_{15} = \frac{1}{A_3 h_3} \quad (5.42)$$

5.4 Thermal Capacitance Calculation in Proposed LPTN Model

For steady state thermal analysis, thermal capacitance is not needed to be considered in the LPTN model. In this thesis, thermal analysis has been carried out for both steady state and transient thermal conditions.

Thermal capacitance can be calculated as,

$$C = mC_p = \rho V C_p = \rho \pi (r_o^2 - r_i^2) l C_p \quad (5.43)$$

5.5 Temperature Calculation in Proposed LPTN Model

5.5.1 Steady State Thermal Analysis

In the steady state analysis, time variation is not considered and thus the below matrix format equation can be used for determining the temperature rise [112],

$$[T] = [G]^{-1} [P] \quad (5.44)$$

where, $[T]$ is the temperature column vector, $[P]$ is the loss column vector, and $[G]$ is the thermal conductance square vector which is the inverse of thermal resistance.

5.5.2 Transient Thermal Analysis

In the transient thermal analysis, time variation is considered and thus thermal capacitance is included. The below matrix format equation can be used for determining the rate of temperature rise with time variation [112],

$$\frac{d}{dt} [T] = [C]^{-1} [P] - [C]^{-1} [G] [T] \quad (5.45)$$

where, $[C]$ is the thermal capacitance diagonal matrix.

5.6 Predicted Temperature of PMSM Prototypes from Proposed LPTN Model

For both IPMSM and SPMSM, forced convection due to the active water-glycol cooling system has been taken into consideration which maintains a constant inlet temperature at

30°C. Moreover, the same flow rate of coolant is considered to maintain constantly forced convection with a constant convection heat transfer coefficient, 1000 W/m²°C for all conditions to analyze the temperature results from the proposed LPTN model.

Thermal analysis using the proposed LPTN model has been carried out for several operating conditions for both motor prototypes for the industrial project purpose. However, only the temperature results for two operating conditions at 70 Nm and 35 Nm in base speeds for both motor prototypes have been presented basically, as the temperature results presented on published papers were for these specific two conditions.

Table 5.3 Steady state temperature of major motor components from LPTN model using initial loss

Name of motor components	Temperature at 70 Nm and base speed		Temperature at 35 Nm and base speed	
	IPMSM	SPMSM	IPMSM	SPMSM
Stator	47.265 °C	35.07 °C	35.615 °C	31.204 °C
Rotor	57.41 °C	39.5 °C	38.805 °C	31.68 °C
Winding	70.54 °C	40.65 °C	44.596 °C	33.26 °C
Magnet	58.08 °C	39.98 °C	39.44 °C	31.84 °C

Further, the thermal investigation has been done at 70 Nm and base speed for both motor prototypes using two-way loss analysis results to check the change in temperature results.

Table 5.4 Steady state temperature of major motor components from LPTN model using final loss results at 70 Nm and base speeds

Name of motor components	Two-way process result	
	IPMSM	SPMSM
Stator	48.205 °C	35.801 °C
Rotor	58.41 °C	40.59 °C
Winding	75.47 °C	41.8 °C
Magnet	59.33 °C	41.08°C

Further, as winding, rotor, and magnets are the most heated parts in the PMSM, temperature rise of these three parts with respect to time has been observed until 120 minutes using the LPTN model for the transient thermal condition. Such a process can show the temperature rise trends of individual motor parts.

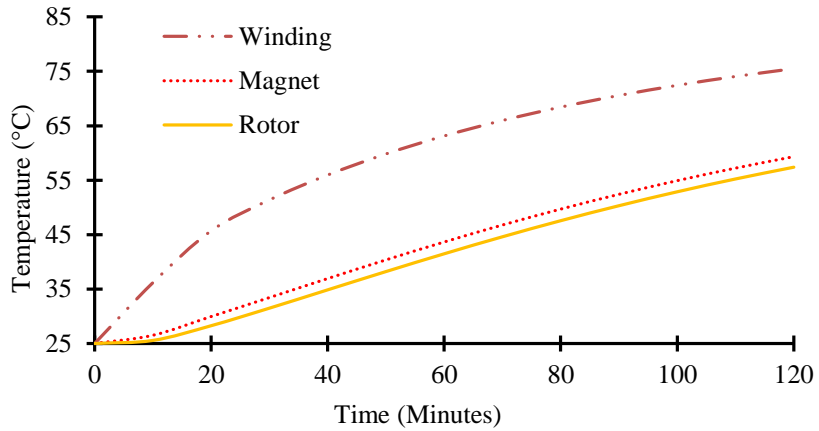


Figure 5.9 Predicted temperature in IPMSM at 70 Nm and 3,000 rpm from LPTN model.

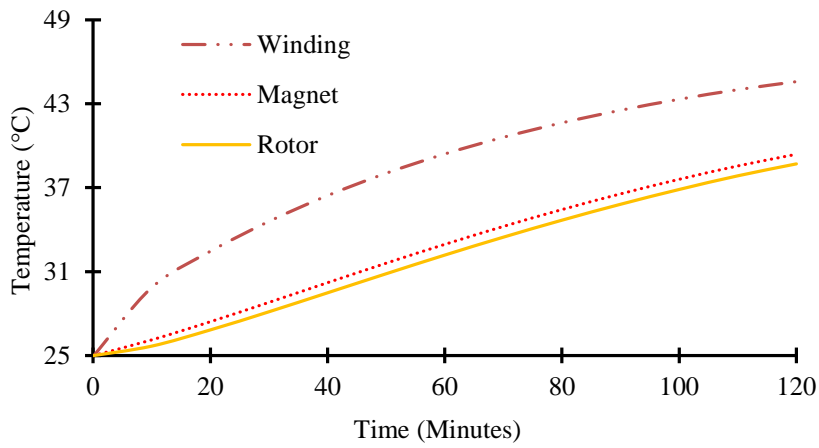


Figure 5.10 Predicted temperature in IPMSM at 35 Nm and 3,000 rpm from LPTN model.

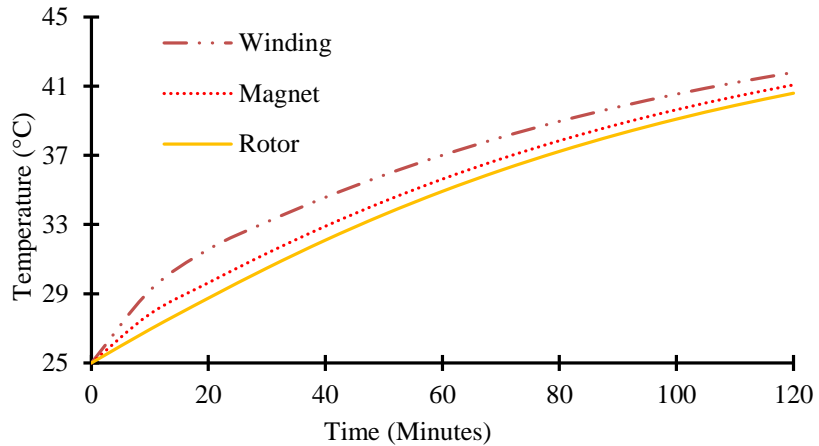


Figure 5.11 Predicted temperature in SPMSM at 70 Nm and 405 rpm from LPTN model.

From the above graphs, it is clear that in the SPMSM, rotor and magnets have high temperature rise as winding, unlike IPMSM where only winding has a comparatively higher temperature rise. Because, in SPMSM, the external surface of rotor and magnets

dissipate heat mostly through air gap convection, while in the IPMSM, rotor and magnets dissipate heat mostly by conduction through the shaft in a comparatively quicker way [113].

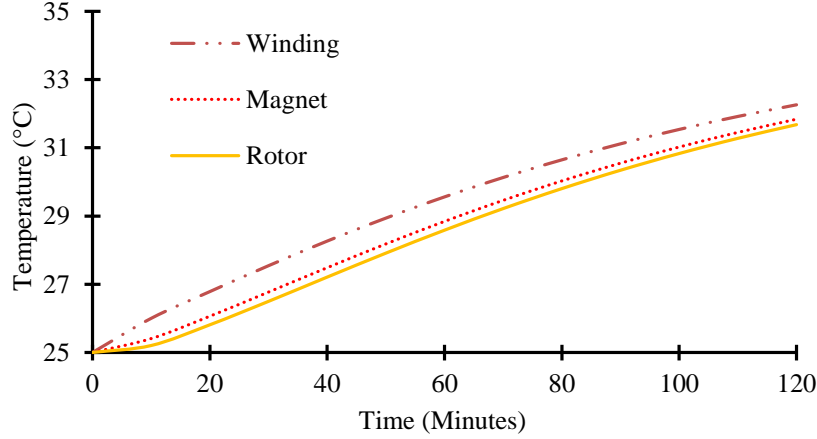


Figure 5.12 Predicted temperature in SPMMSM at 35 Nm and 405 rpm from LPTN model.

For this reason, there is no significant difference between the temperature of the rotor and magnet with the temperature of windings in SPMMSM. From the overall LPTN results, it is clear that both motors have better thermal stability and performance since temperature trends are within the expected tolerance limits for the analyzed operating conditions.

Chapter 6

A Novel Hybrid Technique for Computationally Efficient FEA Thermal Modeling Approach of PMSMs

6.1 FEA Process for Thermal Analysis of Motor

ANSYS numerical software tool has been utilized for the overall process from motor design to thermal analysis. The overall process has been carried out through the coupling of ANSYS Electronics and ANSYS Mechanical tools in ANSYS Workbench. Motor design and electromagnetic analysis of designed motor have been done using RMXprt and Maxwell respectively in ANSYS Electronics. Finally, thermal analysis of the motor has been done using ANSYS Steady State Thermal in ANSYS Mechanical. Losses are feed into the thermal analysis process as heat generation source through the coupling of Maxwell and Steady State Thermal in ANSYS Workbench.

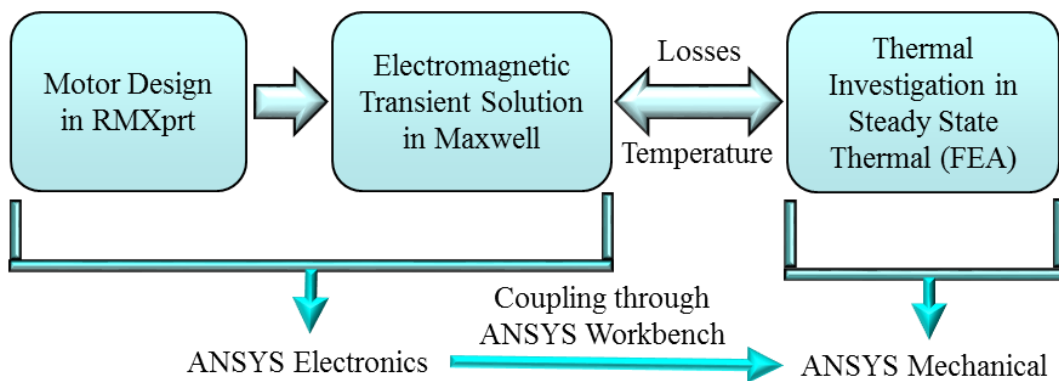


Figure 6.1 The overall process in ANSYS for thermal analysis of motor.

6.2 Proposed FEA Thermal Model

Three basic steps are followed as usual for the proposed FEA thermal model. They are pre-process, solver and post-process. Pre-processing involves geometry creation, meshing, and defining boundary conditions. Solver involves the solving process of the problem. Finally, post-processing involves mainly data visualization.

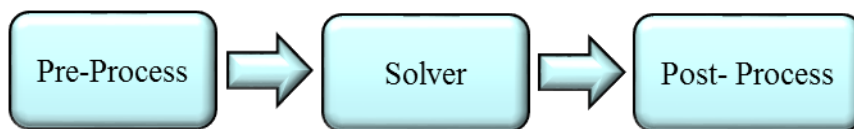


Figure 6.2 Basic steps for numerical FEA thermal model.

6.2.1 Meshing for FEA Thermal Model

A detail grid generation and grid independence study have been carried out for mesh convergence. Unlike numerical CFD, the numerical FEA process is less sensitive to the change in the mesh structure since FEA only deals with static solid geometry. Therefore, there is no significant change in final results based on grid size and thus moderate meshing has been used.

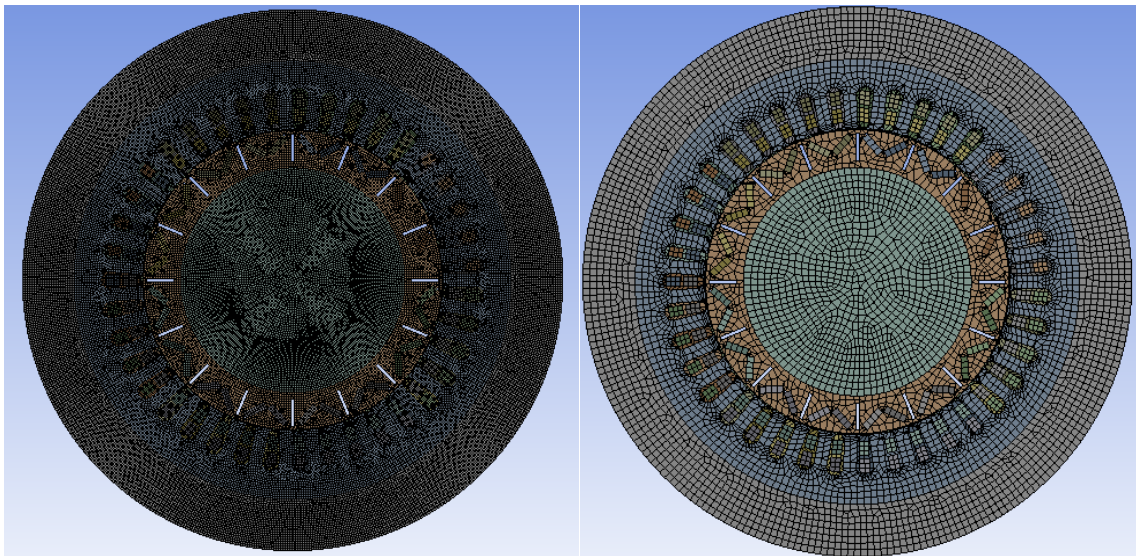


Figure 6.3 Two different mesh structures for numerical FEA thermal model.

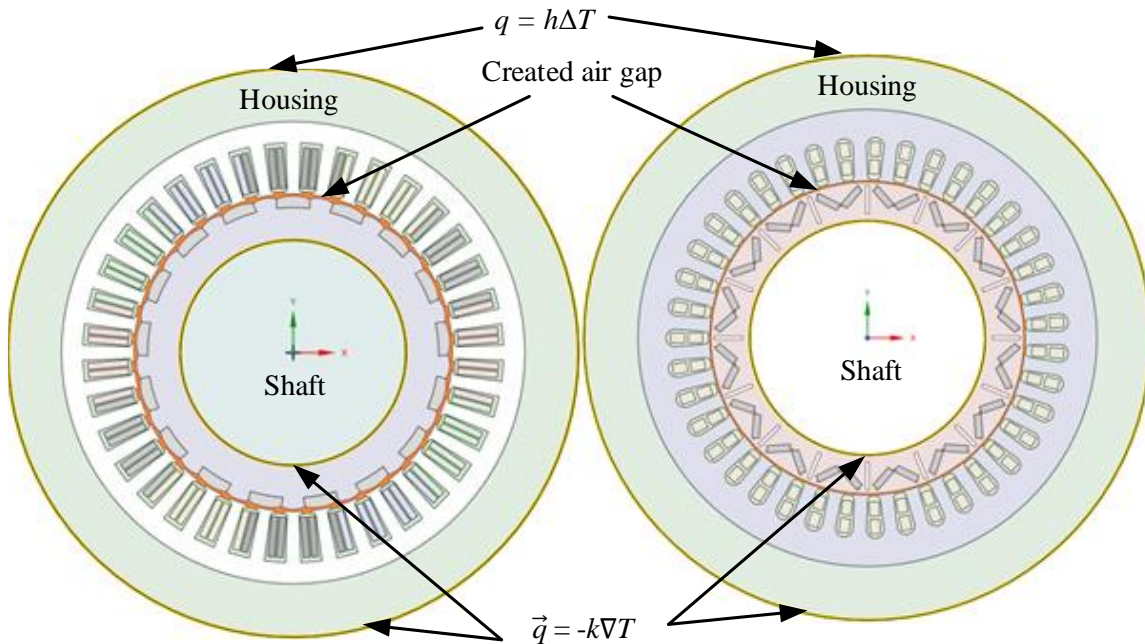


Figure 6.4 Strategies and boundary conditions for numerical FEA thermal model.

6.2.2 Strategy and Boundary Conditions in Proposed FEA Thermal Model

Determined motor losses have been taken as heat generation sources to predict final motor temperature. A convection boundary has been applied on the edge of the housing to address the cooling effect. The flow rate and temperature of the incoming coolant are almost constant to provide a constant cooling effect at continuous loading condition, unlike dynamic drive cycle loading condition. Therefore, a constant convection heat transfer coefficient, $1000 \text{ W/m}^2\text{°C}$ has been considered at constant inlet coolant temperature, 30°C . Further, some strategies have been presented for simplifying the overall FEA process and addressing the drawbacks of the conventional FEA thermal analysis process of the motor. These strategies are described below in separate subsections.

6.2.3 Simplification Strategy for FEA Thermal Modeling

In most cases, the radial section of motor geometry is used for simplified 2D FEA thermal analysis. In the radial section of motor geometry, bearing and endcap of the motor cannot be considered. Therefore, 2D FEA cannot address the heat flow from shaft to housing through bearing and endcap. To characterize this unaddressed heat flow, an additional conduction boundary has been applied in between shaft and housing. To implement this additional conduction boundary, a mutual contact region between shaft and housing has been created and a manual mutual conductance has been used instead of program-controlled conductance in the mutual contact region. 3D FEA can be carried out also without considering complex bearing and end cap geometry by using such a simplification strategy.

To characterize the heat flow from shaft to housing through bearing and end cap, a simplified LPTN model has been developed as shown in Figure 5.7. In the developed LPTN model, the outer race of the bearing and inner part of the end cap towards the housing lumped together as one node and inner race of the bearing towards the shaft is taken as another node. Further, the bearing balls are taken as a middle node and in between the nodes, thermal resistances are placed.

In this case, heat due to bearing loss is considered to be fully consumed by sealing and lubrication and the conductivity of sealing and bearing is neglected for simplification

as it does not have a significant effect on the considered heat flow. Therefore, the thermal resistance, R_b as shown in Figure 5.7 that permits the heat flow from shaft to housing can be determined using only physical dimensions of bearing.

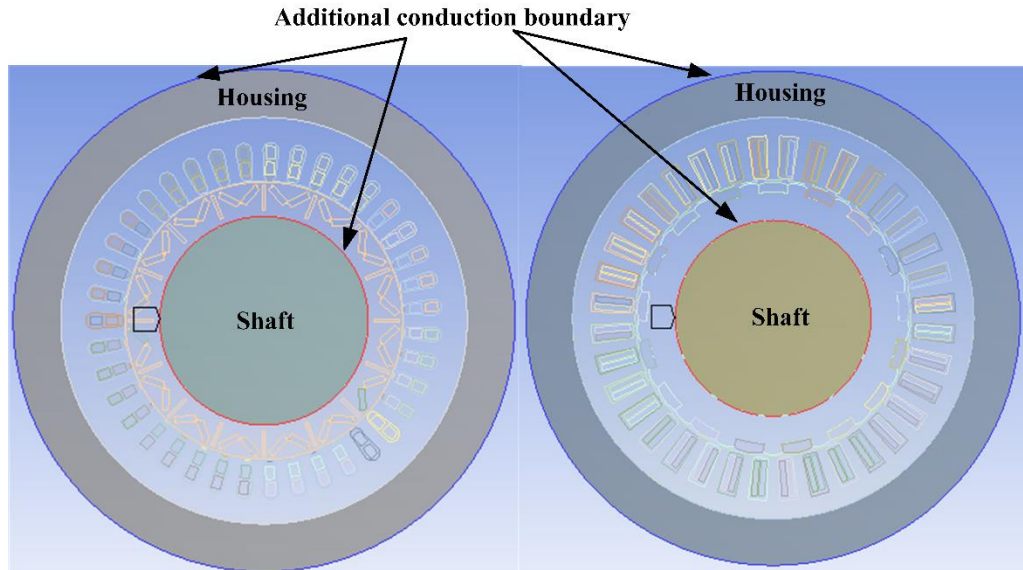


Figure 6.5 Simplification strategy for numerical FEA thermal model in both IPMSM and SPMSM.

The general expression (5.34) for the thermal resistance of bearing constructed from the experimental results [28], [78] can be used to determine the thermal resistance, R_b . Since symmetry of the motor is considered in the LPTN model, the same amount of heat flows through two bearings in a parallel position. Therefore, the mutual conductance to characterize the heat flow from the shaft to housing through bearing and end cap will be the inverse of $\frac{1}{2} R_b$.

6.2.4 Air Gap Creation Strategy in Proposed FEA Thermal Model

Unlike the CFD analysis, the FEA tool is not capable of analyzing fluid flow. Therefore, in conventional FEA thermal analysis of PMSM, a convection boundary at a constant air temperature is basically used in the air gap to characterize the heat flow. However, in actual practical cases, with the increase in motor operating temperature, air temperature in the air gap increases. Further, air friction loss in the air gap also contributes to the increase in air temperature. Such an increase in air temperature actually affects the heat flow phenomena in the air gap. When PMSM operates in a low operating temperature range, due to low air temperature, heat flows from both stator and rotor towards the air gap through convection. However, when PMSM operates in a high

operating temperature range, due to high air temperature, heat flow is different. As the rotor has a higher temperature than the air temperature, still a little amount of heat flows from the rotor towards the air gap through convection.

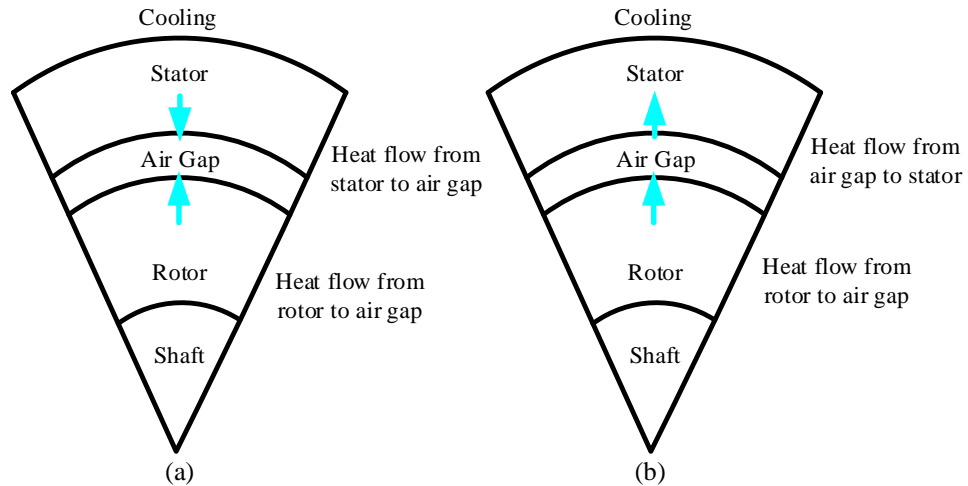


Figure 6.6 Heat flow in air gap. (a) Low operating temperature. (b) High operating temperature.

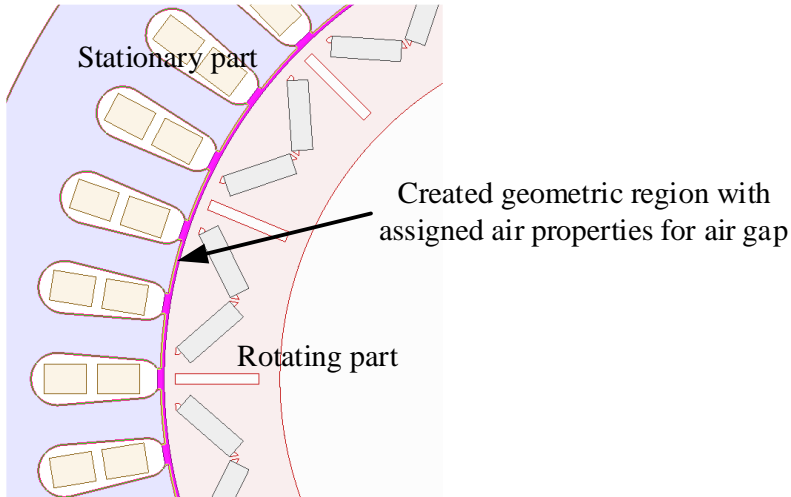


Figure 6.7 Created geometric region with assigned air properties for air gap in the motor geometry.

On the other hand, due to higher cooling effects on the stator edge, the stator has lower temperature comparatively and thus heat flows from the air gap to the stator towards the active cooling system of PMSM. However, convection boundary at a constant air temperature applied in conventional FEA thermal analysis cannot address such variation in air gap heat flow. Such convection boundary only removes more and more heat from both stator and rotor with the rise in motor operating temperature, since the temperature gradient between rising motor temperature and constant air temperature

increases at a significant rate. Therefore, such a convection boundary in the air gap is a misrepresentation of the heat flow in the air gap. During a higher range of motor operating temperatures, it predicts less motor temperature especially the temperature of the rotor. Further, it cannot consider air friction loss as a heat generation source. However, in PMSM used for the high-speed application, air friction loss cannot be neglected due to high angular speed. Therefore, a unique air gap creation strategy has been developed to characterize the air gap heat flow in an accurate way. Such a strategy allows the change in air temperature with the rise in operating temperature of PMSM. Thus it is helpful to address the air gap heat transfer in correct way. Further, the created geometric region for air gap can consider air friction loss as heat generation source. In this strategy, a manual thermal conductance has been applied instead of program-controlled conductance in the contact region of the created geometric region for air gap with both stator and rotor. Such thermal conductance can be determined from the inverse of thermal resistance due to convection in the air gap, R_{ag} [18].

6.3 Predicted Temperature of PMSM Prototypes from Proposed FEA Model

The FEA process is helpful to show overall temperature distribution throughout the motor. This process makes sure that there is no sudden rise in any individual winding or magnet temperature which in turn ensures there is no fault in the motor design. Thermal analysis using the proposed FEA thermal model has been carried out for several operating conditions for both motor prototypes for the industrial project purpose. However, only the temperature results for two operating conditions at 70 Nm and 35 Nm in base speeds for both motor prototypes have been presented in both Figure 6.8 and 6.9.

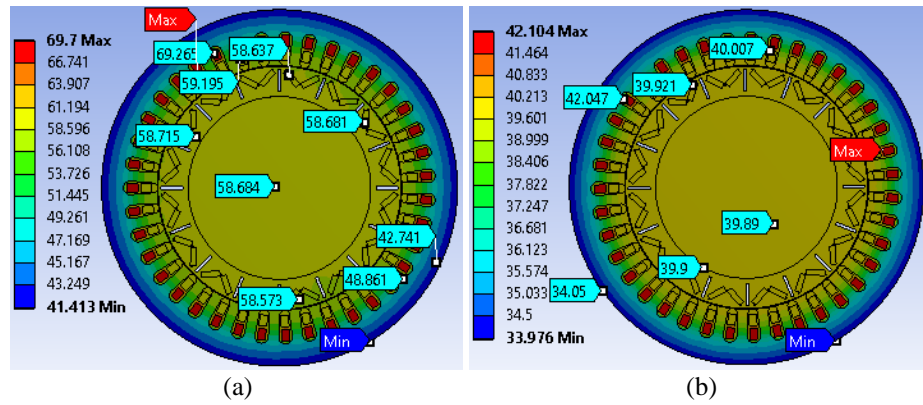


Figure 6.8 Temperature distribution map in IPMSM at 3,000 rpm from FEA thermal model.
(a) 70 Nm. (b) 35 Nm.

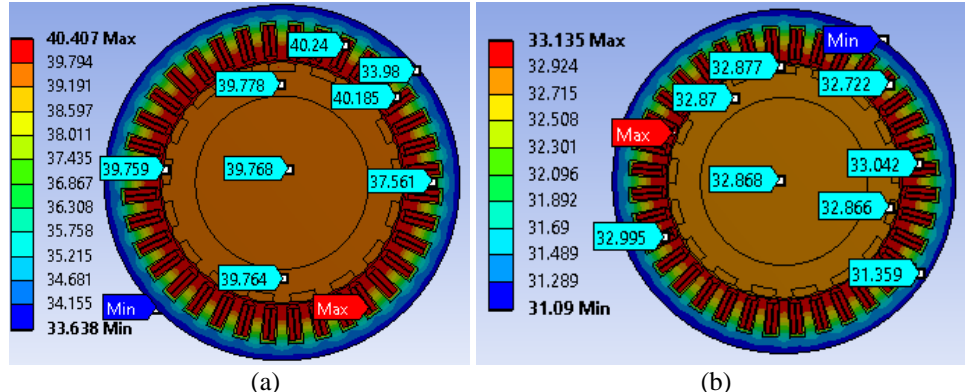


Figure 6.9 Temperature distribution map in SPMMSM at 405 rpm from FEA thermal model. (a) 70 Nm.
 (b) 35 Nm.

Further, the thermal investigation has been done at 70 Nm and base speed for both motor prototypes using two-way loss analysis results to check the change in temperature results like the LPTN model. The comparison of FEA temperature results using one-way and two-way process are presented in Figure 6.10 and 6.11 both IPMSM and SPMMSM prototypes respectively.

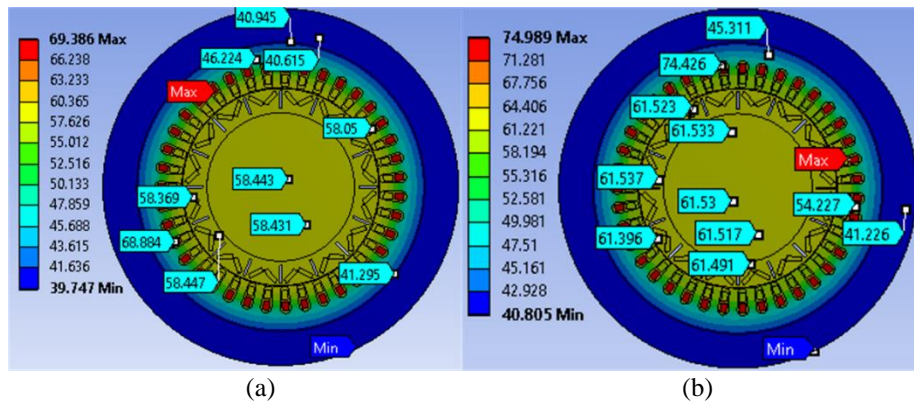


Figure 6.10 Temperature distribution map in IPMSM at 70 Nm and 3,000 rpm from FEA thermal model.
 (a) One-way analysis. (b) Two-way analysis.

Further, the 3D FEA process has also been carried out. 3D FEA has been performed mainly to address the end region passive cooling effect. Since end winding is the most heated part of the motor prototypes, the temperature distribution range is higher in the 3D FEA process. Further, as the end region passive cooling convection coefficient is applied on the rotor and stator end surfaces exposed to the inner air and end winding, the results are more accurate comparatively in the 3D FEA process. The 3D FEA temperature results are presented in Figure 6.12.

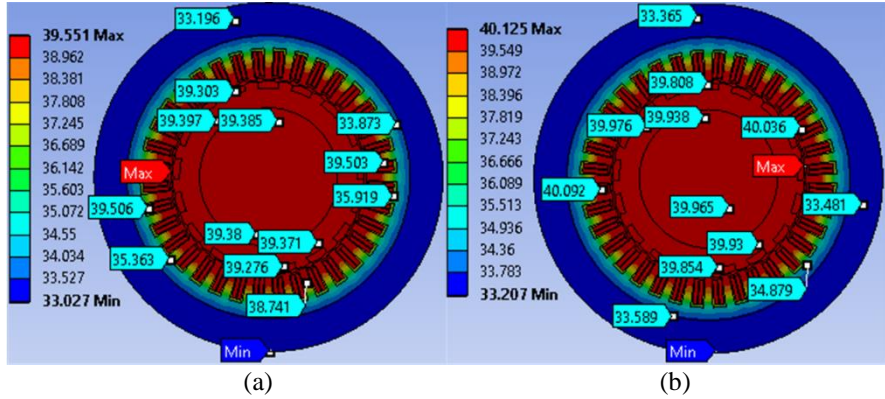


Figure 6.11 Temperature distribution map in SPMSM at 70 Nm and 405 rpm from FEA thermal model.
(a) One-way analysis. (b) Two-way analysis.

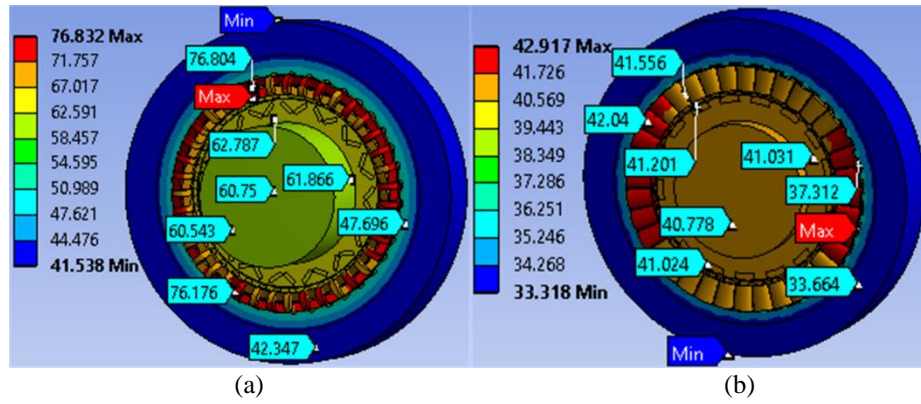


Figure 6.12 Temperature distribution map at 70 Nm and base speeds from numerical 3D FEA thermal models. (a) IPMSM. (b) SPMSM.

Like the LPTN model, FEA results show the same trend of temperature rise. In SPMSM, temperature distributions across the winding, rotor, and magnet are almost similar. On the other hand, the winding of IPMSM has a comparatively higher temperature distribution range than the rotor and magnets. Further, temperature distribution across all windings and magnets is almost uniform for both motor prototypes. Thus, the motor design does not have any fault. Finally, since the temperature distribution range is within the expected tolerance level, it further justifies the better thermal performance of both motor prototypes.

The total computational time is about 24 minutes for 3D FEA process using Intel(R) Core (TM) i7-2600, 3.40 GHz, 16 GB RAM workstation. Further, 3D CFD process with only moderate number of iterations, 500 using same work station takes more than 5 hours, around 320 minutes. However, the computational time for the proposed 2D FEA process using same workstation is less than 15 minutes.

Chapter 7

Validation of The Proposed LPTN and FEA Thermal Models

7.1 Comparison of LPTN and FEA Thermal Models

From Table 7.1 and 7.2, it is clear that analyzed temperature results from both LPTN and FEA thermal models at rated condition show close agreement. In IPMSM, the temperature difference between LPTN and FEA is about 1-2.3 °C at the rated operating condition. The maximum temperature difference in percentage is about 3.8% at the rated operating condition.

Table 7.1 Comparison of LPTN and FEA temperature results at the rated condition in IPMSM

At 70 Nm loading torque condition and base speed, 3,000 rpm				
Major Motor Components	LPTN Temp. Results	FEA Temp. Results	Difference	In percentage
Stator	48.205 °C	46.59 °C	1.6	3.5%
Rotor	58.41 °C	60.74 °C	2.3	3.8%
Winding	75.47 °C	74.57 °C	0.9	1.2%
Magnet	59.33 °C	61.523 °C	2.2	3.6%

In SPMSM, the temperature difference between LPTN and FEA is about 1-1.7 °C at the rated operating condition. The maximum temperature difference in percentage is about 4.2% at the rated operating condition.

Table 7.2 Comparison of LPTN and FEA temperature results at the rated condition in SPMSM

At 70 Nm loading torque condition and base speed, 405 rpm				
Major Motor Components	LPTN Temp. Results	FEA Temp. Results	Difference	In percentage
Stator	35.801 °C	34.68 °C	1.1	3.2%
Rotor	40.59 °C	39.705 °C	0.9	2.2%
Winding	41.8 °C	40.107 °C	1.7	4.2%
Magnet	41.08 °C	39.89 °C	1.2	3%

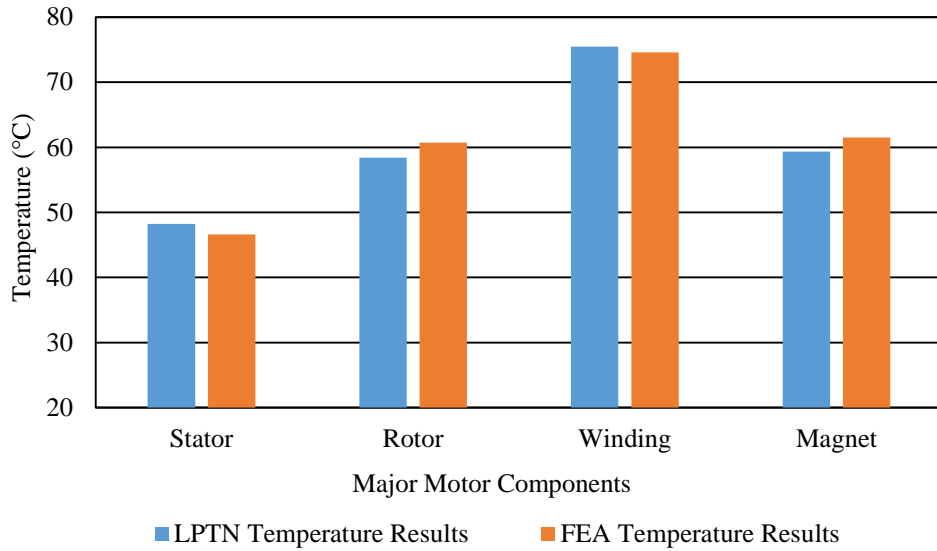


Figure 7.1 Comparison of LPTN and FEA temperature results for IPMSM at 70 Nm and 3,000 rpm.

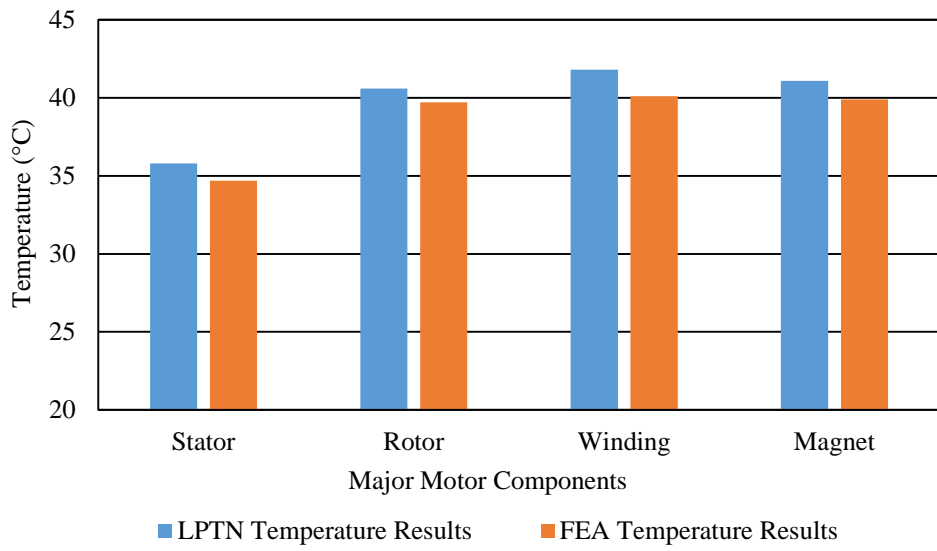


Figure 7.2 Comparison of LPTN and FEA temperature results for SPMSM at 70 Nm and 405 rpm.

7.2 Experimental Validation of Thermal Models

A loading test has been carried out for SPMSM only at a really low operating condition, 35 Nm and 100 rpm within limited scope for experimental validation. Further, LPTN and FEA have been carried out in this specific condition for SPMSM to check the difference between analyzed results and test results. Since the IPMSM prototype is designed for high speed application and it needs a higher starting current rating, the loading test has not been performed for this prototype. Because the existing Siemens test bench and control system in the lab is not capable of running both motors at high speed and high

torque conditions for a longer period at least more than one hour. Without a longer period loading test, steady state operating temperature for the motor cannot be reached. Therefore, below presented experimental validation of thermal models are for only SPMSM prototype at 35 Nm and 100 rpm.

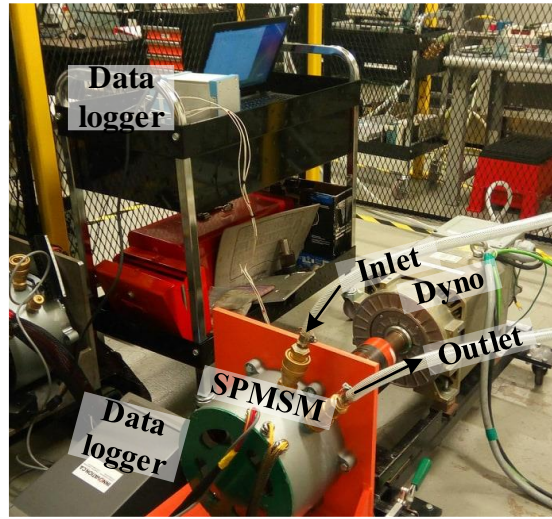


Figure 7.3 Loading test of SPMSM at 35 Nm and 100 rpm.

Thermocouple K type temperature sensors (approximate error range $\pm 2^\circ\text{C}$) are embedded inside the motors to measure the temperatures of main windings. Further, the resistance temperature detector (RTD) type temperature sensors can be used for other stationary parts of the motor and infrared radiation (IR) sensor can be used for rotating parts of the motor. By using such temperature sensors with a data logger, temperature rise with the variation of time can be recorded. However, only steady state thermal analyses of SPMSM using both proposed FEA and LPTN model have been conducted at 35 Nm and 100 rpm. Therefore, only steady state temperature of SPMSM has been recorded with the help of thermal imager after one-hour loading test at the same operating condition.

Table 7.3 Comparison of LPTN and measured temperature results in SPMSM

At 35 Nm loading torque condition and 100 rpm speed				
Major Motor Components	LPTN Temp. Results	Measured Temp.	Error	Error in percentage
Winding	26.35 °C	26.7 °C	0.35	1.3%
Magnet	25.25 °C	24.7 °C	0.55	2.2%

Table 7.4 Comparison of FEA and measured temperature results in SPMSM

At 35 Nm loading torque condition and 100 rpm speed				
Major Motor Components	FEA Temp. Results	Measured Temp.	Error	Error in percentage
Winding	25.92 °C	26.7 °C	0.78	2.9%
Magnet	25.19 °C	24.7 °C	0.49	2%

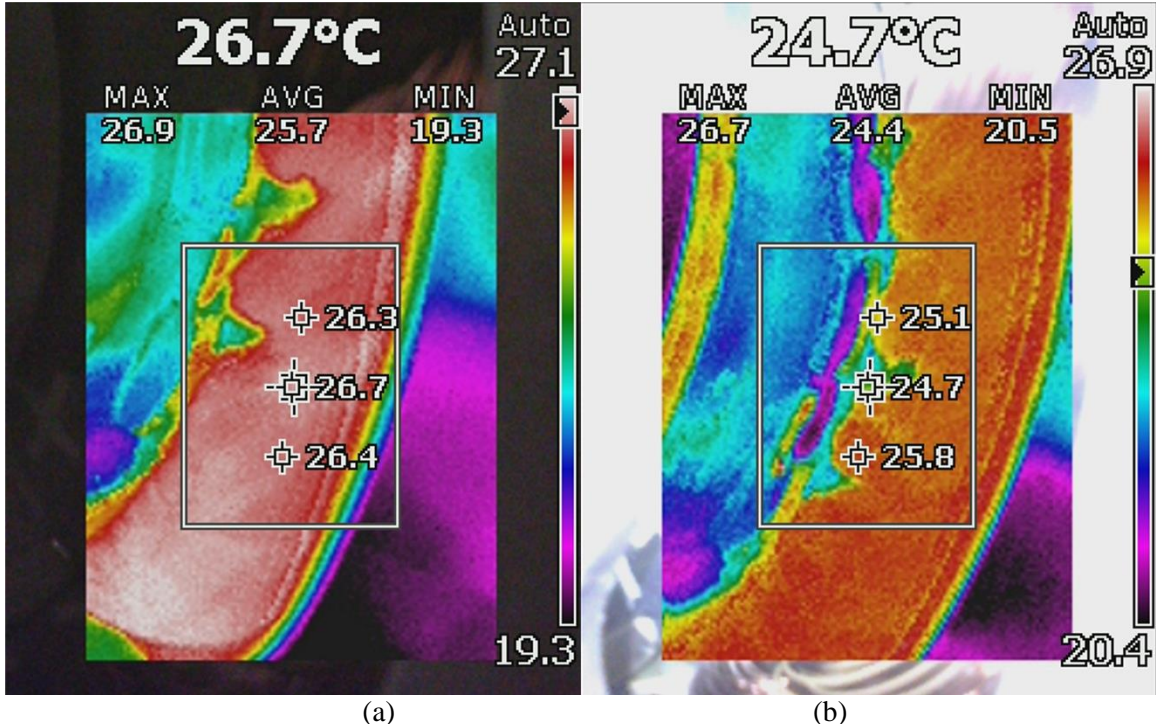


Figure 7.4 Captured temperature profile during loading test of SPMSM at 35 Nm and 100 rpm. (a) Winding temperature. (b) Magnet Temperature.

From Table 7.3 and 7.4, it is clear that predicted LPTN and FEA temperature results have a close agreement with measured temperature results. However, such low torque and speed operating condition and using a thermal imager to measure the temperature cannot show the actual error percentage in the thermal models. Because such low torque and speed operating condition is not thermally challenging. Further, the thermal imager actually measures the temperature at any specific point of the motor part and in the rotating part, it is difficult to point out the exact location. Therefore, high torque and speed operating condition and embedded temperature sensors in each motor part are recommended for better thermal testing. Yet, such thermal test at low operating condition can still reflect the reliability of the processes used in thermal models.

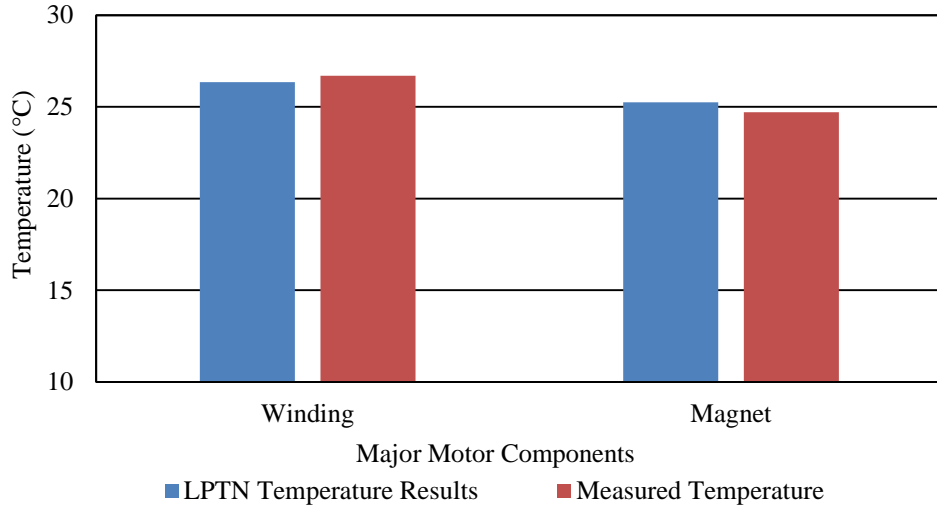


Figure 7.5 Comparison of LPTN and measured temperature results in SPMSM at 35 Nm and 100 rpm.

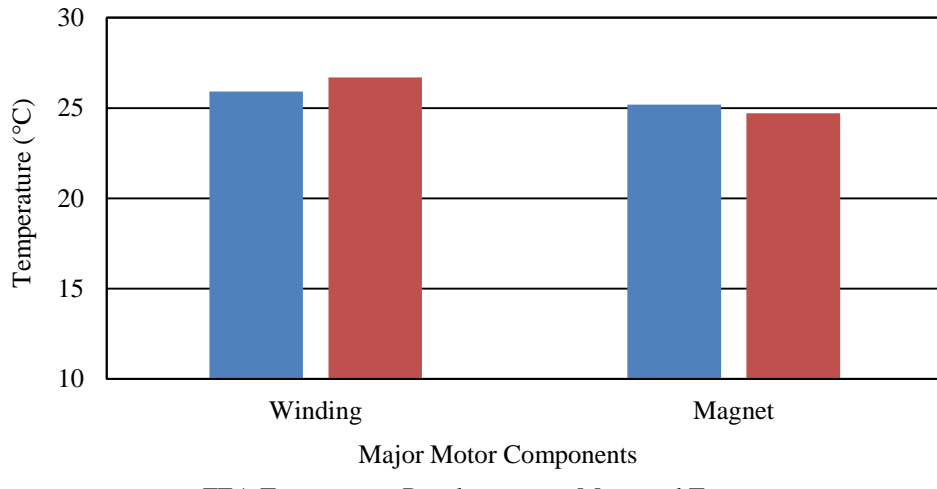


Figure 7.6 Comparison of FEA and measured temperature results in SPMSM at 35 Nm and 100 rpm.

7.3 Comparison of One-way and Two-way Electro-thermal Analysis Results

It is clear that due to higher winding temperature and higher temperature coefficient of resistivity of winding ($\alpha_T = 0.0039 \text{ K}^{-1}$), there is a significant increase in copper loss. On the other hand, due to less magnet temperature and less temperature coefficient of resistivity of the magnet ($\alpha_T = 0.0002 \text{ K}^{-1}$), the increase in resistivity of the magnet is negligible. However, due to the higher reverse temperature coefficient of the coercivity of magnet ($\alpha_T = 0.005 \text{ K}^{-1}$), there is a considerable reduction in magnetic flux density which in turn results in a slight decrease in solid loss of magnet. The temperature coefficient of permeability of lamination steel is not considered during analysis due to the good stability of steel properties even at a high range of operating temperatures of the motor.

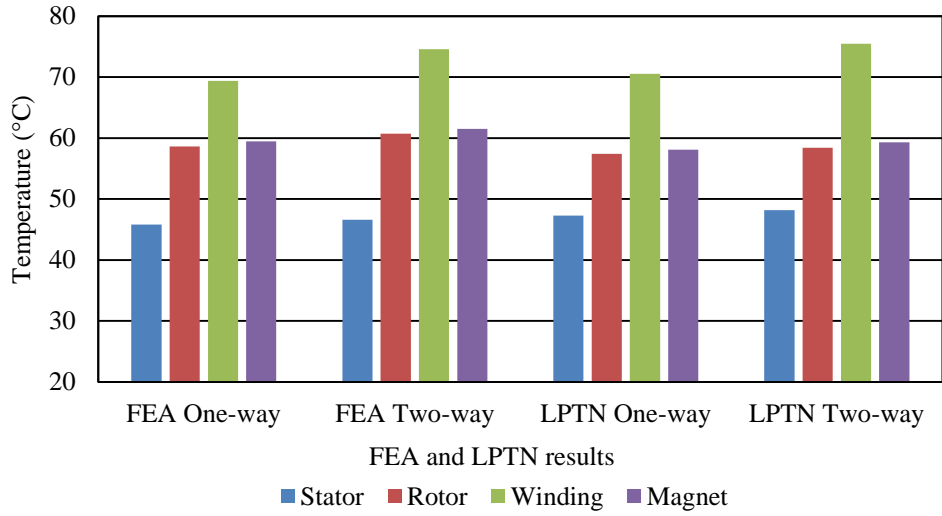


Figure 7.7 Comparison of one-way and two-way electro-thermal co-analysis results for both FEA and LPTN in IPMSM at rated condition.

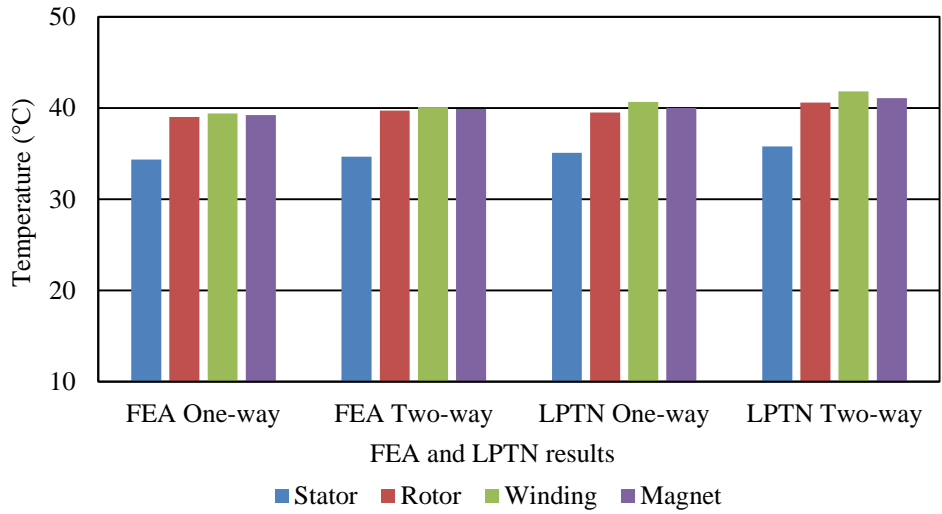


Figure 7.8 Comparison of one-way and two-way electro-thermal co-analysis results for both FEA and LPTN in SPMSM at rated condition.

Still, there is a slight decrease in core loss due to the reduction in magnetic flux. Such a change in losses surely has a considerable effect in final motor temperature prediction that can be seen from the one-way and two-way analysis temperature results comparison shown in Table 5.4 for LPTN and Figure 6.10 and 6.11 for FEA.

From comparison as shown in Figure 7.7 and 7.8, it is clear that due to the overall increase in the total final loss of IPMSM during two-way electro-thermal co-analysis, there is a considerable increase in overall motor temperature. There is a comparatively more increase in winding temperature than the temperature of other motor parts due to

higher temperature rise and higher temperature coefficient of winding. During conventional one-way electro-thermal co-analysis, the maximum error exists in the winding part. Such two-way electro-thermal analysis is helpful to minimize this error.

7.4 Validation of Thermal Analysis Strategy of Windings in LPTN

Since the DC test has been carried out, the rotating parts stay still and thus power flows through specific windings only [103]. Since, winding resistance, R_{Cu} and the amount of DC current supply, I is known, the power flow, P_{Cu} can be calculated as I^2R which is the only heat generation source in this case. Further, temperature gradient, ΔT can be determined from the monitored temperatures using thermocouple K type (approximate error range $\pm 2^\circ\text{C}$) during the DC test and thus thermal resistance of winding can be found easily from calculated heat flow and temperature gradient. Since the temperature dependence of resistivity of copper is considered during analysis, temperature-dependent, R_{Cu} has been considered during calculation as follows [104],

$$R_{Cu} = R_{Cu0}(1 + 0.0039 \times \Delta T) \quad (7.1)$$

Since SPMSM has a low current rating, variac has been used to supply reduced AC voltage to the rectifier and then it has been converted into DC supply to carry out the DC test. On the other hand, since IPMSM has a high current rating, it has been connected to the direct high voltage DC supply in the lab to carry out the DC test.

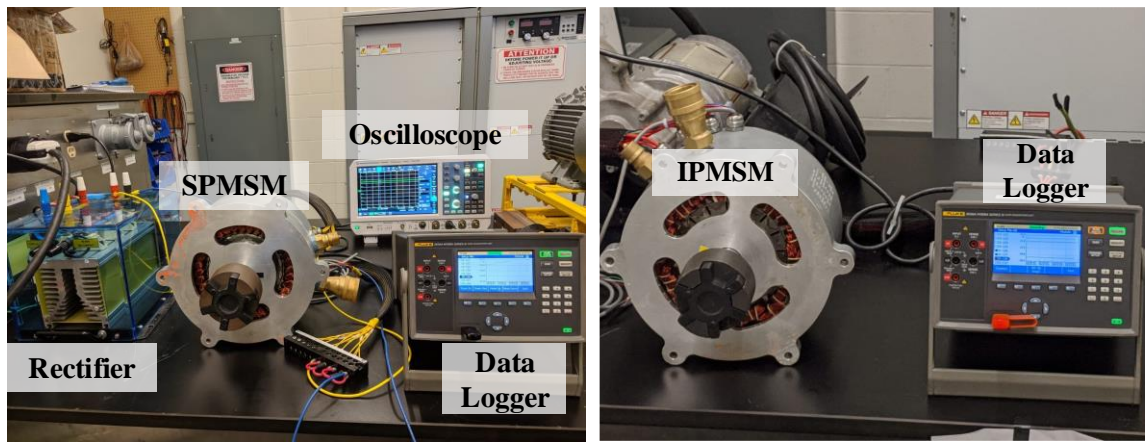


Figure 7.9 DC Test of SPMSM and IPMSM respectively

Table 7.5 Comparison of windings thermal resistance

Thermal resistance of winding ($^{\circ}\text{C/W}$)	IPMSM		SPMSM	
	Calculated	Measured	Calculated	Measured
	0.051525	0.059	0.027063	0.03

In Table 7.5, the measured thermal resistances for windings of both motors from the DC tests are close to the calculated thermal resistances of windings for the LPTN model. Further, it can be seen in the experimental validation section that the predicted temperature of windings for SPMSM shows good agreement with measured temperature from experiments. Thus, the strategy of slot geometry transformation into a rectangular shape can be used for thermal resistance calculation of any multilayer windings in the LPTN model.

7.5 Validation of Equivalent Space Strategy of Magnets in LPTN

To implement an equivalent space strategy for V-shape magnets of IPMSM in LPTN, firstly, FEA thermal analysis of IPMSM with horizontally positioned magnets has been carried out using the same losses at 70 Nm and 3000 rpm. It shows the difference between V-shape and horizontally positioned magnet is negligible. Therefore, the effect of the change in position and shape on magnet temperature is not considerable. Thus, the equivalent space strategy can be used for the thermal resistance calculation of any magnet regardless of its position in the rotor.

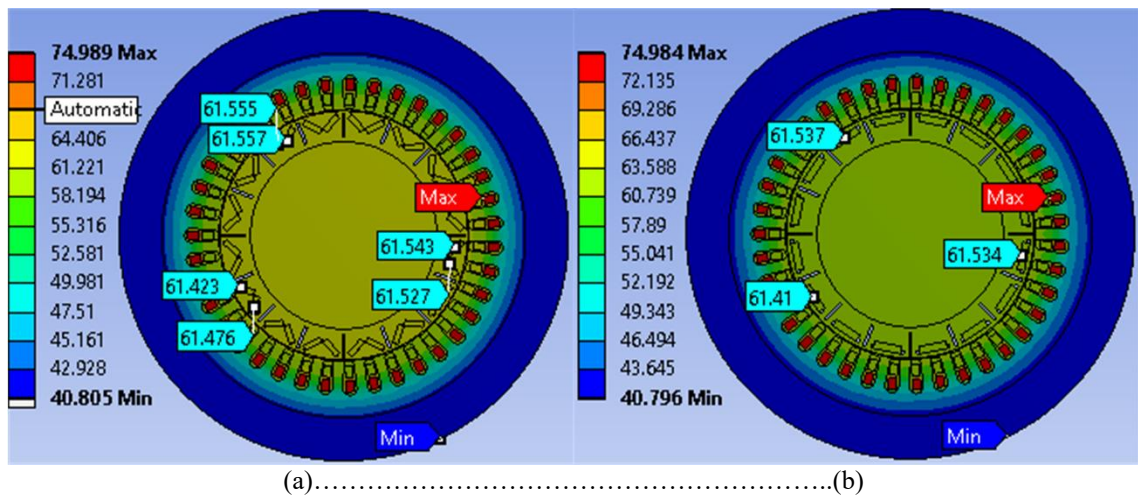


Figure 7.10 Comparison of predicted magnet temperatures in IPMSM prototype from FEA. (a) V-shape magnets. (b) Horizontally positioned magnets.

7.6 Explanation of Air Gap Creation Strategy in FEA

Convection boundary at constant air temperature at the air gap removes more and more heat from rotor especially with the rise in motor operating temperature, since temperature gradient increases. However, in the actual case, due to air friction loss and rise in motor temperature, air temperature continuously increases in the air gap and thus heat removal from rotor due to air gap convection gets less. Therefore, the predicted rotor temperature from FEA is considerably less than the actual case. Hence, the air gap creation strategy has been implemented in the proposed FEA model to consider air friction loss as a heat generation source and the change in air temperature in the air gap. Therefore, the predicted rotor temperature of IPMSM from proposed FEA is comparatively higher than conventional FEA using convection boundary at constant air temperature, 22 °C in the air gap. Although the predicted rotor temperature difference is less than 1°C only at rated condition, this difference can be more at higher operating conditions. For SPMSM, this temperature difference is not significant, since the range of motor operating temperature at rated condition is much lower comparatively.

Table 7.6 Comparison of predicted rotor temperature from FEA Models

Predicted rotor temperature of IPMSM	Conventional 2D FEA	Proposed 2D FEA
	60 °C	60.74 °C

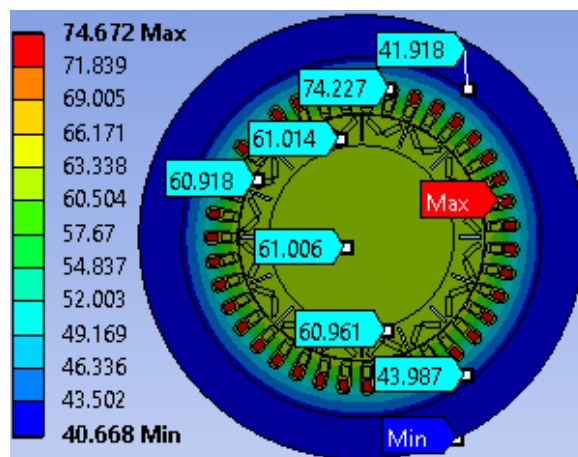


Figure 7.11 Temperature results from conventional FEA process using convection boundary at air temperature, 22°C in air gap.

Chapter 8

Cooling Design Process and Cooling Performance

Investigation of PMSMs

8.1 Cooling Design Process

Although cooling design optimization is not the focus of this thesis at all, still some suggestions have been made in this section regarding cooling design optimization of traction motor to pave the way for future research on the cooling design of the designed traction motors in the lab.

The newly designed IPMSM and SPMSM have torque density of 13 Nm/kg and 13.72 Nm/kg respectively without housing which is far better than torque density range of the commercially available EV motors, 5 to 8 Nm/kg. However, when housing with the integrated active cooling system is considered, the torque density of both motors fall significantly below 6 Nm/kg. The main reason behind this is that the housing with integrated active cooling system design is not optimized. Since most of the portion of the housing basically consists of an active cooling system, an effective design optimization process is needed for the active cooling system of the designed motor prototypes. It is really challenging and time consuming to use repetitive CFD analysis for the cooling design optimization process to get a high performance as well as a compact cooling design structure of traction motors. Therefore, an basic algorithm has been developed from background study on the cooling design optimization of traction motors to get an optimal cooling design of the motor prototypes. In this case, CFD analysis can be used later to check the performance results of the optimized cooling design. Further small modifications such as any angular turn of fluid flow path etc. can be done using CFD analysis for further increase in cooling performance of the optimized cooling design.

The below steps are involved in the developed algorithm for cooling design optimization of traction motors [9], [100]-[102]:

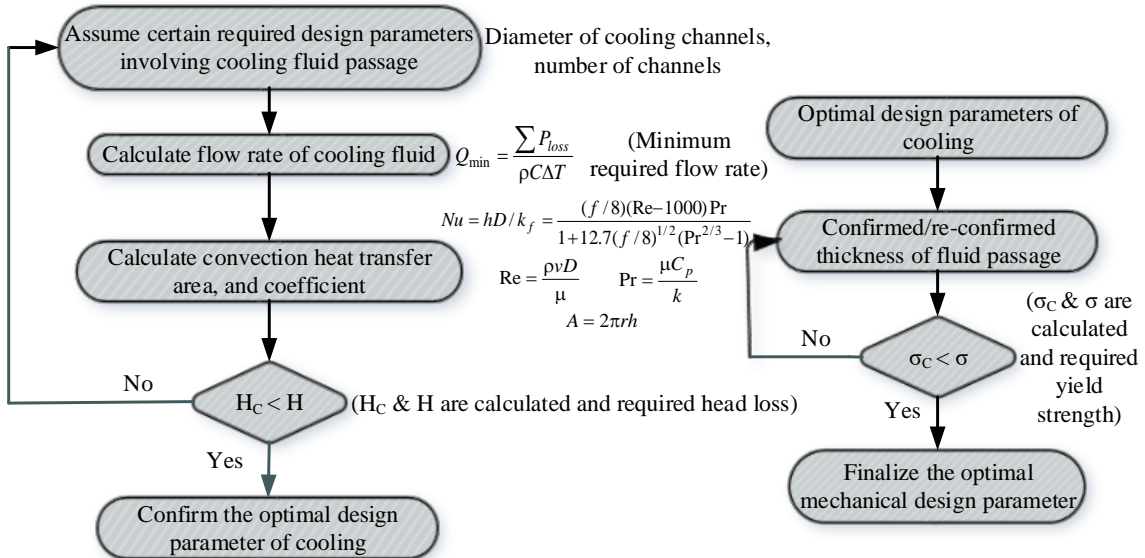


Figure 8.1 Basic step algorithm for cooling design optimization of traction motor.

Step-1: The first step is to assume the required design parameters involving cooling fluid passage. In this case, the required design parameters are the diameter of cooling channels and the number of channels for better cooling performance.

Step-2: The second step is to calculate the flow rate of cooling fluid. The required minimum flow rate can be calculated as [9],

$$Q_{min} = \frac{\sum P_{loss}}{\rho C_p \Delta T} \quad (8.1)$$

where, P_{loss} is the total motor loss responsible for heat generation, ρ is the density of cooling fluid, C_p is the specific heat capacity of cooling fluid and ΔT is the allowable temperature rise for cooling fluid. Loss data and allowable temperature rise for cooling fluid can be determined from electro-thermal co-analysis.

Step-3: The third step is to calculate the convection heat transfer coefficient and area for the assumed design parameters in step-1. The active cooling system for both designed motor prototypes is circumferential cooling jacket and the nature of the fluid flow inside the cooling system is always fully developed turbulent flow, $3000 < Re < 10^6$ due to high cooling flow rate to get the higher cooling effect. Therefore, the Nusselt number equation (2.1) can be used for calculating the convection heat transfer coefficient. Further, since

stator has a cylindrical structure and cooling system is built on the stator surface, the convection heat transfer area can be determined as,

$$A = 2\pi r l \quad (8.2)$$

However, as electro-thermal co-analysis for both motor prototypes has been done already for different convection heat transfer coefficients, the reverse process can be used to assume design parameters for the better one among all considered convection heat transfer coefficients for electro-thermal co-analysis.

Step-4: Energy equations are used at inlet and outlet and the head loss is calculated from the difference. During this process, any loss that affects flow velocity and heat transfer such as friction loss of cooling pipes, minor loss in valves, bends, tees or any other component needs to be considered carefully. If the calculated head loss is larger than the required head loss for heat removable, the above steps need to be carried out again. The amount of heat removable suggestion can be got from the electro-thermal co-analysis. On the other hand, if the calculated head loss is satisfied, the assumed design parameters can be considered as optimal design parameters.

Step-5: The final step is the stress analysis of the optimal cooling design. It can confirm the required minimum thickness of the cooling pipe to withstand the electromagnetic force and any other acting force during motor operation.

8.2 Cooling Performance Investigation

The main purpose of this cooling performance investigation process is to develop a two-way electro-thermal co-analysis strategy for CFD analysis. Such a process can predict both thermal performance and electromagnetic performance of the motor while the motor is operating with active cooling system. There are few published literature on CFD analysis for cooling performance investigation of traction motor [100]-[102]. From this literature, the concept regarding geometry setup, meshing, boundary, and turbulence modeling can be obtained for CFD analysis. However, such CFD analysis is only capable of showing the thermal performance of the motor considering the active cooling system. Therefore, the main focus of this section is to introduce a two-way electro-thermal co-analysis strategy for such CFD analysis to predict both thermal and electromagnetic

performance of the motor. Since the main target of any motor design process is achieving better electromagnetic performance, implemented active cooling system should ultimately serve for targeted electromagnetic performance during the motor design process. Therefore, the two-way electro-thermal co-analysis process must be used during CFD analysis to ensure the electromagnetic performance of the motor under the predicted operating temperature of the motor. Therefore, for developing the CFD modeling, conventional ways from published literature are followed and in addition to these steps, the same two-way electro-thermal co-analysis strategy like FEA has been introduced into CFD modeling to predict electromagnetic performance under predicted temperature distribution from CFD analysis.

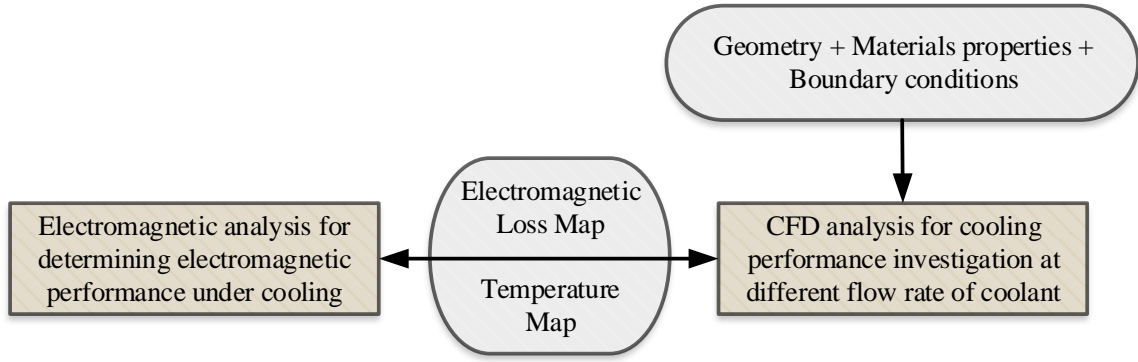


Figure 8.2 Two-way electro-thermal co-analysis process during CFD analysis.

In this process, the fluid field and temperature field are coupled to analyze the distribution of temperature throughout all parts of the newly designed IPMSM prototype and flow resistance distribution of cooling fluid considering the active cooling system of the newly designed IPMSM prototype. The temperature field is calculated using the same Thermodynamics concept for the conduction and convection heat transfer phenomena as FEA. Further, the fluid flow field in cooling channels are governed by the laws of conservation of mass, conservation of momentum and conservation of energy and these laws are described by the below governing equations for incompressible fluid [98], [114]:

Governing equation for the law of conservation of mass,

$$\frac{\partial v_x}{\partial x} + \frac{\partial v_y}{\partial y} + \frac{\partial v_z}{\partial z} = 0 \quad (8.3)$$

Governing equation for the law of momentum,

$$\begin{cases} F_x - \frac{1}{\rho} \frac{\partial p}{\partial x} + \nu \left(\frac{\partial^2 v_x}{\partial x^2} + \frac{\partial^2 v_y}{\partial y^2} + \frac{\partial^2 v_z}{\partial z^2} \right) = \frac{dv_x}{dt} \\ F_y - \frac{1}{\rho} \frac{\partial p}{\partial y} + \nu \left(\frac{\partial^2 v_x}{\partial x^2} + \frac{\partial^2 v_y}{\partial y^2} + \frac{\partial^2 v_z}{\partial z^2} \right) = \frac{dv_y}{dt} \\ F_z - \frac{1}{\rho} \frac{\partial p}{\partial z} + \nu \left(\frac{\partial^2 v_x}{\partial x^2} + \frac{\partial^2 v_y}{\partial y^2} + \frac{\partial^2 v_z}{\partial z^2} \right) = \frac{dv_z}{dt} \end{cases} \quad (8.4)$$

Governing equation for the law of conservation of energy,

$$\frac{\partial T}{\partial t} + \frac{\partial(v_x T)}{\partial x} + \frac{\partial(v_y T)}{\partial y} + \frac{\partial(v_z T)}{\partial z} = \frac{k_f}{\rho C_p} \left(\frac{\partial^2 T}{\partial x^2} + \frac{\partial^2 T}{\partial y^2} + \frac{\partial^2 T}{\partial z^2} \right) + S_T \quad (8.5)$$

For any CFD model, a mesh convergence study is necessary to keep the proper balance between computational time and accuracy. The detailed mesh convergence study has been presented already in previously published literature. Since the motor has several parts with different physical dimensions, the meshing has been carried out by assigning separate element size corresponding to every specific motor part. Such meshing will ensure element sizes are well below the limit of the minimum physical dimension of the specific part [100]. The presented CFD is limited in scope and the purpose of this presented CFD is to only set up the initial stage for future planning of cooling design optimization of newly designed IPMSM prototype using the CFD analysis.

Further, inlet boundary condition for incoming fluid and outlet boundary condition for outgoing fluid has been set up. In the inlet boundary, the velocity calculated from flow rate, 8 LPM and area of the channels and the constant temperature, 40 °C of the incoming fluid is assigned. Since the fluid flow inside the cooling channel is turbulent according to calculated Reynold's number, the standard $k-\epsilon$ model is used as the turbulence model [100]. The turbulence control equation for the standard $k-\epsilon$ model is [114],

$$\begin{cases} \rho \frac{\partial k_e}{\partial t} + \rho \frac{\partial(k_e u_i)}{\partial x_i} = \frac{\partial}{\partial x_j} \left[\left(\mu + \frac{\mu_t}{\sigma_{k_e}} \right) \frac{\partial k_e}{\partial x_j} \right] + G_{k_e} - \rho \epsilon_e \\ \rho \frac{\partial \epsilon_e}{\partial t} + \rho \frac{\partial(\epsilon_e u_i)}{\partial x_i} = \frac{\partial}{\partial x_j} \left[\left(\mu + \frac{\mu_t}{\sigma_{\epsilon_e}} \right) \frac{\partial \epsilon_e}{\partial x_j} \right] + \frac{C_{1\epsilon_e} \epsilon_e}{k_e} G_{k_e} - C_{2\epsilon_e} \rho \frac{\epsilon_e^2}{k_e} \end{cases} \quad (8.6)$$

In this formula, u_i is the time velocity, G_{ke} is the generating term of the turbulent kinetic energy, k_e due to the average velocity gradient. The remaining parameters are adjustable constants taken from comprehensive data fitting for a wide range of turbulent flows [98]. The standard $k-\epsilon$ model employs constant values, $C_{1\epsilon}=1.44$, $C_{2\epsilon}=1.92$, $C_\mu=0.09$, $\sigma_{ke}=1.00$ and $\sigma_{ee}=1.30$ and calculates turbulent viscosity, μ_t as follows [98], [114],

$$\mu_t = \rho C_\mu \frac{k_e^2}{\epsilon_e} \quad (8.7)$$

For near wall treatment, standard wall functions are used in the $k-\epsilon$ turbulence modeling.

After the CFD setup is completed, motor losses are imported for the selected zone as heat generation sources for thermal analysis. Later the predicted temperature results are imported into electromagnetic analysis to predict torque under operating temperature. This two-way process can be carried out with several iterative processes. Such a strategy will be helpful for ensuring an optimized cooling design for targeted torque at a certain operating condition.

In this case, thermal analysis has been carried out considering steady state thermal condition at the rated condition for newly design IPMSM prototype.

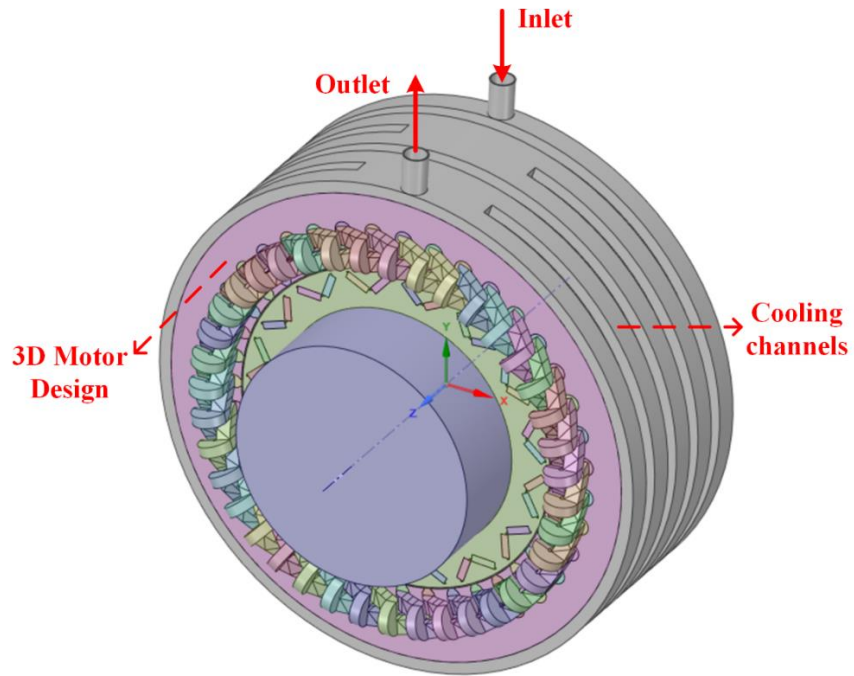


Figure 8.3 3D motor geometry with cooling channels for CFD analysis.

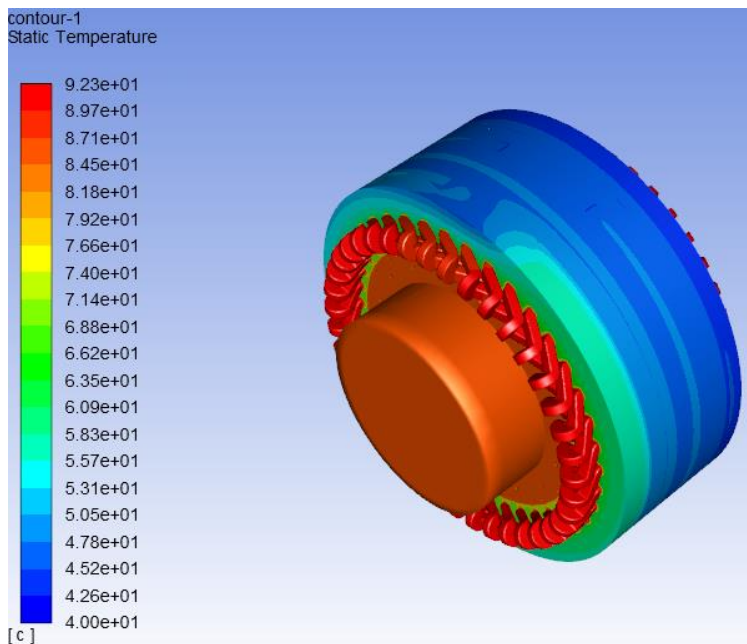


Figure 8.4 Predicted temperature distribution of IPMSM from CFD analysis.

Table 8.1 Predicted torque considering the operating temperature of IPMSM

Motor torque considering operating temperature	At initial temperature, 22 °C	At predicted temperature
	70 Nm	61.8 Nm

Such a two-way electro-thermal co-analysis process is also helpful for flow rate investigation of cooling fluid. From such flow rate investigation, a suitable flow rate with a high convective cooling effect can be obtained for a certain operating condition of the motor. As a result, the motor torque rating at that specific operating condition will be close to the torque rating under the initial motor temperature.

Chapter 9

Conclusions

9.1 Overall Research Summary

For fulfilling the first research objective, a LPTN model has been developed to predict temperatures of the designed IPMSM and SPMSM prototypes in this thesis. In the first research contribution, a simplification strategy for the proposed analytical LPTN model has been developed by considering only major heat flow phenomena for thermal resistance calculation. Such a simplification strategy reduces the over-complexity of the calculation process which further reduces the overall calculation time. On the other hand, since all major heat flow phenomena that have a significant contribution to motor temperature rise are considered during the calculation, it keeps the accuracy level within the accepted limit. Therefore, the proposed LPTN model can be used as a fast and reliable temperature prediction method for PMSM. In the second research contribution, the universal thermal analysis strategies for a wide range of winding configurations and positions of magnets has been developed to use the proposed LPTN model as a universal thermal representation model for all types of PMSMs. Therefore, the same LPTN model is capable of analyzing the temperature results of both SPMSM and IPMSM prototypes.

Further, a FEA thermal model has been developed to predict temperature distribution maps of the designed IPMSM and SPMSM prototypes in this thesis. In the third research contribution, a simplification strategy has been implemented for the proposed FEA thermal model by assigning an additional conduction boundary to address the heat flow from shaft to housing without considering complex bearing and end cap geometry. Further, in the fourth research contribution, a unique air gap creation strategy has been implemented in the proposed FEA thermal model to address the heat transfer through the air gap in an efficient way for better accuracy. These implemented strategies in the proposed FEA thermal model makes the overall FEA process computationally more efficient by keeping the proper balance between the simplification and accuracy level of the process. Thus, it can be used as a fast and reliable motor design fault detection method.

For fulfilling the second research objective, thermal tests have been conducted for the experimental validation of the developed LPTN and FEA thermal models. The DC test has been conducted for the validation of winding thermal resistance calculation used in the LPTN model for both motor prototypes. Further, a loading test has been conducted for SPMSM within a limited scope for the comparison of measured and analyzed temperature results. Such experimental tests are helpful to validate the reliability of the developed thermal models so that the thermal models can be used for any PMSM prototype in the future. From the experimental validations, it can be said that the predicted temperature results from both thermal models has close agreement with experimental results. Therefore, it can be concluded that the developed thermal models are reliable.

Finally, from the predicted temperature results of the thermal models below terms have been found for the designed IPMSM and SPMSM prototypes,

1. Selection of correct insulation type H, since it can allow up to 125 °C rated temperature rise.
2. Selection of correct bearing type suitable for such temperature rise.
3. Suggestions on cooling requirements obtained from the temperature rise pattern of both motor prototypes.
4. No motor design fault in both motor prototypes.

Therefore, it can be concluded that both motor prototypes have a thermally sustained design.

At last for fulfilling the third research objective, efficient ways have been suggested for cooling design and cooling performance investigation process of PMSMs. In the fifth research contribution, a basic step algorithm has been developed to provide the basic guidelines of the cooling design process of PMSMs. The developed step algorithm defines the step by step process for cooling design and thus can be used as a basic cooling design optimization guideline for PMSMs. Further, a CFD thermal model using the proposed two-way electro-thermal co-analysis strategy has been developed for suggesting an efficient way for the cooling performance investigation process of both motor

prototypes in the future. Such two-way electro-thermal co-analysis strategy stated in the sixth and last research contribution has been developed for better accuracy in thermal modeling. This co-analysis is helpful for better prediction of both thermal and electromagnetic performance of PMSMs. Therefore, such CFD modeling with two-way electro-thermal co-analysis will be helpful for suggesting suitable flow rates of cooling fluid at several operating conditions for both targeted thermal and electromagnetic performance of PMSM.

Therefore, in summary, it can be said that several efficient ways of thermal modeling have been suggested in this thesis which can address the thermal issues of PMSMs properly.

9.2 Future Scopes

9.2.1 Future Work in the area of Thermal Design and Analysis

Future possible research work in the area of thermal design and analysis of PMSMs has been described below:

1. More detail thermal analysis of both IPMSM and SPMSM prototypes can be carried out using the developed LPTN and FEA thermal models for several operating conditions considering both continuous and dynamic drive cycle loads. Further, experimental validation of the developed LPTN and FEA thermal models can be carried out for both IPMSM and SPMSM prototypes in a broader scope at several operating conditions. Furthermore, a detailed parametric sensitivity analysis of the proposed LPTN model can be done in the future.
2. I-beam type magnets of IPMSM are the exceptions for the presented universal thermal analysis strategy of the magnets. Therefore, necessary changes can be made in the presented universal thermal analysis strategy of the magnets to incorporate I-beam type magnets also.
3. The presented universal thermal resistance calculation strategy for different double layers winding configurations is one of the parts of ongoing research work on thermal resistance calculation for future multilayer winding configurations. For simplification,

heat transfer between winding layers is neglected in the presented universal thermal resistance calculation strategy for double layers winding configurations.

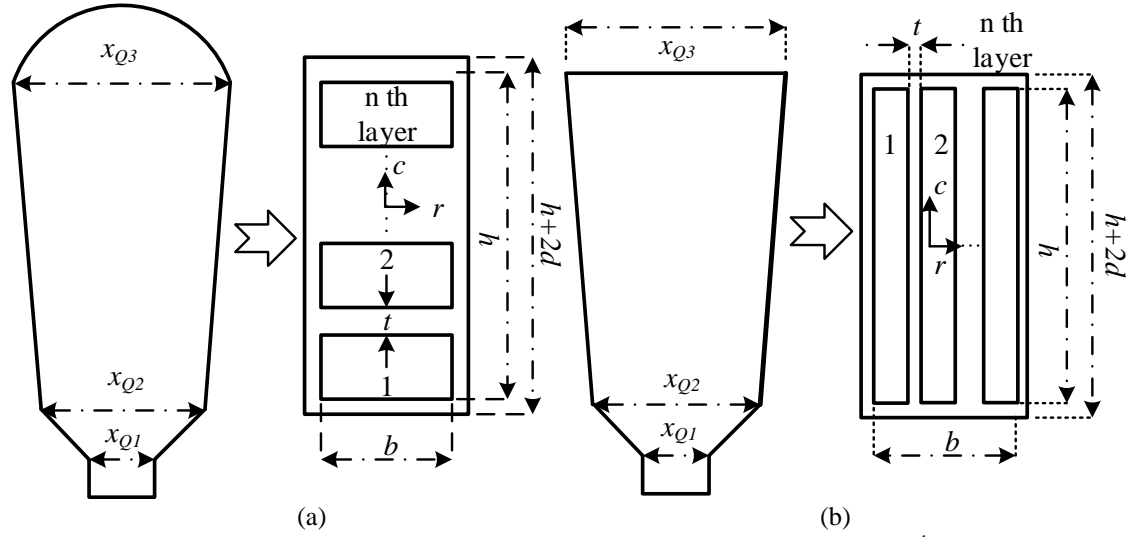


Figure 9.1 Layer by layer temperature prediction topology in LPTN model for n^{th} layer winding configurations. (a) FSDW. (b) FSCW.

However, a small temperature gradient always exists between the winding layers. For double layers FSCW configuration of SPMSM prototype, this temperature gradient is negligible. On the other hand, for double layers FSDW configuration of IPMSM prototype, this temperature gradient is not negligible which can be noticed from the predicted temperature distribution map of IPMSM from the FEA thermal model. The reason behind this is that the lower layer of FSDW is near to the air gap natural convection cooling. Therefore, layer by layer temperature prediction topology for windings is the best approach for thermal analysis of windings. Thus, the development of a universal thermal resistance calculation strategy of any present or future n^{th} layer winding configuration of the motor with layer by layer temperature prediction topology is the future goal of the ongoing research work on thermal resistance calculation for multilayer winding configurations.

4. To increase the torque density of both IPMSM and SPMSM prototypes, extra material has been scraped from the rotor to reduce the overall weight of the motors. Such a process leaves some additional air gaps in the rotor of the manufactured prototypes shown in Figure 2.6. Because of less rotor material, it reduces the rotor core loss and further the created additional air gap is responsible for a small amount of natural

convection cooling. Thus, the predicted rotor and magnet temperature of the designed prototypes from thermal models is more compared to the measured temperatures of manufactured prototypes. To address this issue, a Nusselt number equation will be introduced for natural convection cooling of additional air gaps in the rotor. Therefore, the development of basic step algorithm process for generating the Nusselt number equation to address the convection heat transfer in additional air gaps of traction motors is another possible future work in this field.

5. Unlike IM, PMSM does not have rotor bars or fins in the rotor. Therefore, the end region air flow in the PMSM is comparatively more smooth. Hence, the same developed empirical equations for calculating the combined convection coefficient in the end region of IM cannot provide a better prediction of the coefficient. Thus, the development of an empirical equation for calculating the combined convection coefficient to address the complex end region heat transfer phenomenon of the PM traction motor can be another future possible research scope.

9.2.2 Future Work in the area of Thermal Management

Future possible research work in the area of thermal management of PMSMs has been described below:

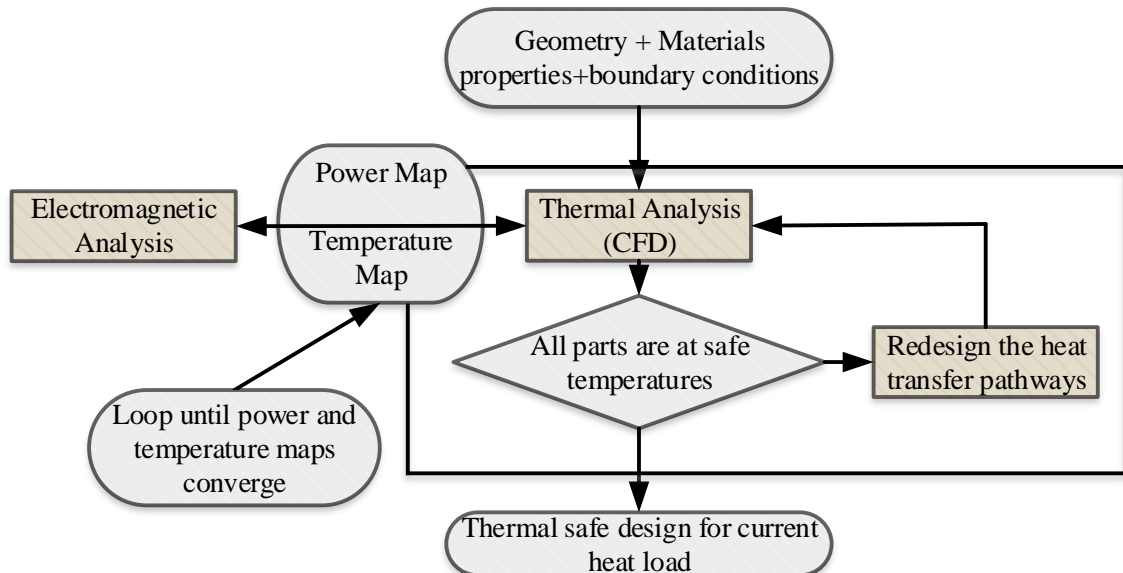


Figure 9.2 Cooling design optimization process for targeted electromagnetic performance using CFD analysis in ANSYS Workbench.

1. Optimized cooling design for full-scale prototypes of both IPMSM and SPMSM can be developed using the step algorithm in the future for better performance of the prototypes.
2. A detailed cooling performance investigation can be conducted using the developed CFD analysis to figure out the proper flow rate of cooling fluid for the better thermal and electromagnetic performance of the motor prototypes.
3. Developed two-way electro-thermal co-analysis strategy in CFD analysis can be further extended for cooling design optimization for the targeted electromagnetic performance shown in Figure 9.2.
4. Validation of suggested CFD analysis can be conducted in the future using a prototype for optimized cooling. Further, a detail mesh convergence and turbulence modeling investigation can be carried out also in the future.

References

- [1] Report on Paris Agreement, United Nations Framework Convention on Climate Change, 22 Oct. 2018 [Online]. Available: <https://unfccc.int/process-and-meetings/the-paris-agreement/the-paris-agreement>.
- [2] Organization for Economic Co-operation and Development (OECD) and International Transport Forum (ITF). (2008, May.). Transport Outlook 2008—Focusing on CO₂ Emissions from Road Vehicles [Online]. Available: <http://www.internationaltransportforum.org/>, accessed on Sep. 2019.
- [3] World Business Council for Sustainable Development (WBCSD). (2004). Mobility: 2030: Meeting the Challenges of Sustainability [Online]. Available: <http://www.wbcsd.org/>, accessed on Sep. 2019.
- [4] M. Ehsani, Y. Gao, and A. Emadi, *Modern Electric, Hybrid Electric, and Fuel Cell Vehicles – Fundamentals, Theory, and Design*, 2nd ed., NY: CRC Press, 2010.
- [5] L. D. Marlino, "Report on Toyota Prius Motor Thermal Management," Oak Ridge National Laboratory, 2005.
- [6] Z. Li, G. Feng, C. Lai, W. Li, and N. C. Kar, "Current Injection-based Multiple Parameters Estimation for Dual Three-phase IPMSM Considering VSI Nonlinearity," *IEEE Transactions on Transportation Electrification*, vol. 5, pp. 405 – 415, 2019.
- [7] G. Liao and J. Xi, "Intelligent Monitoring and Overheating Protection System for Motor," in *International Conference on Computing, Control and Industrial Engineering*, Wuhan, 2010, pp. 308–311.
- [8] J. Fan et al., "Thermal Analysis of Permanent Magnet Motor for the Electric Vehicle Application Considering Driving Duty Cycle," *IEEE Trans. on Mag.*, vol. 46, no. 6, pp. 2493–2496, June 2010.
- [9] F. JinXin, Z. ChengNing, W. ZhiFu and E. G. Strangas, "Thermal analysis of water cooled surface mount permanent magnet electric motor for electric vehicle," in *International Conference on Electrical Machines and Systems*, Incheon, 2010, pp. 1024–1028.

- [10] X. Fan, B. Zhang, R. Qu, J. Li, D. Li and Y. Huo, "Comparative thermal analysis of IPMSMs with integral-slot distributed-winding (ISDW) and fractional-slot concentrated-winding (FSCW) for electric vehicle application," in *IEEE International Electric Machines and Drives Conference (IEMDC)*, Miami, FL, 2017, pp. 1–8.
- [11] X. Zhang, Q. Lu, Y. Zhang, X. Huang and Y. Ye, "Thermal characteristics study of a water-cooled permanent magnet linear motor," in *Ninth International Conference on Ecological Vehicles and Renewable Energies (EVER)*, Monte-Carlo, 2014, pp. 1–9.
- [12] Y. Gai et al., "Cooling of Automotive Traction Motors: Schemes, Examples, and Computation Methods," *IEEE Transactions on Industrial Electronics*, vol. 66, no. 3, pp. 1681–1692, March 2019.
- [13] D. A. Staton and A. Cavagnino, "Convection Heat Transfer and Flow Calculations Suitable for Electric Machines Thermal Models," *IEEE Transactions on Industrial Electronics*, vol. 55, no. 10, pp. 3509–3516, Oct. 2008.
- [14] S. Seghir-Ouali, D. Saury, S. Harmand, O. Phillipart, and D. Laloy, "Convective heat transfer inside a rotating cylinder with an axial air flow," *Int. J. Thermal Sci.*, vol. 45, pp. 1166–1178, 2006.
- [15] D. J. Womac, S. Ramadhyani, and F. P. Incropera, "Correlating equations for impingement cooling of small heat sources with single circular liquid jets," *J. Heat Transfer*, vol. 115, pp. 106–115, 1993.
- [16] G. Arslan and M. Ozdemir, "Correlation to predict heat transfer of an oscillating loop heat pipe consisting of three interconnected columns," *Energy Convers. Manage.*, vol. 49, pp. 2337–2344, 2008.
- [17] F. Ahmed, E. Ghosh and N. C. Kar, "Transient thermal analysis of a copper rotor induction motor using a lumped parameter temperature network model," in *IEEE Transportation Electrification Conference and Expo*, 2016, pp. 1–6.
- [18] F. Ahmed and N. C. Kar, "Analysis of End-Winding Thermal Effects in a Totally Enclosed Fan-Cooled Induction Motor with a Die Cast Copper Rotor," *IEEE Transactions on Industry Applications*, vol. 53, no. 3, pp. 3098–3109, May–June 2017.

- [19] D. Staton, A. Boglietti and A. Cavagnino, "Solving the more difficult aspects of electric motor thermal analysis in small and medium size industrial induction motors," *IEEE Transactions on Energy Conversion*, vol. 20, no. 3, pp. 620–628, Sept. 2005.
- [20] Y. Gai et al., "On the Measurement and Modeling of the Heat Transfer Coefficient of a Hollow-Shaft Rotary Cooling System for a Traction Motor," *IEEE Transactions on Industry Applications*, vol. 54, no. 6, pp. 5978–5987, Nov.–Dec. 2018.
- [21] A. Boglietti and A. Cavagnino, "Analysis of the end-winding cooling effects in TEFC induction motors," *IEEE Transactions on Industry Applications*, volume 43, issue 5, pp. 1214–1222, 2007.
- [22] C. Micallef, S. J. Pickering, K. Simmons, and K. Bradley, "Improvements in air flow in the end region of a large totally enclosed fan cooled induction motor," in *Proc. of IEEE International Electric Machines and Drives Conference (IEMDC'05)*, San Antonio, May 2005.
- [23] A. Boglietti, A. Cavagnino, D. Staton, M. Popescu, C. Cossar, and M.I. McGilp, "End space heat transfer coefficient determination for different induction motor enclosure types", *IEEE Trans. on Industry Applications*, vol. 45, No. 3, May/June 2009, pp. 929–937.
- [24] E. Schubert, "Heat Transfer Coefficients at End Windings and Bearing Covers of Enclosed Asynchronous Machines," *Elektrie*, vol. 22, April 1968. pp160–162. (Translation ERA/IB 2846).
- [25] A. Boglietti, A. Cavagnino, D. Staton, and M. Popescu, "Impact of different end region cooling arrangements on endwinding heat transfer coefficients in electric motors," in *Proc. IEEE Conf. on Industrial Electronics*, 978–1–4244–4649–0/09.
- [26] A. Boglietti, A. Cavagnino, M. Lazzari, and M. Pastorelli, "A simplified thermal model for variable speed self cooled industrial induction motor," in *IEEE Transactions on Industry Applications*, volume.39, no.4, August 2003, pp. 945–952.
- [27] C. Micallef, S. J. Pickering, K. A. Simmons, and K. J. Bradley, "An Alternative Cooling Arrangement for the End Region of a Totally Enclosed Fan Cooled (TEFC)

- Induction Motor," in *4th IET Conference on Power Electronics Machines and Drives*, pp. 309–309, (2008).
- [28] G. Kylander, Thermal Modelling of Small Cage Induction Motors, Ph.D. thesis, School of Electrical and Computer Engineering, Chalmers University of Technology, Goteborg, Sweden, February 1995, Technical Report No. 265.
 - [29] B. Zhang, R. Qu, J. Wang, W. Xu, X. Fan, and Y. Chen, "Thermal Model of Totally Enclosed Water–Cooled Permanent–Magnet Synchronous Machines for Electric Vehicle Application," *IEEE Transactions on Industry Applications*, vol. 51, pp. 3020–3029, 2015.
 - [30] F. Harahap and J. H. N. McManus, "Natural convection heat transfer from horizontal rectangular fin arrays," *J. Heat Transfer*, vol. 89, pp. 32–38, 1967.
 - [31] S. Mukundan, H. Dhulipati, J. Tjong and N. C. Kar, "Parameter Determination of PMSM Using Coupled Electromagnetic and Thermal Model Incorporating Current Harmonics," *IEEE Transactions on Magnetics*, vol. 54, no. 11, pp. 1–5, Nov. 2018, Art no. 8110505.
 - [32] O. Wallscheid and J. Böcker, "Global Identification of a Low–Order Lumped–Parameter Thermal Network for Permanent Magnet Synchronous Motors," *IEEE Transactions on Energy Conversion*, vol. 31, no. 1, pp. 354–365, March 2016.
 - [33] O. Wallscheid and J. Böcker, "Design and identification of a lumped–parameter thermal network for permanent magnet synchronous motors based on heat transfer theory and particle swarm optimisation," in *17th European Conference on Power Electronics and Applications (EPE'15 ECCE–Europe)*, Geneva, 2015, pp. 1–10.
 - [34] Q. Lu, X. Zhang, Y. Chen, X. Huang, Y. Ye and Z. Q. Zhu, "Modeling and Investigation of Thermal Characteristics of a Water–Cooled Permanent–Magnet Linear Motor," *IEEE Transactions on Industry Applications*, vol. 51, no. 3, pp. 2086–2096, May–June 2015.
 - [35] A. M. EL-Refaie, N. C. Harris, T. M. Jahns and K. M. Rahman, "Thermal analysis of multibarrier interior PM synchronous Machine using lumped parameter model," *IEEE Transactions on Energy Conversion*, vol. 19, no. 2, pp. 303–309, June 2004.

- [36] L. Zhiyong, W. Xuehuan and C. Linhong, "Thermal analysis of PMSM based on lumped parameter thermal network method," in *19th International Conference on Electrical Machines and Systems*, 2016.
- [37] B. Zhang, R. Qu, J. Wang, J. Li, W. Xu and Y. Chen, "Electromagnetic–Thermal Coupling Analysis of Permanent Magnet Synchronous Machines for Electric Vehicle Applications Based on Improved $(\mu+1)$ Evolution Strategy," *IEEE Transactions on Magnetics*, vol. 51, no. 4, pp. 1–10, April 2015.
- [38] L. Mo, T. Zhang and Q. Lu, "Thermal Analysis of a Flux-Switching Permanent-Magnet Double-Rotor Machine With a 3-D Thermal Network Model," *IEEE Transactions on Applied Superconductivity*, vol. 29, no. 2, pp. 1-5, March 2019.
- [39] P. Ponomarev, M. Polikarpova and J. Pyrhönen, "Thermal modeling of directly–oil–cooled permanent magnet synchronous machine," in *XXth International Conference on Electrical Machines*, 2012, pp. 1882–1887.
- [40] B. Zhang, R. Qu, X. Fan and J. Wang, "Thermal and mechanical optimization of water jacket of permanent magnet synchronous machines for EV application," in *IEEE International Electric Machines & Drives Conference*, Coeur d'Alene, 2015, pp. 1329–1335.
- [41] P. Ponomarev, M. Polikarpova and J. Pyrhönen, "Conjugated fluid–solid heat transfer modeling of a directly–oil–cooled PMSM using CFD," in *Int. Symposium on Power Electronics Power Electronics, Electrical Drives, Automation and Motion*, Sorrento, 2012, pp. 141–145.
- [42] A. Nollau and D. Gerling, "Novel cooling methods using flux-barriers," *International Conference on Electrical Machines*, Berlin, 2014, pp. 1328–1333.
- [43] A. Nollau and D. Gerling, "A flux barrier cooling for traction motors in hybrid drives," *IEEE International Electric Machines & Drives Conference*, Coeur d'Alene, 2015, pp. 1103-1108.
- [44] A. Fatemi et al., "Design of an Electric Machine for a 48–V Mild Hybrid Vehicle," *IEEE Energy Conversion Congress and Exposition*, Portland, OR, 2018, pp. 2278–2285.

- [45] Y. Zhang, S. McLoone, W. Cao, F. Qiu and C. Gerada, "Power Loss and Thermal Analysis of a MW High-Speed Permanent Magnet Synchronous Machine," *IEEE Transactions on Energy Conversion*, vol. 32, pp. 1468–1478, Dec. 2017.
- [46] T. D. Kefalas and A. G. Kladas, "Thermal Investigation of Permanent-Magnet Synchronous Motor for Aerospace Applications," *IEEE Transactions on Industrial Electronics*, vol. 61, pp. 4404–4411, 2014.
- [47] L. Hosain, R. B. Fdhila, K. Ronnberg, "Air-Gap Flow and Thermal Analysis of Rotating Machine using CFD", in *the 8th International Conference on Applied Energy –ICAE2016*.
- [48] M. Kasprzak, J. W. Jiang, B. Bilgin and A. Emadi, "Thermal analysis of a three-phase 24/16 switched reluctance machine used in HEVs," *IEEE Energy Conversion Congress and Exposition*, 2016, pp. 1–7.
- [49] J. Tang and Y. Liu, "Design and Experimental Verification of a 48 V 20 kW Electrically Excited Synchronous Machine for Mild Hybrid Vehicles," in *XIII International Conference on Electrical Machines*, Alexandroupoli, 2018, pp. 649–655.
- [50] M. Zeraouila, M. E. H. Benbouzid and D. Diallo, "Electric motor drive selection issues for HEV propulsion systems: a comparative study," in *IEEE Vehicle Power and Propulsion Conference*, Chicago, IL, 2005.
- [51] E. Ghosh, F. Ahmed, A. Mollaeian, J. Tjong and N. C. Kar, "Online parameter estimation and loss calculation using duplex neural — Lumped parameter thermal network for faulty induction motor," *IEEE Conference on Electromagnetic Field Computation*, 2016, pp. 1–1.
- [52] S. Mezani, N. Takorabet and B. Laporte, "A combined electromagnetic and thermal analysis of induction motors," *IEEE Transactions on Magnetics*, vol. 41, no. 5, pp. 1572–1575, May 2005.
- [53] A. Boglietti, A. Cavagnino, M. Parvis and A. Vallan, "Evaluation of radiation thermal resistances in industrial motors," *IEEE Transactions on Industry Applications*, vol. 42, no. 3, pp. 688–693, May–June 2006.

- [54] O. I. Okoro, "Steady and transient states thermal analysis of a 7.5-kW squirrel-cage induction machine at rated-load operation," *IEEE Transactions on Energy Conversion*, vol. 20, no. 4, pp. 730–736, 2005.
- [55] C. Kral, A. Haumer and T. Bauml, "Thermal Model and Behavior of a Totally-Enclosed-Water-Cooled Squirrel-Cage Induction Machine for Traction Applications," *IEEE Transactions on Industrial Electronics*, vol. 55, no. 10, pp. 3555–3565, Oct. 2008.
- [56] A. Boglietti, E. Carpaneto, M. Cossale and S. Vaschetto, "Stator-Winding Thermal Models for Short-Time Thermal Transients: Definition and Validation," *IEEE Transactions on Industrial Electronics*, vol. 63, no. 5, pp. 2713–2721, May 2016.
- [57] C. Kral, A. Haumer, M. Haigis, H. Lang and H. Kapeller, "Comparison of a CFD Analysis and a Thermal Equivalent Circuit Model of a TEFC Induction Machine with Measurements," *IEEE Transactions on Energy Conversion*, vol. 24, no. 4, pp. 809–818, Dec. 2009.
- [58] X. Wang, J. Du, G. Peng, H. Lv, "Thermal Comparison of a CFD analysis and a lumped parameter model of an air-cooled induction machine for EVs", *International Journal of Applied Electromagnetics and Mechanics*, vol. 54, no. 1, pp. 37–56, 2017.
- [59] J. Gong, F. Gillon and P. Brochet, "Magnetic and thermal 3D finite element model of a Linear Induction Motor," in *IEEE Vehicle Power and Propulsion Conference*, Lille, 2010, pp. 1–6.
- [60] R. Pechanek, V. Kindl, B. Skala, "Transient Thermal Analysis of Small Squirrel Cage Motor through Coupled FEA", *MM Science Journal*, pp. 560–563, 2015.
- [61] Z. Ye, W. Luo, W. Zhang and Z. Feng, "Simulative analysis of traction motor cooling system based on CFD," in *International Conference on Electric Information and Control Engineering*, 2011, pp. 746–749.
- [62] M. Hettegger, B. Streibl, O. Biro and H. Neudorfer, "Measurements and Simulations of the Convective Heat Transfer Coefficients on the End Windings of an Electrical Machine," *IEEE Transactions on Industrial Electronics*, vol. 59, no. 5, pp. 2299–2308, 2012.

- [63] Y. Zhang, J. Ruan, T. Huang, X. Yang, H. Zhu and G. Yang, "Calculation of Temperature Rise in Air-cooled Induction Motors Through 3-D Coupled Electromagnetic Fluid–Dynamical and Thermal Finite–Element Analysis," *IEEE Transactions on Magnetics*, vol. 48, no. 2, pp. 1047–1050, 2012.
- [64] Z. Huang, F. Marquez, M. Alakula and J. Yuan, "Characterization and application of forced cooling channels for traction motors in HEVs," in *XXth Int. Conf. on Electrical Machines*, 2012, pp. 1212–1218.
- [65] S. Moon, J. Yun, W. Kim and J. Kim, "Thermal–flow analysis and cooling performance enhancement of a totally enclosed fan–cooled motor," in *International Conference on Electrical Machines and Systems*, Busan, 2013, pp. 2028–2030.
- [66] S. H. Moon, Y. H. Jung and K. W. Kim, "Numerical investigation on thermal–flow characteristics of a totally enclosed fan cooled induction motor," in *XXII International Conference on Electrical Machines*, Lausanne, 2016, pp. 1928–1933.
- [67] C. Ulu, O. Korman and G. Kömürgöz, "Electromagnetic and thermal analysis/design of an induction motor for electric vehicles," in *8th International Conference on Mechanical and Aerospace Engineering*, Prague, 2017, pp. 6–10.
- [68] A. Gudi, A. Singh and B. Agarwal, "Electric machine stator thermal sensitivity analysis using CFD," in *IEEE Transportation Electrification Conference (ITEC–India)*, Pune, 2017, pp. 1–6.
- [69] D. Kim, D. Hong, J. Choi, Y. Chun, B. Woo and D. Koo, "An Analytical Approach for a High Speed and High Efficiency Induction Motor Considering Magnetic and Mechanical Problems," *IEEE Transactions on Magnetics*, vol. 49, no. 5, pp. 2319–2322, May 2013.
- [70] C. W. Somerton, L. J. Genik, D. Beavers, and T. Jammer, "A Nusselt Number Correlation Classification System," in *Proceedings of the American Society of Engineering Education*, 1999.
- [71] F.P. Incropera and D.P. DeWitt, *Introduction to Heat Transfer*, 9th ed. NY: John Wiley & Sons, 2011.
- [72] Y. A. Cengel, *Heat Transfer: A Practical Approach*, 2nd ed. Boston: WCB McGraw–Hill, 1993.
- [73] A. Bejan, *Convection Heat Transfer*, 3rd ed. NY: John Wiley & Sons, 2004.

- [74] B. Guo, Y. Huang, Y. Guo and J. Zhu, "Thermal Analysis of the Conical Rotor Motor Using LPTN with Accurate Heat Transfer Coefficients," *IEEE Transactions on Applied Superconductivity*, vol. 26, no. 7, pp. 1–7, Oct. 2016.
- [75] N. Simpson, R. Wrobel and P. H. Mellor, "A General Arc-Segment Element for Three-Dimensional Thermal Modeling," *IEEE Transactions on Magnetics*, vol. 50, no. 2, pp. 265-268, Feb. 2014.
- [76] R. Wrobel and P. H. Mellor, "A General Cuboidal Element for Three-Dimensional Thermal Modelling," *IEEE Transactions on Magnetics*, vol. 46, no. 8, pp. 3197–3200, Aug. 2010.
- [77] X. Hu, "Optimizing the Thermal Design in Electric Machines with Simulation", ANSYS Inc., April 17, 2018.
- [78] J. Lindstrom, "Development of an Experimental Permanent-Magnet Motor Drive", Chalmers University of Technology, Goteborg, Sweden, Rep. no. 312L, April, 1999.
- [79] J. P. Holman, *Heat Transfer*, 10th edition, NY: McGraw–Hill, 2010.
- [80] W. S. Janna, *Engineering Heat Transfer*, NY: Van Nostrand, 1988.
- [81] A. F. Mills, *Heat Transfer*, Englewood Cliffs, NJ: Prentice Hall, 1999.
- [82] K. Bennion, E. Cousineau, X. Feng, C. King, and G. Moreno, "Electric Motor Thermal Management R&D", IEEE Power and Energy Society general meeting, Denver, CO, July 26–30, 2015.
- [83] A. Boglietti, A. Cavagnino, D. Staton, M. Shanel, M. Mueller and C. Mejuto, "Evolution and Modern Approaches for Thermal Analysis of Electrical Machines," *IEEE Transactions on Industrial Electronics*, vol. 56, no. 3, pp. 871–882, March 2009.
- [84] M. Rosu, P. Zhou, D. Lin, D. M. Ionel, M. Popescu, F. Blaabjerg, V. Rallabandi, and D. Staton, "Thermal Problems in Electrical Machines," in *Multiphysics Simulation by Design for Electrical Machines, Power Electronics and Drives*, Wiley–IEEE, 2017.
- [85] F. JinXin, Z. ChengNing, W. Zhifu, A. R. Tariq, C. E. Nino, and E. G. Strangas, "Design and thermal analysis of traction motor for electric vehicle based on driving

- duty cycle,"in *Digests of the 14th Biennial IEEE Conference on Electromagnetic Field Computation*, Chicago, IL, 2010, pp. 1-1.
- [86] C. Pohlandt, and M. Geimer, "Thermal models of electric machines with dynamic workloads," *Landtechnik*, vol. 70, no. 4, pp. 97-112, July 2015.
 - [87] G. Li, J. Ojeda, E. Hoang, M. Gabsi and M. Lecrivain, "Thermal–Electromagnetic Analysis for Driving Cycles of Embedded Flux-Switching Permanent-Magnet Motors," *IEEE Transactions on Vehicular Technology*, vol. 61, no. 1, pp. 140–151, Jan. 2012.
 - [88] S. Ramarathnam, A. K. Mohammed, B. Bilgin, A. Sathyan, H. Dadkhah and A. Emadi, "A Review of Structural and Thermal Analysis of Traction Motors," *IEEE Transactions on Transportation Electrification*, vol. 1, no. 3, pp. 255–265, Oct. 2015.
 - [89] H. Li and Y. Shen, "Thermal Analysis of the Permanent–Magnet Spherical Motor," *IEEE Transactions on Energy Conversion*, vol. 30, no. 3, pp. 991–998, Sept. 2015.
 - [90] P. H. Mellor, D. Roberts, and D. R. Turner, "Lumped parameter thermal model for electrical machines of TEFC design," in *IEEE Proceedings B – Electric Power Applications*, vol. 138, no. 5, pp. 205–218, Sept. 1991.
 - [91] A. H. Mohamed, A. Hemeida, A. Rasekh, H. Vansompel, A. Arkkio and P. Sergent, "A 3D Dynamic Lumped Parameter Thermal Network of Air-Cooled YASA Axial Flux Permanent Magnet Synchronous Machine" *Energies*, vol. 11, no. 4, pp. 774-790, 2018.
 - [92] N. Simpson, R. Wrobel and P. H. Mellor, "An Accurate Mesh-Based Equivalent Circuit Approach to Thermal Modeling," *IEEE Transactions on Magnetics*, vol. 50, no. 2, pp. 269-272, Feb. 2014.
 - [93] J. Chin, S. Hwang, H. Park and J. Hong, "Thermal Analysis and Verification of PMSM Using LPTN Considering Mechanical Components and Losses," in *XIII International Conference on Electrical Machines (ICEM)*, Alexandroupoli, 2018, pp. 1323-1329.
 - [94] "Introduction - ANSYS Fluent Heat Transfer Modeling", ANSYS Inc., Dec 28, 2017.

- [95] J. Kuria and P. Hwang, "Investigation of Thermal Performance of Electric Vehicle BLDC Motor," *International Journal of Mechanical Engineering*, vol. 1, no. 1, Mar. 2012.
- [96] L. Li, J. Zhang, C. Zhang, and J. Yu, "Research on Electromagnetic and Thermal Issue of High-Efficiency and High-Power-Density Outer-Rotor Motor," *IEEE Transactions on Applied Superconductivity*, vol. 26, no. 4, pp. 1–5, June 2016.
- [97] K. Bennion, E. Cousineau, X. Feng, C. King, and G. Moreno, "Electric Motor Thermal Management R&D", in IEEE Power and Energy Society general meeting, Denver, CO, July 26–30, 2015.
- [98] H. Versteeg and W. Malalasekra, *An Introduction to Computational Fluid Dynamics – The Finite Volume Method*, 2nd edition, Pearson Education Ltd., 2016.
- [99] P. Lindh *et al.*, "Multidisciplinary Design of a Permanent-Magnet Traction Motor for a Hybrid Bus Taking the Load Cycle into Account," *IEEE Transactions on Industrial Electronics*, vol. 63, no. 6, pp. 3397-3408, June 2016.
- [100] L. Cuiping, G. Zhengwei, L. Junhui, Z. Bing, and D. Xiucui, "Optimal design of cooling system for water cooling motor used for mini electric vehicle," in *20th International Conference on Electrical Machines and Systems (ICEMS)*, Sydney, NSW, 2017, pp. 1-4.
- [101] Z. Rehman and K. Seong, "Three-D Numerical Thermal Analysis of Electric Motor with Cooling Jacket", *Energies*, vol. 11, no. 92, Jan. 2018.
- [102] Y. Yang et al., "Thermal management of electric machines", *IET Electric Systems in Transportation*, vol. 7, no. 2, pp. 104-116, 2017.
- [103] S. Ayat, R. Wrobel, J. Goss, and D. Drury, "Experimental calibration in thermal analysis of PM electrical machines," *IEEE Energy Conversion Congress and Exposition (ECCE)*, Milwaukee, WI, 2016, pp. 1-8.
- [104] C. Kral, A. Haumer and S. B. Lee, "A Practical Thermal Model for the Estimation of Permanent Magnet and Stator Winding Temperatures," *IEEE Transactions on Power Electronics*, vol. 29, no. 1, pp. 455-464, Jan. 2014.
- [105] G. D. Demetriades, H. Z. d. I. Parra, E. Andersson, and H. Olsson, "A Real-Time Thermal Model of a Permanent-Magnet Synchronous Motor," *IEEE Transactions on Power Electronics*, vol. 25, no. 2, pp. 463-474, Feb. 2010.

- [106] S. Mukundan, H. Dhulipati, G. Feng, J. Tjong, and N. C. Kar, "Modeling and Analysis of Novel Star-Delta Winding Configuration with Odd Slot Numbers for Reduced Space Harmonics Using Winding Function," in *proc. of IEEE International Electric Machines & Drives Conference (IEMDC)*, San Diego, CA, USA, 2019, pp. 1910–1916.
- [107] D. G. Dorrell, D. A. Staton, J. Kahout, D. Hawkins and M. I. McGilp, "Linked Electromagnetic and Thermal Modelling of a Permanent Magnet Motor," in *3rd IET International Conference on Power Electronics, Machines and Drives – PEMD*, Dublin, Ireland, 2006, pp. 536–540.
- [108] S. Mezani, N. Takorabet, and B. Laporte, "A combined electromagnetic and thermal analysis of induction motors," *IEEE Transactions on Magnetics*, vol. 41, no. 5, pp. 1572–1575, May 2005.
- [109] Q. Guo, C. Zhang, L. Li, J. Zhang, and M. Wang, "Maximum Efficiency per Torque Control of Permanent–Magnet Synchronous Machines," *Applied Sciences*, vol. 6, no. 12, p. 425, Dec. 2016.
- [110] O. V. Tikhonova and A. T. Plastun, "Electromagnetic calculation of induction motor by “ANSYS Maxwell”," in *IEEE Conference of Russian Young Researchers in Electrical and Electronic Engineering (EICONRus)*, Moscow, 2018, pp. 822-826.
- [111] J. Pyrhonen, T. Jokinen and V. Hrabovcova, *Design of Rotating Electrical Machines*, John Wiley & Sons, Ltd. ISBN: 978-0-470-69516-6, 2008.
- [112] P. S. Ghahfarokhi, A. Kallaste, A. Belahcen and T. Vaimann, "Steady state and transient thermal analysis of the stator coil of a permanent magnet generator," in *The 18th International Scientific Conference on Electric Power Engineering (EPE)*, Kouty nad Desnou, 2017, pp. 1-5.
- [113] N. Zhao and W. Liu, "Loss Calculation and Thermal Analysis of Surface-Mounted PM Motor and Interior PM Motor," *IEEE Transactions on Magnetics*, vol. 51, no. 11, pp. 1-4, Nov. 2015.
- [114] Wang Fujun. Analysis of computational fluid dynamics [M]. Beijing: *Tsinghua University press*, 2004.

Appendices

Appendix A: List of Publications

Journals

- [1] **P. Roy**, S. Mukundan, H. Dhulipati, F. Ahmed, M. Towhidi, Z. Li, E. Ghosh, and N. C. Kar “Universal Thermal Representation of Interior and Surface Mounted PMSMs for Electric Vehicle Application,” to be submitted in *the IEEE Journal of Emerging and Selected Topics in Industrial Electronics*, 2020.
- [2] **P. Roy**, S. Mukundan, M. Towhidi, F. Ahmed, Z. Li, and N. C. Kar, “A Comprehensive Review of Thermal Design and Analysis of Traction Motors,” to be submitted in *the IEEE Journal of Emerging and Selected Topics in Industrial Electronics*, 2020.

Conference Publications

- [1] **P. Roy**, A. Bourgault, F. Ahmed, M. Towhidi, S. Mukundan, H. Dhulipati, E. Ghosh, and N. C. Kar “Thermal Representation of Interior and Surface Mounted PMSMs for Electric Vehicle Application,” in *the IEEE 45th Annual Conference of the Industrial Electronics Society*, Lisbon, Portugal, October 2019.
- [2] F. Ahmed, **P. Roy**, M. Towhidi, G. Feng and N. C. Kar, “CFD and LPTN Hybrid Technique to Determine Convection Coefficient in End-winding of TEFC Induction Motor with Copper Rotor”, in *the IEEE 45th Annual Conference of the Industrial Electronics Society*, Lisbon, Portugal, October 2019.
- [3] **P. Roy**, M. Towhidi, F. Ahmed, A. J. Bourgault, S. Mukundan, A. Balamurali, and N. C. Kar, “A Comprehensive Review of Thermal Design and Analysis of Traction Motors,” in *the IEEE 28th International Symposium on Industrial Electronics*, Vancouver, Canada, June 2019.
- [4] A. J. Bourgault, **P. Roy**, E. Ghosh, and N. C. Kar, “A Survey of Different Cooling Methods for Traction Motor Application,” in *the IEEE Canadian*

Conference on Electrical and Computer Engineering (CCECE), Edmonton, Canada, May 2019.

- [5] **P. Roy**, A. J. Bourgault, and N. C. Kar, “Review of Thermal Design & Analysis of Traction Motors”, poster paper at *EECOMOBILITY (ORF) & HEVPD&D CREATE conference*, Windsor, Ontario, Canada, April 2019.
- [6] **P. Roy**, M. Towhidi, F. Ahmed, S. Mukundan, H. Dhulipati, and N. C. Kar, “A Novel Hybrid Technique for Thermal Analysis of Permanent Magnet Synchronous Motor Used in Electric Vehicle Application,” accepted for presentation in *SAE World Congress Experience Conference*, Detroit, MI, USA, April 21-23, 2020.
- [7] **P. Roy**, A. J. Bourgault, M. Towhidi, Z. Li, S. Mukundan, G. Rankin, and N. C. Kar, “A Step Algorithm for Effective Cooling Design and Cooling Performance Investigation of PM Traction Motors,” submitted in *IEEE International Magnetics Conference*, Montreal, Canada, May 2020.

Technical Report

- [1] **P. Roy**, “Development of Mechanical Devices in EPT-150 for Targeted Speed and Torque”, in NSERC CREATE project at D&V Electronics Ltd., November 2018.

Appendix B: Research Activities, Memberships, Scholarships and Courses

Industrial Project Contributions

1. NSERC Engage Project with TM4 Inc.
 - Parameter sorting of developed lumped parameter thermal network model for thermal analysis of surface mounted permanent magnet synchronous machines for electric vehicle application.
2. NSERC CREATE Project at D&V Electronics Ltd.
 - Design and development of mechanical transmission system in EPT-150 for targeted speed and torque.
 - Worked with R&D team of the company on several design works, documentations, supplier sourcing, and testing.
3. NSERC CRD Project with Ford Motor Company Ltd. and D&V Electronics Ltd.
 - Equip the electric power train for thermal testing with drives and drive cycle based testing.
 - Development of an algorithm for acceleration and deceleration profile of DUTs in EPT-150 and determination of thermal characteristics of brake resistors under the acceleration and deceleration cycle
4. BorgWarner Motor Testing
 - Thermal testing of BorgWarner motor using EPT.
5. ORF Project with Ford Motor Company Ltd. and D&V Electronics Ltd.
 - Thermal analysis of multi-phase e-motor for direct-drive application.
 - Cooling design optimization and cooling performance investigation of multi-phase e-motor for direct-drive application.
6. Gates Project
 - Thermal analysis of designed axial flux permanent magnet motor.
7. NREL-BorgWarner Project Proposal
 - Thermal management of BorgWarner inverter.

Other Activities

1. NSERC CREATE Internship in D&V Electronics Ltd.
2. Poster Presentation at the EECOMOBILITY (ORF) & HEVPD&D CREATE conference.
3. Oral Presentation at the IEEE 28th International Symposium on Industrial Electronics, Vancouver, Canada, June 2019.
4. Oral Presentation at the IEEE 45th Annual Conference of the Industrial Electronics Society, Lisbon, Portugal, October 2019.

Memberships

1. IEEE Student Membership
2. IES Student Membership
3. SAE Student Membership
4. IEEE Young Professionals Membership – Assistant Treasurer at IEEE Young Professionals in Windsor Section
5. Nominated for Golden Key International Honour Society Membership because of the merit position within the top 15% of my program at the University of Windsor.

Scholarships

1. Research Grant received from Canada Research Chair Program in Electrified Transportation Systems, Centre for Hybrid Automotive Research and Green Energy, 2018 – 2019.
2. University of Windsor Teaching Assistantship, 2018-2019.

Courses Taken

1. Power System Analysis & Control
2. Practical CFD & Turbulence Modeling
3. Advanced Energy Storage System for Hybrid Electric Vehicle
4. Analysis - Electric Machines
5. Engineering Technical Communications
6. Introduction to Project Management

Appendix C: Permission for Using Publications

12/17/2019

Rightslink® by Copyright Clearance Center



RightsLink®



A Comprehensive Review of Thermal Design and Analysis of Traction Motors



Conference Proceedings:

2019 IEEE 28th International Symposium on Industrial Electronics (ISIE)

Author: Pratik Roy

Publisher: IEEE

Date: June 2019

Copyright © 2019, IEEE

Thesis / Dissertation Reuse

The IEEE does not require individuals working on a thesis to obtain a formal reuse license, however, you may print out this statement to be used as a permission grant:

Requirements to be followed when using any portion (e.g., figure, graph, table, or textual material) of an IEEE copyrighted paper in a thesis:

- 1) In the case of textual material (e.g., using short quotes or referring to the work within these papers) users must give full credit to the original source (author, paper, publication) followed by the IEEE copyright line © 2011 IEEE.
- 2) In the case of illustrations or tabular material, we require that the copyright line © [Year of original publication] IEEE appear prominently with each reprinted figure and/or table.
- 3) If a substantial portion of the original paper is to be used, and if you are not the senior author, also obtain the senior author's approval.

Requirements to be followed when using an entire IEEE copyrighted paper in a thesis:

- 1) The following IEEE copyright/ credit notice should be placed prominently in the references: © [year of original publication] IEEE. Reprinted, with permission, from [author names, paper title, IEEE publication title, and month/year of publication]
- 2) Only the accepted version of an IEEE copyrighted paper can be used when posting the paper or your thesis online.
- 3) In placing the thesis on the author's university website, please display the following message in a prominent place on the website: In reference to IEEE copyrighted material which is used with permission in this thesis, the IEEE does not endorse any of [university/educational entity's name goes here]'s products or services. Internal or personal use of this material is permitted. If interested in reprinting/republishing IEEE copyrighted material for advertising or promotional purposes or for creating new collective works for resale or redistribution, please go to http://www.ieee.org/publications_standards/publications/rights_rights_link.html to learn how to obtain a License from RightsLink.

If applicable, University Microfilms and/or ProQuest Library, or the Archives of Canada may supply single copies of the dissertation.

BACK

CLOSE

© 2019 Copyright - All Rights Reserved | Copyright Clearance Center, Inc. | Privacy statement | Terms and Conditions
Comments? We would like to hear from you. E-mail us at customercare@copyright.com



RightsLink®



Thermal Representation of Interior and Surface Mounted PMSMs for Electric Vehicle Application



Conference Proceedings:
IECON 2019 - 45th Annual Conference of the IEEE Industrial Electronics Society
Author: Pratik Roy
Publisher: IEEE
Date: Oct. 2019

Copyright © 2019, IEEE

Thesis / Dissertation Reuse

The IEEE does not require individuals working on a thesis to obtain a formal reuse license, however, you may print out this statement to be used as a permission grant:

Requirements to be followed when using any portion (e.g., figure, graph, table, or textual material) of an IEEE copyrighted paper in a thesis:

- 1) In the case of textual material (e.g., using short quotes or referring to the work within these papers) users must give full credit to the original source (author, paper, publication) followed by the IEEE copyright line © 2011 IEEE.
- 2) In the case of illustrations or tabular material, we require that the copyright line © [Year of original publication] IEEE appear prominently with each reprinted figure and/or table.
- 3) If a substantial portion of the original paper is to be used, and if you are not the senior author, also obtain the senior author's approval.

Requirements to be followed when using an entire IEEE copyrighted paper in a thesis:

- 1) The following IEEE copyright/ credit notice should be placed prominently in the references: © [year of original publication] IEEE. Reprinted, with permission, from [author names, paper title, IEEE publication title, and month/year of publication]
- 2) Only the accepted version of an IEEE copyrighted paper can be used when posting the paper or your thesis online.
- 3) In placing the thesis on the author's university website, please display the following message in a prominent place on the website: In reference to IEEE copyrighted material which is used with permission in this thesis, the IEEE does not endorse any of [university/educational entity's name goes here]'s products or services. Internal or personal use of this material is permitted. If interested in reprinting/republishing IEEE copyrighted material for advertising or promotional purposes or for creating new collective works for resale or redistribution, please go to http://www.ieee.org/publications_standards/publications/rights/rights_link.html to learn how to obtain a license from RightsLink.

If applicable, University Microfilms and/or ProQuest Library, or the Archives of Canada may supply single copies of the dissertation.

BACK

CLOSE

Vita Auctoris

NAME: Pratik Roy

PLACE OF BIRTH: Comilla, Bangladesh

YEAR OF BIRTH: 1994

EDUCATION: Comilla Zilla School, S.S.C., Bangladesh, 2009
Comilla Victoria Govt. College, H.S.C., Bangladesh, 2011
Khulna University of Engineering and Technology (KUET),
B.Sc., Bangladesh, 2016
University of Windsor, M.A.Sc., Windsor, ON, 2020